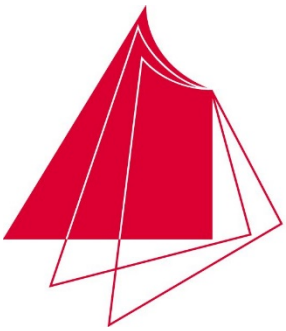

Hochschule Karlsruhe
Technik und Wirtschaft
UNIVERSITY OF APPLIED SCIENCES

Master Thesis

Thermal Characterization of the Valencian Silo-Yard

Processing and 3D visualization of thermal images of the FLIR One camera

Place	:	Karlsruhe University of Applied Science (HSKA) Information Management and Media (IMM) International Master Program Geomatics
Name	:	Juan Pedro Carbonell Rivera
Date of Presentation	:	August 2016
First Referee	:	Prof. Dr. Heinz Saler
Second Referee	:	Prof. Dr. Tilman Müller
Supervisor	:	Dipl.-Ing. (FH) Konrad Berner

Terms of reference

Master Thesis

for

Juan Pedro Carbonell Rivera, BSc

Title: **Thermal Characterization of the Valencian Silo-Yard –**
Processing and 3D visualization of thermal images of the FLIR One camera

1 INTRODUCTION

Documentation of cultural heritages is an important task of humanity. Geodesy hereby delivers a significant impact. Modern geodetic methods like Terrestrial Laserscanning and UAV photogrammetry are particularly able to produce high accurate geometric and thematic information within a reasonable time.

The Silos of Burjassot are a Spanish national monument in the area of Valencia. Three universities, Universidad Politécnica de Valencia, Aristoteles University Thessaloniki and Hochschule Karlsruhe worked together with funding from the Landesstiftung Baden-Württemberg to apply several geodetic methods, like geodetic network measurement, terrestrial and UAV photogrammetry, thermography and GPR to obtain a 3d model of the silos and their surroundings in Burjassot.

The measurement and the processing of the data have been split between several students of the above mentioned universities.

2 OBJECTIVES

The proposed thesis can be subdivided into the following subparts:

1. Participation in the field campaign of Burjassot from April 11 to 15 and taking thermal images with FLIR One.
2. Software Development under Android operating system for thermal and RGB image processing.
3. Photogrammetric processing of RGB images.
4. Orientation of thermal images based on the orientation parameters of the RGB images.
5. Visualization of the 3D silo model with Unity game engine.

3 REFERENCES

Flir Systems 2011. *Thermal imaging guidebook for industrial applications*. p. 48, available at: http://www.flirmedia.com/MMC/THG/Brochures/T820264/T820264_EN.pdf.

Planck, M. 1914. *The Theory of Heat Radiation*. F. Blakiston Son & Co, available at: https://www.gutenberg.org/files/40030/40030-pdf.pdf

Valls Ayuso A., García García F., Ramírez Blanco M. J., & Benlloch Marco J. 2015. *Understanding subterranean grain storage heritage in the Mediterranean region: The Valencian silos (Spain).* Valencia: Elsevier.

Valls Ayuso A., Ramírez Blanco M. J. & Llinares Millán J. 2014. *Silos de Burjassot (S.XVI). Origen y desarrollo constructivo. Evolución de sus estructuras y estado de conservación. PhD thesis at* UPV, Valencia.

The written part of the thesis, an internet presentation, the slides of the presentation and the abstract for the audience have to be handed over on a CD.

Duration:	6 months	1st Referee:	Prof. Dr. Heinz Saler
Handing out :	1st March 2016	2nd Referee:	Prof. Dr. Tilman Müller
Closing date :	1st September 2016	Supervisor:	Dipl.-Ing. (FH) Konrad Berner

Prof. Dr. Heinz Saler

Declaration of Authorship

I declare that the work presented here is, to the best of my knowledge and belief, original and the result of my own investigations, except as acknowledged, and has not been submitted, either in part of whole, for a degree at this or any other university. Formulations and ideas taken from other sources are cited as such. This work has not been published.

Karlsruhe, August 2016

Juan Pedro Carbonell Rivera

Acknowledgement

First and foremost my special thanks goes to Prof. Dr.-Ing. Heinz Saler for the professional and technical support of all the questions and problems that I have met during accomplishing this master thesis. In particular I would like to appreciate the kind help of Dipl.-Ing. Konrad Berner for the creative and dynamic motivation and suggestion to fulfil the requirements of this study for every steps of its success. Without their assistance and dedicated involvement in every steps through the process, this thesis paper would have never been accomplished. I would like thank the other professors of IMM for their support and understanding over the study period of the International Master in Geomatics.

I would like to show my gratitude to Prof. Dr. José Luis Lerma García for his strong during the data collection and their invaluable help guiding this project. Due to his patience and great interest in my paper, this master thesis was successfully accomplished.

Getting through my thesis and the study period I required more than academic support, and I have many people to thank for listening to me and understand me. I cannot begin to express my gratitude and appreciation for their friendship. Especially my Spanish colleagues in this adventure David Arenas Serrano, Vahram Dilbaryan and David Montalvá España have been unwavering in their personal support during this time in Karlsruhe. For many memorable evenings out and in, I must thank to Arturo González, Myriam de Miguel and William Odoi. Thanks to my friends in Spain, Joan Baptista Albuixech, Brais Ausina, Daniel Borao, Ángel García, Francisco Román Parra and Jesús Loreto Rosendo without their motivation this way would have been much more difficult, even impossible.

Most importantly, none of this could have happened without my family. My father Pedro Carbonell López, my mother María Remedios Rivera Fernández, my godmother Manuela Rivera Fernández and my grandparents. They have made all this possible supporting me in good and bad times. This thesis stand as a testament to your unconditional love and encouragement.

Abstract

This master thesis is part of the international project "Responsibility for Cultural Heritage" created by the universities Aristotle University of Thessaloniki, Hochschule Karlsruhe Technik und Wirtschaft and Polytechnic University of Valencia. Thermal Characterization of the Valencian Silo-Yard is the outcome of the work done in the Silos of Burjassot.

This project is focused on the Silos of Burjassot, an architecture and civil engineering work built as reservoir for the wheat that was consumed in Valencia, providing in shortage periods and keeping in prosperity times.

During the international campaign done between the 11th to 15th April an interior thermal characterization of different silos was performed, in order to create different documentation about the current state of conservation of the monument and pathologies that affect it. This thermal characterization was performed with low-cost hardware, developing software under Android operating system, to obtain images in the visible and infrared spectrum. After data collection, different 3D models of the silos was created from multispectral imagery with a viewer to freely view different parts of the Silos of Burjassot. Finally, different documentation of conditions and pathologies were did from the different products created.

Resumen

Esta tesina de máster es parte del proyecto internacional “Responsibility for Cultural Heritage” creado por las universidades Aristotle University of Thessaloniki, Hochschule Karlsruhe Technik und Wirtschaft y la Universidad Politécnica de Valencia. Caracterización Térmica del Patio de los Silos Valenciano es el resultado del trabajo realizado en Los Silos de Burjassot.

Este proyecto está centrado en Los Silos de Burjassot, una obra de arquitectura e ingeniería civil construida como almacén del trigo que era consumido en Valencia, proporcionándolo en periodos de escasez y manteniéndolo en periodos de prosperidad.

Durante la campaña internacional realizada entre el 11 y el 15 de abril fue realizada una caracterización térmica interior de diferentes silos, a fin de crear diferente documentación sobre el estado actual de conservación del monumento y patologías que le afectan. Esta caracterización térmica fue realizada con hardware de bajo coste, desarrollando software bajo sistema operativo Android, para obtener imágenes en el espectro visible e infrarrojo. Después de la toma de datos, diferentes modelos 3D de los silos fueron creados a partir de las imágenes multiespectrales, junto con un visor para ver libremente las diferentes partes de Los Silos de Burjassot. Finalmente, fue realizada diferente documentación de las condiciones y patologías a partir de los diferentes productos creados.

Resum

Aquesta tesina de màster es part del projecte internacional “Responsibility for Cultural Heritage” creat per les universitats Aristotle University of Thessaloniki, Hochschule Karlsruhe Technik und Wirtschaft y la Universitat Politècnica de València. Caracterització tèrmica del Pati de les Sitges Valencià es el resultat del treball realitzat en Les Sitges de Burjassot.

Aquest projecte està centrat en Les Sitges de Burjassot, una obre d’arquitectura i enginyeria civil construïda com a magatzem del blat consumisc en València, proporcionant-lo en períodes de escassesa i mantenint-lo en períodes de prosperitat.

Durant la campanya internacional realitzada entre el 11 y el 15 d’abril va ser realitzada una caracterització tèrmica interior de diferents sitges, amb la fi de crear diferent documentació sobre l’estat actual del monument i les patologies que li afecten. Aquesta caracterització tèrmica va ser realitzada amb hardware de baix cost, desenvolupant software sota sistema operatiu Android, per a obtindre imatges en el espectre visible e infraroig. Després de la toma de dades, diferent models 3D de les sitges varen ser creades utilitzant imatges multiespectrals, amb un visor per a vore lliurement les diferents parts de Les Sitges de Burjassot. Finalment, va ser realitzada diferent documentació de les condicions i patologies a partir dels diferents productes creats.

Table of Contents

List of Figures

List of Equations

List of Tables

1 Basic Concepts

This theoretical part explains the basic concepts associated with the infrared thermography, also it explains in detail this technique nowadays.

In the following pages, the basic concepts of the infrared thermography will be discussed (Balageas, 2007).

1.1 Heat and temperature concepts

To define the concept of heat one must understand that matter is composed of tiny particles called atoms and molecules, and the constant movement of these particles causes a type of energy called "thermal energy".

One of the most used units to measure the thermal energy of a material is *Temperature.* All matter contains measurable thermal energy.

Temperature is a measure of heat energy that represents the average temperature of a body or material. Therefore, the temperature is not energy, but it is a measure of the energy and depends on the velocity of the particles in a material or substance. This is the difference between heat and temperature, because the heat is affected by other variables such as the type, size, and the number of particles of the material.

The relation between the particles and the temperature is found in the absolute zero (Zielinski, 2008), the coldest theoretical temperature, at which the thermal motion of atoms and molecules reaches its minimum - classically, this would be a state of motionlessness, but quantum uncertainty dictates that the particles still possess a finite zero-point energy. In addition to this, a real system or object can never be brought to a temperature of absolute zero by thermodynamic means. Absolute zero is denoted as 0 K on the Kelvin scale, −273.15 °C on the Celsius scale, and −459.67 °F on the Fahrenheit scale.

There are three scales to measure the temperature previously used: Celsius, Fahrenheit and Kelvin (Arora, 2004).

1.2 Heat transmission

The energy is transferred from the higher temperature region to the lower temperature whenever there is a temperature difference. According to the concepts of thermodynamics, this transmitted energy is called heat. (Kaviany, 2014)

The laws of thermodynamics explain the transfer of energy, but always refer to systems that are in equilibrium, and can only be used to predict the amount of energy required to change a system from one state of equilibrium to another, so they do not serve to predict how quickly these changes may occur.

Thus, for a complete analysis of heat transfer it is necessary to consider fundamental mechanisms of transmission:

- *Conduction or diffusion*: The transfer of energy between objects that are in physical contact. Thermal conductivity is the property of a material to conduct heat and is evaluated primarily in terms of Fourier's Law for heat conduction.
- *Convection*: The transfer of energy between an object and its environment, due to fluid motion. The average temperature, is a reference for evaluating properties related to convective heat transfer.
- *Radiation*: The transfer of energy by the emission of electromagnetic radiation.

In the following lines these three mechanisms will be explained in more detail.

1.2.1 Conduction

This form of heat transmission is performed from one body to another being in contact, and it needs a mass to transport heat. It transmits kinetic energy (vibration of the molecules, atoms, ions, electrons...) by contact and requires a differential temperature for such transfer to occur.

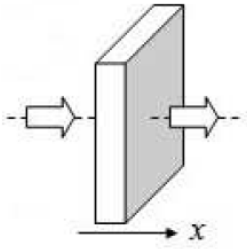

Figure 1. Conduction of heat.

Fourier's law is the law governing this transmission, this relates heat flow with the temperature field at different points of the environment, provides that the flow is proportional to the temperature gradient and easier to transmit heat in the environment.

$$Q = -\lambda \frac{\partial T}{\partial x} = \lambda \cdot \Delta T$$

Equation 1. Fourier's law.

Where λ is the material's conductivity (W·m−1·K−1), and ΔT is the temperature gradient (K·m−1).

1.2.2 Convection

Convection is one of the three forms of heat transfer and it is characterized because it is produced through a fluid (air, water) that transports heat between different temperature zones. Convection occurs solely through fluid materials. When these fluid materials are heated, they increase in volume and therefore, decreases its density and displaces the fluid located at the top which has a lower temperature. The convection is the transport of heat through the up and down streams of fluid.

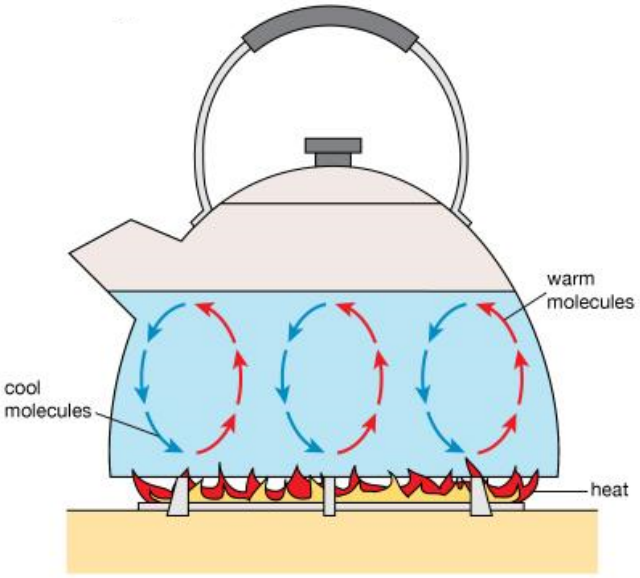

Figure 2. Convection of heat.

The heat transfer involves the transport of heat in a volume and mix of macroscopic elements of hot and cold portions of a gas or a liquid. The exchange of energy between a solid surface and a fluid or by means of a pump, a fan or other mechanical device (mechanical or assisted convection) is also included.

In the transfer of free or natural heat in which a fluid is hotter or colder and in contact with a solid surface, it causes a circulation due to density differences resulting from a temperature gradient in the fluid.

Heat transfer by convection is expressed with Newton's law of cooling.

$$\frac{dT}{dt} = -k(T - T_{\propto})$$

Equation 2. Newton's law of cooling.

Where k is the heat transfer coefficient (W/(m2 K)). T is the temperature of the object's surface and interior (since these are the same in this approximation), and finally, $T_{\propto}$ is the temperature of the environment; i.e. the temperature suitably far from the surface.

1.2.3 Radiation

Thermal radiation is a process of emission of internal energy of a body using electromagnetic waves. The source of this energy emission is at the molecular and atomic agitation of any body temperature above absolute zero. Following Fourier‘s law, all the surfaces emit energy in the form of radiation. (Equation 1)

This energy propagation material does not need to be transmitted, it is able to do so in a vacuum. These electromagnetic waves propagate at the speed of light (c = 299 792 458 m/s) in vacuum. The behaviour of this phenomenon corresponds to two theories simultaneously, the wave theory and the particle theory in which radiation interacts with matter through discrete quanta of energy or photons. It spreads in all directions and the full range of all waves is known as the electromagnetic spectrum.

The human eye only detects a spectrum corresponding to the range of radiation wavelengths between $3.8 \cdot 10^{-7}\ m$ and $7.6 \cdot 10^{-7}\ m$, which it is known as visible radiation.

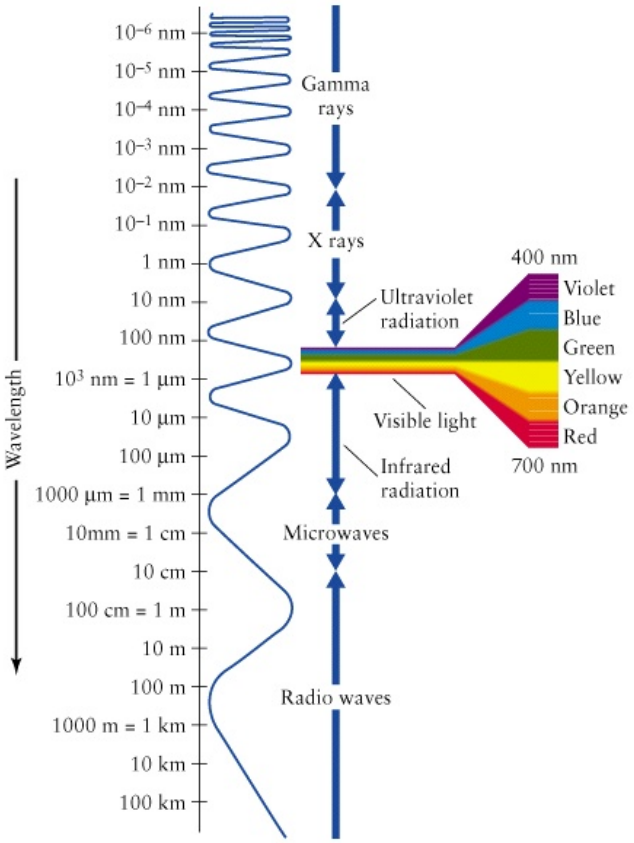

Figure 3. Visible spectrum.

1.3 Infrared radiation

Infrared radiation is a type of thermal radiation by its wavelength range which is not visible to the human eye (Cusido, Devant and Riba, 1996) .

Originally, its discoverer Sir Frederick William Herschel, named them as "heat rays" and then Infrared, because they are under the level of energy of red. The amount of energy that radiates a body is directly related to the temperature of the bodies, so as hotter radiates energy.

If the body emits more energy than it absorbs it is considered "hot", this principle is the basis which the infrared radiation was originally identified. One of the features that has spread its applicability in various branches, can be detected optically using technological equipment without contact with the body or substance directly, as is the case with the thermal imaging camera.

1.4 Radiation of a black body

Heat balance equation is based on that part of the radiation energy emitted. The radiation in each body is absorbed, reflected and transmitted to varying degrees. This concept creates a classification of bodies or matter:

- The "black body" is that one absorbs all radiation incident on it, from any wavelength.
- The "white body" or mirror, which reflects all radiation.
- The "transparent body" allowing passage of any electromagnetic waves in his wavelength.

Black Body radiation occurs when the radiant body has a very weak interaction with the surrounding environment and can be considered in a state of thermal equilibrium, and it emits the same amount of radiant energy that it absorbed. This is another reason why, it is also called the "perfect radiator". The concept of the black body is considered ideal, because in reality there is no body that perfectly absorbs all radiation (Planck, 1914) , however, this principle serves as a reference model for the calculation and measurement of other features derived as emissivity.

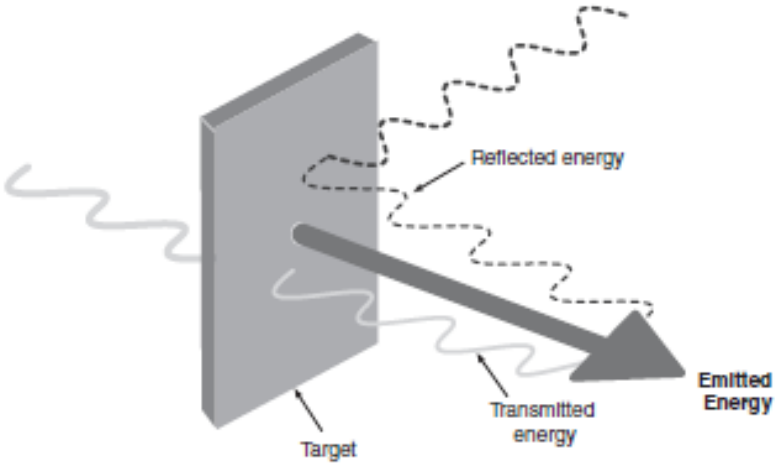

Figure 4. Radiation components.

1.5 Emissivity

The degree of radiation or emissivity, is a characteristic of the black bodies that express the efficiency of a surface as a radiator (or absorber) of electromagnetic radiation. In other words, it is a property of the surface of the bodies that determines its ability to radiate energy. The emissivity refers to the percentage of energy emitted by a real body in function of the maximum energy that can irradiate a black body at the same temperature.

$$Emissivity = \frac{radiation\ emitted\ of\ an\ object\ at\ temperature\ T}{radiation\ emitted\ of\ a\ black\ body\ at\ temperature\ T}$$

Equation 3.Emissivity.

This factor explains how an object radiates infrared energy; a good radiator (easily seen objects in the camera) has an emissivity close to unity (ε ≈ 1). Contrary to the bad radiators (objects hard to see by the camera), which have an emissivity (ε) near to zero (ε ≈ 0).

The emissivity depends on several factors, here the most important are listed according to their order of importance:

- Type of material.

- The surface of the material (polished, oxidized).
- Surface geometry (cavity effects, etc.).

The emissivity can also change for other reasons, less common measurement situations, such as:

- Material temperature levels.
- Wavelengths (IR short wave).

Emissivity values vary from one material to another. Metals with a rough or oxidized surface have a higher emissivity than a polished surface.

Some examples are as follows:

Aluminum Foil	0.04
Asphalt	0.93
Black Body Matt	1.00
Brass Dull Plate	0.22
Brass Polished	0.03
Brick, red rough	0.93
Concrete	0.85
Ice smooth	0.97
Sand	0.76
Plant Leaves	0.96

Figure 5. Emissivity values (Lillesand, 2008).

There is a relationship between the emissivity and reflectivity of an object, for an opaque body and for practical purposes this simplified relationship is as follows:

$$Emissivity + Reflectivity = 1$$

Also a highly reflective material is a poor emitter of infrared energy and therefore has a low emissivity value.

1.6 Infrared thermography

Thermography testing is more complex than inexperienced operators in thermography can imagine. This complexity has several origins:

- The physical nature itself of the measurement by the camera.
- The complexity of the observed object (it will be called here "system", in order to emphasize its complexity).
- The existence of heat transfer between this system and the environment.
- The existence of other possible sources of heat.

Some part of these transfers may be under the control of the operator (in the case of active thermography) or totally independent of the operator (passive thermography). Therefore one can say that the thermography measurement is a process between three actors:

- Operator in the passive or active test with his system (in this case the camera).
- The system observed.
- The environment observed.

These interrelationships (Balageas, 2007), where the fact that the nature is thermal involve all modes of heat transfer (radiation, convection and conduction) and the different production of heat of different natures. It is not possible to make a thermographic diagnostic with quality without:

- Information about the camera.
- Information about the formation of the observed "structure, material, etc."
- A minimum knowledge in heat transfer.

1.7 Camera: Principles and characteristics

A thermographic camera is a device that forms visible images to the human eye by means of infrared emissions of the electromagnetic spectrum of the detected bodies. They are noncontact systems, sensitive to the radiation emanating from the surface, this energy depends on the temperature of the surface and its features.

Moreover, knowing the spectral response of the detector, you can find out the electrical output signal and by amplifying that, it generates a visible image.

Mathematically it can be determined and the Steffan-Boltzmann's law describes the maximum of total radiation that is released by a surface, where it is considered that the measurement objectives and the background are perfect black objects. Steffan-Boltzmann's law establishes that the emissive potential of a real surface that is less than a black body at the same absolute temperature (T) body is given by:

$$E = \varepsilon \cdot \sigma \cdot T_e^4$$

Equation 4. Steffan-Boltzmann's law.

Where ε is a radiant surface property, called emissivity. With values in the range 0≤ ε ≤1, it depends on the type of material and the condition of its surface. T_e is the effective temperature, the temperature of a black body that would emit the same total amount of electromagnetic radiation. σ is the constant of proportionality in the Stefan–Boltzmann law: "the total intensity radiated over all wavelengths increases as the temperature increases".

1.7.1 Emissivity calculation

Firstly, thermal imaging cameras give a temperature value for each point, regardless that for the same temperature, two materials can radiate infrared energy with very different intensities. A very

graphic example is a metal cup with a black tape to insulate that are at the same temperature, but the tape and metal cup emit infrared energy with very different intensities (Figure 6).

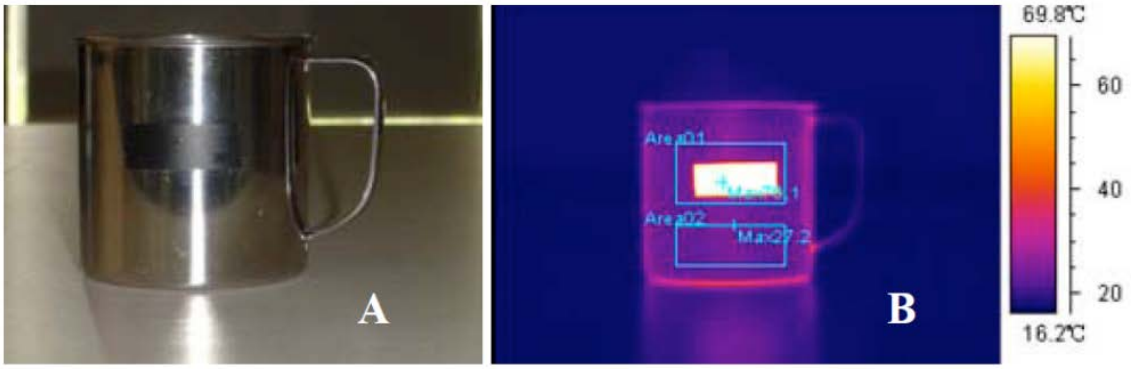

Figure 6. A) Metal cup with tape, B) View with thermographic image.

Although the objects physically are located at the same temperature, the thermography presents different temperatures, this is due to the different emissivity between metal and tape. All infrared instruments (such as thermal imaging cameras) allow one to choose within a wide range of emissivity, the most suitable for measurement. It is therefore important to know the factors that change the characteristic of the material and how it affects actual temperature readings. To know the emissivity of an object under study, all that is needed is a known emissivity to be used as reference, in this case a tape to insulate with emissivity of 0.95, is used as a reference, then different steps are required to determine the emissivity of the object under study (Flir Systems, 2011).

1.7.2 Resolution and optic

Visual or spatial resolution affects the clarity with which we can see the components or equipment under study. Often when a problem is diagnosed, it must distinguish the real source of the problem, between two or more possible sources, located very close to one another. It stands for resolution, the fineness or minimum distance between elements that the infrared detector can observe. A higher resolution provides better image and this depends on several factors such as the detector design, the number of pixels that it is able to generate in the picture, and of course, the quality of the optics used plays a very important role.

Appropriate lenses should be used for the application. It is a good idea, in addition to standard camera lens to have wide-angle lenses, macro and telephoto lenses. The user must know the minimum focusing distance, in relation to each lens. Also according to the lens used, the relationship of the distance object should be modified. The user should always use a relationship that allows one to see the object as large as possible in order to distinguish the finer details. The spatial resolution is defined as the relationship between the sensor size and the distance between the lens and the sensor. If the spatial resolution is low, the user can use the camera farther away (or for the same distance, smaller objects can be displayed).

Space constraints play an important role in the selection of lenses. Each lens must be calibrated in particular to the thermal camera. It should be noted that when purchasing a new lens, the camera must be sent to the manufacturer to perform calibration of both.

1.7.3 Temperature range and thermal sensitivity

Problems can go unnoticed by the thermographer, if not do an appropriate selection of the temperature range and sensitivity or gain of the camera. Ranges must be adjusted to contain the image of the desired information. Due to temperature variations of the inspected equipment, it is necessary for the adjustment range and thermal sensitivity, to be carried out very frequently. Modern thermographic equipment automatically set both controls, however, these are not always the best for each study. The experienced thermographer must optimize the image information through making adjustments manually.

1.7.4 Perspective

Using proper perspective is of course very convenient, but it is much more critical for diagnosis. Once a problem is identified, it should be reviewed from various perspectives for more information to confirm that the diagnosis is correct. There are several reasons, why a problem occurs in the image, but when looked at from another perspective, it disappears. For example, a solar reflection in an electrical connection of a transformer elements. A problem must be observed not only in front, but also from the side, above and below if it is possible. Often, one has to place the thermal imaging camera, overhead, or near the floor, or in confined areas. Having a rotating or external display is a good idea, to facilitate the work.

2 The Valencian Silo-Yard in Burjassot

A silo (from the Greek *σιρός – siros*, "pit for holding grain") is a structure for storing bulk materials. Silos are used in agriculture to store grain (see grain elevators) or fermented feed known as silage. Archaeological ruins and ancient texts show that silos were used in ancient Greece as far back as the late 8th century BC, as well as the 5th Millennium B.C site of Tell Tsaf, Israel. The term silo is derived from the Greek *σιρός* (siros), "pit for holding grain". (Buxton, 2003)

2.1 Valencia in the 15th and 16th centuries

During the 15th century, Valencia became a great trading power, taking advantage of the commercial expansion in the Mediterranean Sea. The economy was prosperous and focused on trading through the Mediterranean, which had become increasingly controlled by the Crown of Aragon, mostly from the ports of Valencia and Barcelona (MORTE GARCIA, 2006).

Figure 7. The city of Valencia, Painting of Anton van der Wyngaerde, commissioned by Felipe II. 1563. (Kagan, R. L. and A. van den Wyngaerde, 1986)

This boom was reflected in the growth of artistic and cultural pursuits. Some of the most emblematic buildings of the city were built during this period, including the Serranos Towers (1392), the Miguelete[1] and the Chapel of the Kings of the Convent of Santo Domingo. In painting and sculpture, Flemish and Italian trends had an influence on artists such as Lluís Dalmau, Peris Gonçal and Damià Forment. Literature flourished with the patronage of the court of Alfonso the Magnanimous, supporting authors like Ausiàs March, Roiç de Corella, and Isabel de Villena. By 1460 Joanot Martorell wrote Tirant lo Blanch, an innovative novel of chivalry that influenced many later writers, from Cervantes to Shakespeare. Ausiàs March was one of the first poets to use the everyday language Valencian, instead of the troubadour language, Occitan. Also around this time, between 1499 and 1502, the University of Valencia was founded under the parsimonious name of Estudio General ("studium generale", place of general studies).

In the city of Valencia the *Taula de canvis*[2] was created, functioning partly as a bank and partly as a stock exchange market; altogether it boosted trading (Aldana Fernández, 1988). The local industry, especially textile manufactures, achieved great development and the city of Valencia turned into a Mediterranean trading emporium where traders from all Europe worked. Perhaps the feature which best

[1] Bell tower "El Miguelete" is a gothic style construction started in the fourteen century and finished in the fifteenth. Constructed on an octagonal base, its perimeter is same to its height, more than fifty meters. The bell tower has four bodies of the same height, the last one is the bells hall, open by eight picture windows. Its name, "El Miguelete", comes from the name of its biggest bell "Miguel", made in 1532 and weighing more than ten tons.

[2] The *Taula de canvis* (in Catalan) changing table, or just *Taula*, table, was a financial institution that appeared in different cities of the Crown of Aragon (Valencia, Barcelona, Gerona) in the fifteenth century.

symbolizes this flamboyant period is the Silk Exchange called "*La Lonja*" (Figure 8), one of the finest European examples of civil Gothic architecture and a major trade market in the Mediterranean by the end of the 15th century and throughout the 16th century (Heriard Dubreuil, 1987).

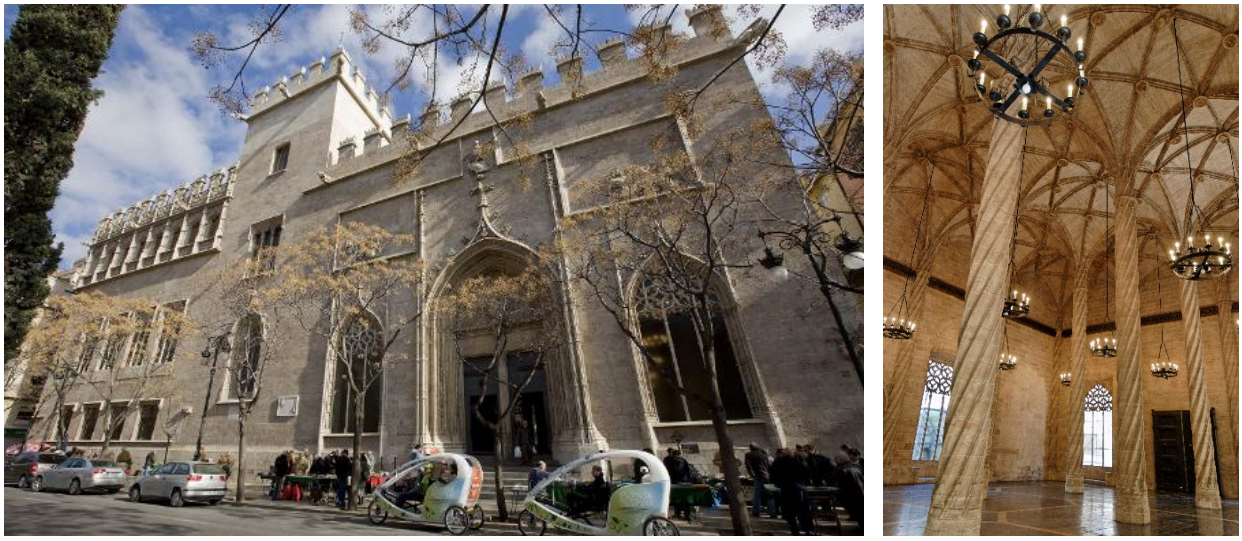

Figure 8. Silk Exchange of Valencia (Revilla, 2015), facade west (left) and interior of the building (right) (García, 2009).

Valencia has a geostrategic location in terms of cereal trade. However, the true potential was not reached due to reduced harvests that plague the city of Valencia. The area due to climate and quality of its soil was not suitable for cultivation of this cereal, which resulted in economic hardship, since wheat generally produced only served to feed the inhabitants of the city during the four months following the harvest.

Two-thirds of the year, the area was covered with foreign wheat supplies (Furió i Diego, A. and U. de València, 1999); through two possible routes: terrestrial and maritime. The most important land supplies were preferably from La Mancha, Aragon and Andalusia. The real safeguard against food shortages, is made from wheat from the Mediterranean, especially from the Italian granaries of Sicily, Napoli, etc.

Throughout the 15th century Urban authorities reacting to shortages acted by accumulating grains, researching the stocks held by leases tithes, traders, bakers and sometimes even requisitioning of them if the gravity of the situation demanded it, encouraging the cereal imports and a placing a ban on removing the existing grain. Furthermore, throughout the 16th century there was an increase in the population of Europe. Valencia, had to wait for the 1540´s to consolidate this population growth, diminished by the plague of 1557 (Betrán, 2006).

2.2 Reasons for the construction of the silos

To resolve these facts (Figure 9) the Council of Valencia decided to build different silos to store the grain and thus have a reservation in case of need, at same time storing the cereals allowed to buy the grain in the period which the cereals had the lowest prices.

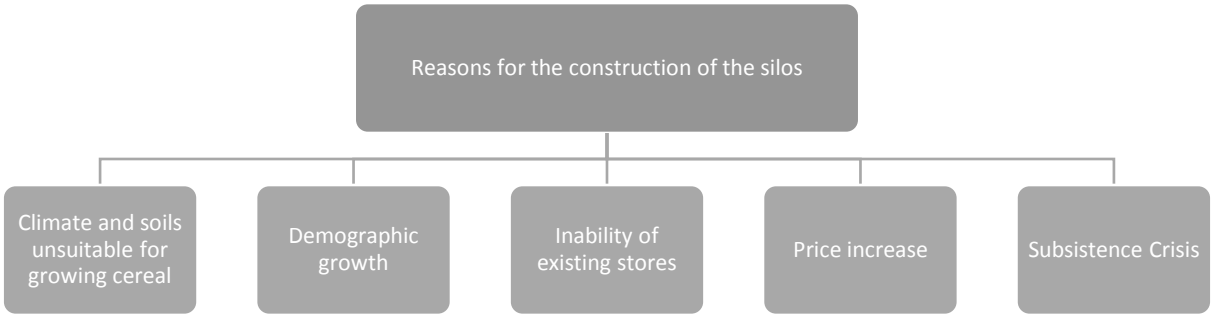

Figure 9. Reasons for the construction of the silos.

2.3 Choice of the location

Due to these factors (previous figure), the large-scale under-ground Valencian silo was constructed in Burjassot, a town located only 5 km away from downtown, in 1573. This location was selected owing to favourable economic, geographical, topographic and geological aspects. It was a civil project undertaken by the Valencia city council (Valls Ayuso, 2014)

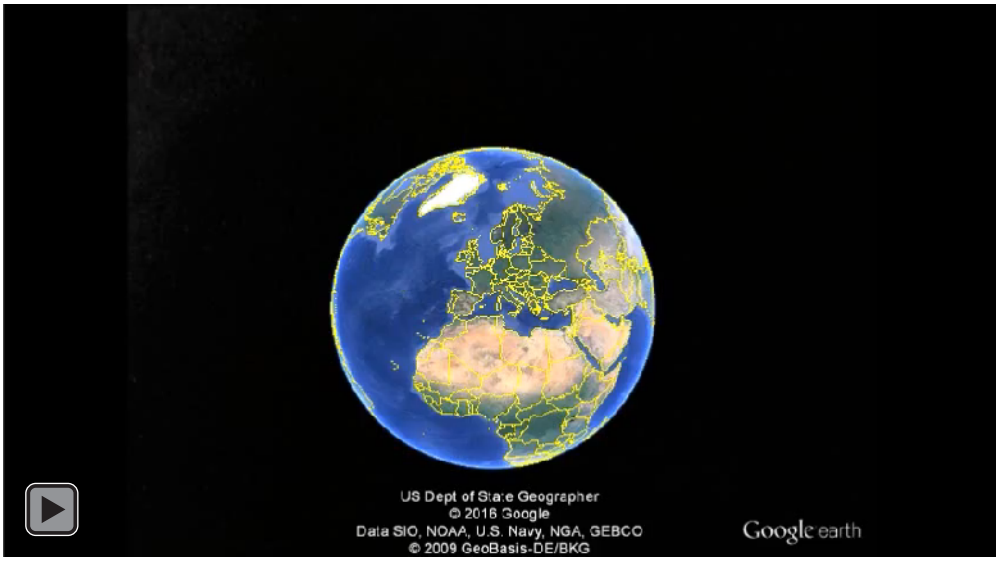

Figure 10. Location of the Valencian Silo-Yard.

2.3.1 Geographic and climatic factors

The Silos of Burjassot are in a remote area of high mountains that hinder the large circulation of air thanks to its relative proximity to the sea, 7 Km., and its height above sea level in Alicante, 60 m, (Lerma, 2012). It enjoys throughout the year maximum sunlight and ventilation, fundamental factors for the preservation of any kind of grain. These subterranean granaries were excavated on the top of a small flat hill. This topography prevents rainwater accumulation. Besides, its elevated position allowed the excavation of underground structures without reaching the groundwater table.

Moreover, climate is slightly drier than in Valencia, because it influences directly in the conservation of cereals, yielding an average of 16.5 °C (Agencia Estatal de Meteorología - AEMET, 2016). The average humidity in Burjassot is 61%. It corresponds to the condition of medium dryness, linked with the formation of the limestone hill where the silos were built. The weather and wind made this part of the reason why Burjassot was the chosen place.

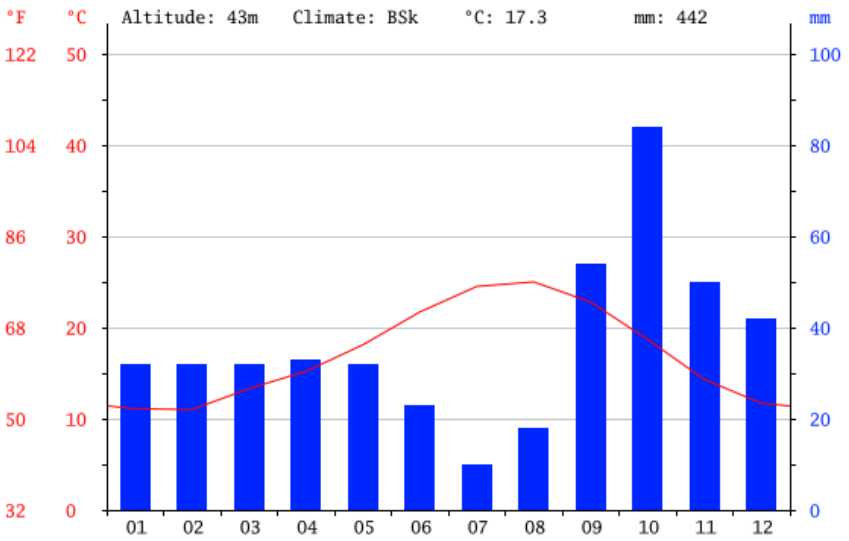

Figure 11. Climograph of Burjassot (Climate-Data.org, n.d.).

2.3.2 Geological factors

The location of the construction was a small hill of limestone, a sedimentary rock composed largely of the minerals calcite and aragonite, with sufficient resistance to erosion. This location is situated in the northeast of Burjassot, with gentle slopes sideways, very dry ground, especially in the higher areas, without evidence of moisture, optimal for the construction of underground deposits.

2.3.3 Other factors

On the one hand, the figure of Bernat Simó was relevant in the final election of this place (Lòpez i García, 1989) Bernat Simó was a citizen of Valencia and an influential member of the oligarchy that controlled the municipal power of Valencia, and on the other hand he was the Lordship of Burjassot, from 1568. This double circumstance made the Council of Valencia[3] gravitate toward this town, choosing it from other possible locations. Bernat Simó bid to the Council of Valencia this area, providing all facilities to build the silos, starting with the construction of three silos to test the excavation within the limits of his Lordship.

The success of the new storage system prompted the Council of Valencia on May 28th 1574, to give the go-ahead to build more silos on the same site. Once the doubts were resolved about the new grain storage system, the same stonemason was hired for the construction of an undetermined number of silos.

The construction started in 1573 and finished 233 years later, ending in 1806. Throughout this time 41 tanks or silos were built (Expósito Navarro, 2005).

[3] The Council of Valencia was a consultative and deliberative representative part of the Juries of Valencia. Juries (in Valencian, *Jurats*) was the supreme executive body of city government, it consisted of four notables or citizens, and two knights.

2.4 Construction

This monumental work of masonry and ashlar was commissioned to master stonemason Sancho de Camino, who made the first three silos as a test, and after verifying its excellent performance, was once again hired to build an unspecified number of silos in the same place where he had built the first three. The first news about the start of the construction of underground reservoirs are dated on July 17th 1573 and informs that a stonemason called Sancho del Camino worked in Burjassot for 7 days, winning the amount of 3 *libras*, 7 *sueldos* and 1 *dinero*[4] in unspecified works, but these would be used to store wheat (Blanes Andrés, 1992; Expósito Navarro, 2005; Marqués, 1979).

On October 5th 1573 there exists a record of a deliberation by the Council of Valencia, justifying different reasons for the construction of the Silos[5] .

The main features of the Silos of Burjassot are the underground construction capable of supplying an important city as Valencia. The only drawback of this underground construction is moisture, but the natural conditions of the place, in a dry hill and easy to dig, and the use of coatings with lime mortar and sand fix the problem, on the other hand its location on a limestone mound avoids stagnant rainwater.

Silos were dug in a clayey soil that presented nodules of carbonates and intercalations of limestone crust substrates. It is a really suitable type of terrain for underground grain storage facilities. It has some advantages such as the easiness of excavation, the consistency and the hydrothermal conditions for wheat preservation as has been stated in several studies about the Mediterranean granaries (Fernández-Posse, 2011; Mestre, 2009; Valls Ayuso, 2014). It presents key biological factors such as low oxygen atmosphere, uniform low temperature and low moisture content, really appropriate for underground grain storage (Mestre, 2009; Valls Ayuso, 2014).

2.5 Construction elements

After the construction of the first six silos between 1573 and 1574, the Council of Valencia decided to order new silos to the stonemason Sancho Del Camino and others to Joan Alfafar. Joan Alfafar was a master builder and managed to apply the technique of building an underground vault that gives the silo the characteristic shape of bottle.

The silo has a double curvature profile, similar to a squat jar or a bottle. The height was variable between seven and ten meters, with a parabolic dome, like the lower wall. Its surface is plastered with a thick layer of lime mortar (Figure 12). Some silos' sections reveals some rows of brick.

[4] The *dinero* (from the Latin *denarius*) was the coin of lower value of the Carolingian Empire, which lasted until the modern era in the monetary systems derived from the Carolingian Empire. The *libra* of silver was divided into two hundred and forty *dineros*, also silver. The *sueldo* was a gold coin of the same weight as the silver *dinero*. As gold and silver maintained until the modern era a parity of 12:1, each *sueldo* was equivalent to twelve *dineros* and the *libra* of silver was equivalent to twenty *sueldos*.

[5] Municipal Archive of Valencia. *Manuals de Consells*, A-98, fol. 126v. Document that informs about the pay from the verger Phelip de la Torre to Sancho de Camino.

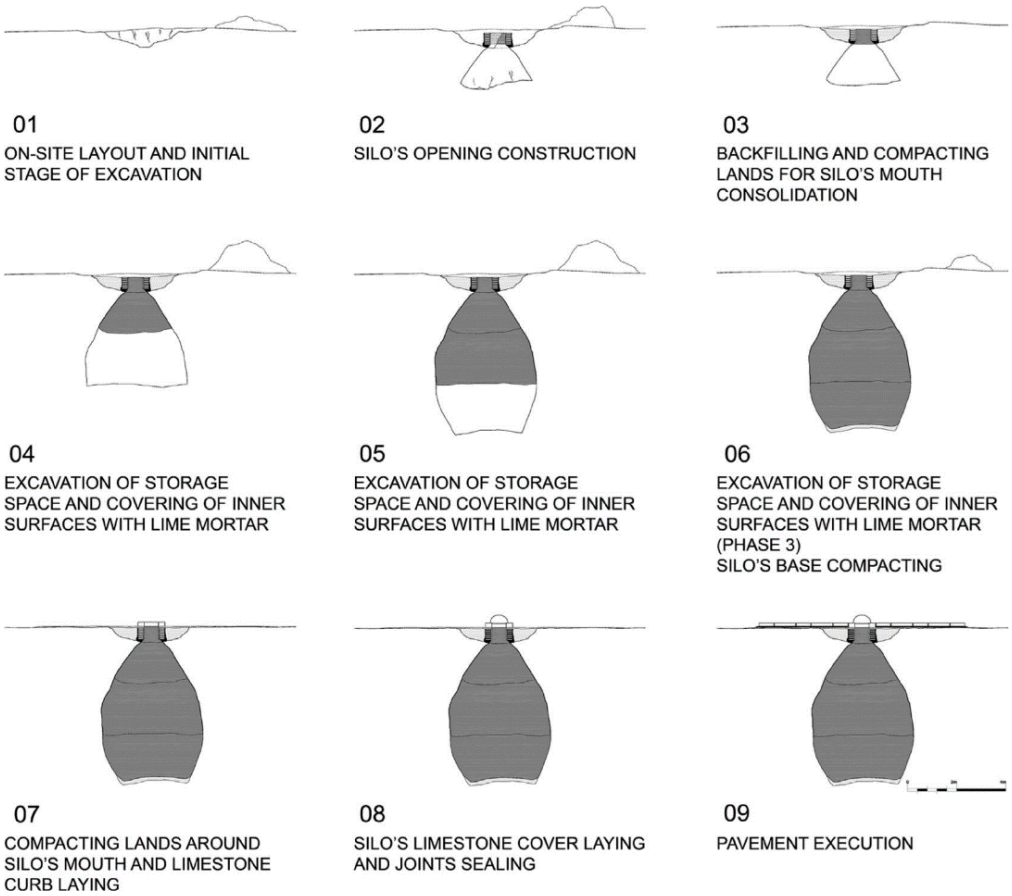

Figure 12. Model of a silo construction process (Valls et al., 2015).

For the preservation of cereal a process was carried out in 3 phases. First of all, a layer of esparto, then reeds above it and then straw was placed on the floor. Straw was used in the mouth of the silo too to absorb the existing moisture as possible.

The cap of Los Silos has a diameter of 60cm. It consists of two pieces:

- A fixed cap, with a form of a truncated pyramid gently sloping, with a lower square base and round surface. On it two numbers that refer to the number of the silo and its ability in *cahíces*[6] were written.

- The second piece is mobile and it is hemispherical stone with rings of cast iron, fixed with lead, whose function was to serve as a gripper to be displaced and at the same time as antitheft chains, the shape and fit are necessary to expel water.

[6] A *cahíz* is an ancient measure of weight for plaster*, it* is equivalent to 201 liters. The Silos of Burjassot have a variable capacity ranging from a minimum of 150 *cahíces* to a maximum of 1.278 *cahíces*.

Figure 13. Cap of the Silo number 28, with a capacity of 400 *cahíces*. 2016.

2.6 The evolution of the monument

2.6.1 Century VXI

In 1575 the master builder Juan de Alfafar was commissioned to create two *botigues* and two *porchades*[7] (Figures 14 and 19). The initial reason was the controversy surrounding the wrongful use of the chapel to store wheat provisionally until it was permanently saved into the Silos (Expósito Navarro, 2005). To build the wooden roof, the carpenter Esteve Ravanals was hired.

Figure 14. Southern facade of one storehouse. 2016.

During this time (1573-1575), new roads were created and improved due to the grain trade, it became the main economic wealth. Also other roads were created for other uses, such as stone transport

[7] Simple buildings like lodges with two sides opened using semicircular arches, closed with a wooden trellis.

from the nearest stone quarries, of *Cantererí*a[8], in the same town of Burjassot, or from Sagunto. All these made Burjassot an important commercial and agricultural center.

During the late sixteenth century important works were made in Los Silos by the Council of Valencia, building the majority of the complex and giving fame to this monument through the centuries.

Miguel Porcar, paved the esplanade, built the stands, the column and the chapiter of the center of the Silo-Yard and the cross (whose lower part is 64 meters above sea level, and matches the level with the platform of the Miguelete[1]). The images of the Virgin and Christ were carved by the sculptor Hieron Munyós.

Figure 15. The Silo-Yard with a replica of the column in front[9], the storehouses (rear left and rear right) and the chapel (rear). Image from Leo Ferrer's Flickr. 2012.

Outfalls of the square as well as the tapes had to adapt to the new slope of the Silo-Yard. This work was carved by master stonemason Guillen Del Rey. A surrounding wall, new silos and a cistern to collect rainwater built by Agosti i Roca were the next works in the Silo-Yard. Finally the construction of the Silos finished in 1596, with 46 deposits.

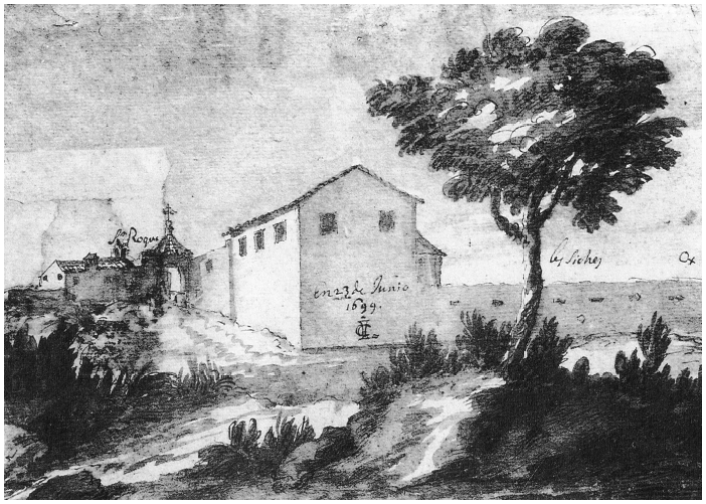

Figure 16. The Silos in 1699 drawn in the same position that in the Figure 14. Juan Conchillos. 1699.

[8] Currently the stone quarry of *Cantererí*a is a neighborhood of Burjassot.
[9] The original column was destroyed in the Spanish Civil War.

2.6.2 Century XVII

In the early seventeenth century, the works of Los Silos suffered a considerable slowdown. The main reason was the expulsion of the *Moriscos*[10] in 1609 causing the fall of cereal consumption. This fact caused a large decrease in the population and a parallel decrease in grain storage in Valencia from the seventeenth century, causing a stoppage in the works of the Silos. This works were not resumed until the mid-18th century.

2.6.3 Century XVIII

The period between 1707 and 1754 was the darkest in the history of Los Silos. In this period they were completely abandoned, not only in terms of construction, but also in economic terms, due to not needing to store cereals in them. In 1754, the Corregidor[11] of Valencia, the Marquess of Malaspina finished with this period of abandonment, conditioning Los Silos to a dual use, military and civilian because the Marquess was previously quartermaster general of the army. During these works in 1755 two significant events occurred, affecting the rehabilitation. The first fact was due to heavy rains in early November, and the second an earthquake, caused by the Lisbon earthquake[12] on the first day of the month.

[10] The Expulsion of the *Moriscos* was decreed by King Felipe III of Spain on April 9, 1609. The *Moriscos* were descendants of Spain's Muslim population that converted to Christianity by coercion or by Royal Decree in the early 16th century. Fighting wars in the Americas, and feeling threatened by the Turks raiding along the Spanish coast, it seems the expulsions were a reaction to a perceived internal problem of the stretched Spanish Empire. Between 1609 through 1614, the Crown systematically expelled *Moriscos* through a number of decrees affecting Spain's various kingdoms, meeting varying levels of success.

[11] A *Corregidor* was a local, administrative and judicial official in Spain and its empire. He was the highest authority of a *Corregimiento*. In the Americas a *Corregidor* was often called an A*lcalde Mayor*. They began to be appointed in fourteenth century Castile and the institution was definitively abolished in 1833. They were the representatives of the royal jurisdiction over a town and its district.

[12] The 1755 Lisbon earthquake, also known as the Great Lisbon earthquake, occurred in the Kingdom of Portugal on Saturday, 1 November, the holiday of All Saints' Day, at around 09:40 local time. In combination with subsequent fires and a tsunami, the earthquake almost totally destroyed Lisbon and adjoining areas. Seismologists today estimate the Lisbon earthquake had a magnitude in the range 8.5–9.0 (Gutscher, Baptista and Miranda, 2006).

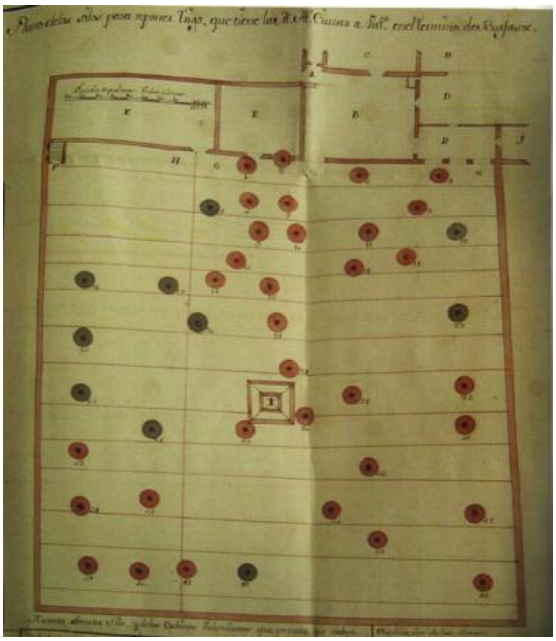

Figure 17. Silos map. José Herrero. 1756. Municipal historical archive of Valencia.

The new rehabilitation in 1788, was supervised by the architect José Herrero and Vicente Pinoel. The second gateway was opened in 1953. Finishing the work on May 31st 1788, after completion of the works of paving of the west corner was accomplished by Andrés Soler.

2.6.4 Century XIX

In the nineteenth century different maintenance works were performed on the silos, and in 1878 the third door opened with an access stairway (Figure 18).

Figure 18. Third door of The Silo-Yard. 2016.

2.6.5 Century XX

In the early years of the twentieth century, Los Silos which until this time were the granary of Valencia, due to high maintenance costs, were hired by the City to private equity, renting The Silos for storing cereals. Therefore, the City Council Valencia took over the facilities and maintenance.

In this age, it started with a playful use of these installations and also, several residents of Burjassot were granted permission to celebrate some festivals on the ground floor of Los Silos.

The Second Republic[13], abandoned these commercial uses, making the request to install the *Escuela de Artes y Oficios of Valencia*[14] into the silos. Once this request was accepted by the City of Valencia, it decided to locate the school in the largest pavilion.

The town hall of Burjassot requested an authorization in 1933 to the City of Valencia to install a public library in one of the outside rooms of Los Silos (Figures 14 and 19). This building was one of the two *porchades*[7], popularly called "*Casa dels Barrons*" or "*embarronat*". This request was rejected.

Figure 19. View of one of the building called "*embarronat*"[7]. 2016.

2.6.5.1 Spanish Civil War

During the Civil War[15] air raid shelters and trenches were installed in Los Silos, using the perimeter wall of the Silo-Yard. Some silos were joined by tunnels to facilitate entry and exit of potential refugees.

The monument began to be used for military purposes in June 1937. Firstly, an acoustic locator[16] (Figure 20) was located on the same pedestal as was the Cross[9] (Lòpez i García, 1994), the chosen location

[13] The Second Spanish Republic (in Spanish: "*Segunda República Española*") was the republican regime that existed in Spain from 1931 to 1939, preceded by the Restoration and followed by Francoist Spain after the Spanish Civil War.
[14] School of Arts and Crafts of Valencia.
[15] The Spanish Civil War widely known in Spain simply as The Civil War or The War, took place from 1936 to 1939 and was fought between the Republicans, who were loyal to the democratic, left-leaning Second Spanish Republic, and the Nationalists, a falangist group led by General Francisco Franco. Although often portrayed as a struggle between democracy and fascism, some historians consider it more accurately described as a struggle between leftist revolution and rightist counterrevolution (Payne, 2014).

[16] The acoustic locators were used from mid-World War I to the early years of World War II to detect enemy aircraft by picking up the noise of their engines. It consists of four acoustic horns, a horizontal pair and a vertical pair,

was due to the excellent loudness conditions of this place and the perfect geolocation because it is a high area, with the same level as the terrace of the Miguelete[1,] and the view of the sea is not hindered.

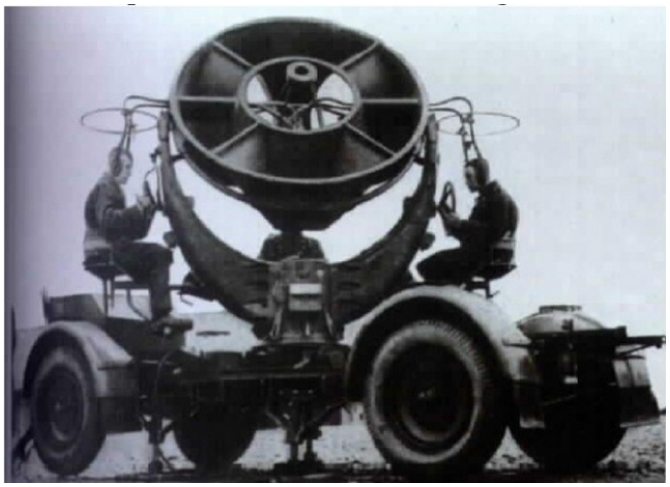

Figure 20. German acoustic locator "Elascop". Manufactured by "Electnacustic". Archive of the Antiaircraft Artillery Regiment No. 72, Spain. 1944.

On February 22nd 1937, a judgment for the execution of shelters and trenches was established in the town of Burjassot. Among several alternatives, the possibility of using the Silos as a refuge was raised. The biggest intervention was the construction of a gallery that connected some silos with others. In addition, the warehouses where the *Escuela de Artes y Oficios of Valencia*[14] were located were used as a preventive prison, and then as a headquarters detachment of the DECA14[17].

The first use of the connected silos by tunnel was as an air-raid shelter for soldiers. Later further excavations were carried out to create another access to other silos to be used as ammunition dumps.

2.6.5.2 Postwar period and dictatorship

During the Francoist Spain[18] in January 1939 an intervention was performed in the *Escuela de Artes y Oficios*[14], which became a school through bricklaying, carpentry and painting works.

Since 1940, Lopez Laguarda established a music school in the embarronat[7] north. A few years later, in 1943 a replica of the cross carved in 1580 was rebuilt (Figure 15). It was made by the director of the School Francisco Marco Diaz-Pintado and one of the most outstanding students (López Laguarda, 1946).

One of the more important events for Burjassot was the demolition of the church of St. Bartolomé de Valencia, which had been looted and burned during the Civil War. This construction was able to save the bell tower and three covers. In 1953, one of this covers was placed on the south facade of the *Escuela de Artes y Oficios*[14].

connected by rubber tubes to stethoscope type earphones worn by the two technicians left and right. The stereo earphones enabled one technician to determine the direction and the other the elevation of the aircraft.

[17] DECA14 was a detachment of Special Defense Against Aircraft (in Spanish, *Defensa Especial Contra Aeronaves*)

[18] Francoist Spain (also historically known as Nationalist Spain during the Spanish Civil War) refers to the period of Spanish history between 1939, when Francisco Franco took control of Spain from the government of the Second Spanish Republic after winning the Civil War, and 1978, when the Spanish Constitution of 1978 went into effect (Gil, 1981).

Figure 21. St. Bartolomé cover church placed on the *Escuela de Artes y Oficios*. 2016.

Until 1975, the Silo-Yard was used for the drying of peanuts, meanwhile it also had a recreational use, like popular fairs, etc.

2.6.5.3 Spanish transition to democracy

During this period[19] the municipalities of Valencia and Burjassot, reached an agreement to transfer Los Silos in usufruct[20] to the municipality of Burjassot, approving the review in 1975.

Finally, in 1979 the City Council of Burjassot began the race to achieve the declaration of National Monument for Los Silos. In 1980 it carried out the repair of different damaged parts and it was installed with a system of lighting. In this reshuffle at this time the brick coating of the Silo number 2 was built (Generalitat Valenciana, 1983).

On March 26th 1982, the Silos of Burjassot were declared a Historical Artistic Monument of National Character by the Ministry of Culture, in accordance with the article 19 of the Regulation of April

[19] The Spanish transition to democracy (in Spanish *Transición española a la democracia*), refers to the restoration of democracy in Spain after the death of Francisco Franco in 1975. The transition began shortly after Franco's death on 20 November 1975, while its completion has been variously said to be marked by the Spanish Constitution of 1978, the failure of an attempted coup on 23 February 1981, or the electoral victory of the Spanish Socialist Workers' Party (PSOE) on 28 October 1982.

[20] A Civil Law term referring to the right of one individual to use and enjoy the property of another, provided its substance is neither impaired nor altered.

16th 1936, by Royal Decree 1185/1982 26th March 1982 (BOE[21]. 9/6/82). In 1985 the monument automatically became *Bien de Interés Cultural*[22].

Currently only the southern *embarronat* and the warehouse are used for crafts, such as sculpture, school-workshop and restoration furniture. A few years ago guide visits were performed inside the six connected silos, but the poor state of conservation of the monument cancelled further visits into the silos.

The Silos of Burjassot have become the hallmark of the town of Burjassot, and due to the population growth have become part of the heart of the town.

[21] The *Boletín Oficial del Estado* (BOE) (English: Official State Gazette) is the official gazette of the Government of Spain and is published every day except Sunday. The content of the BOE is authorized and published, by Royal Assent and with approval from the Spanish Presidency Office.

[22] A *Bien de Interés Cultural* is a category of the heritage register in Spain. The term literally means "Good (in the sense of economics) of Cultural Interest", although a better translation could be "Heritage of Cultural Interest", as Spain protects not only material heritage, like monuments or movable works of art, but also intangible cultural heritage. The category of *Bien de Interés Cultural* dates from 1985 when it replaced the former heritage category of National Monument (in Spanish Monumento Nacional) in order to extend protection to a wider range of cultural property.

3 Project Development

This final project is part of the international project "Responsibility for Cultural Heritage through Geomatics " created by the universities Aristotle University of Thessaloniki, Hochschule Karlsruhe Technik und Wirtschaft and the Polytechnic University of Valencia. Thermal characterization of the Valencian Silo-Yard is the outcome of the work done in the silos of Burjassot.

3.1 Objectives and Planning

“Responsibility for Cultural Heritage through Geomatics” has as targets the development of guidelines and acquisition techniques for the documentation of cultural heritage as well as the transformation in online geodatabases, raising awareness regarding the importance of cultural heritage, creating social competence through the learning of cultural heritage among students and finally, development and sustainable integration of teaching content in the curricula of the participating study programs.

During the international campaign done between the 11th to 15th of April an interior thermal characterization of different silos was performed, in order to create different documentation about the current state of conservation of the monument and pathologies that affect it. This thermal characterization was performed with low-cost hardware, developing software under Android operating system, to obtain images in the visible and infrared spectrum. After data collection, different 3D models of the silos were created from multispectral imagery with a viewer to freely view different parts of the silos of Burjassot. Finally, different documentation of conditions and pathologies were made from the different products created.

The first part of a project is the performance of the project development planning. At the beginning of this Master Thesis a plan with all the steps of this project was created (Figure 22).

Task Name	Duration	Start	Finish
Seminar zur Master Thesis	**30 days**	**Tue 01/03/16**	**Thu 31/03/16**
Creation of Planning	6 days	Tue 01/03/16	Mon 07/03/16
Literature Search	6 days	Mon 07/03/16	Sun 13/03/16
Abstract of Seminar zur Master Thesis	17 days	Mon 14/03/16	Thu 31/03/16
Master-Thesis	**108 days**	**Fri 01/04/16**	**Mon 18/07/16**
Search and Compare of Thermal Cameras	12 days	Tue 01/03/16	Sun 13/03/16
Creation of APP for Flir One Camera	27 days	Mon 14/03/16	Sun 10/04/16
Data Acquisition	5 days	Mon 11/04/16	Fri 15/04/16
Data Processing	27 days	Mon 18/04/16	Sun 15/05/16
Creation of 3D Models	34 days	Mon 16/05/16	Sun 19/06/16
Create visualization of 3D models	28 days	Mon 20/06/16	Mon 18/07/16
Master-Thesis Writting	108 days	Fri 01/04/16	Mon 18/07/16
Kolloquium zur Master Thesis	**15 days**	**Mon 18/07/16**	**Tue 02/08/16**
Presentation for Kolloquium	13 days	Mon 18/07/16	Sun 31/07/16
Defence of the Project	1 day	Mon 01/08/16	Tue 02/08/16

Figure 22. Master Thesis project.

This schedule could be represented as a Gantt chart (Figure 23).

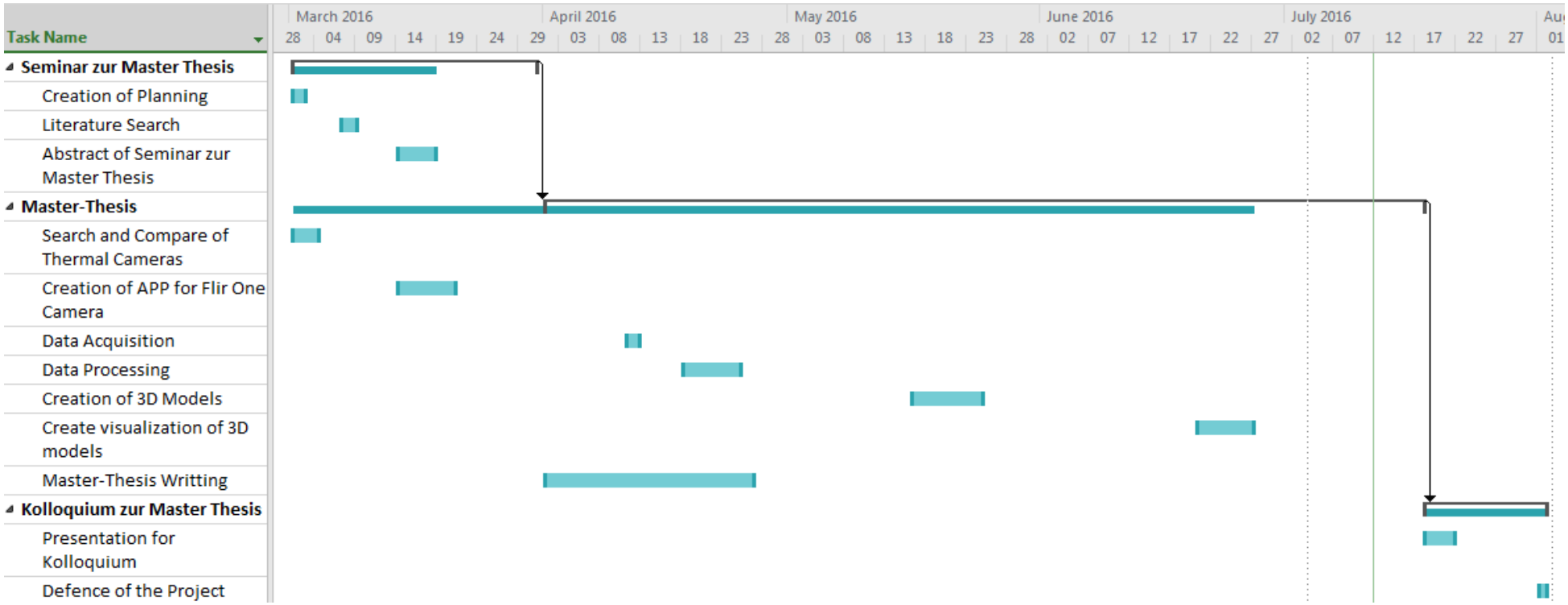

Figure 23. Gantt chart of the Master Thesis.

3.2 Search and Compare of Thermographic Cameras

The first step of this project was the search and comparison of thermographic cameras. During this phase different e-shops, forums and webpages of different producers were consulted. For this task the following requirements were followed (Figure 24).

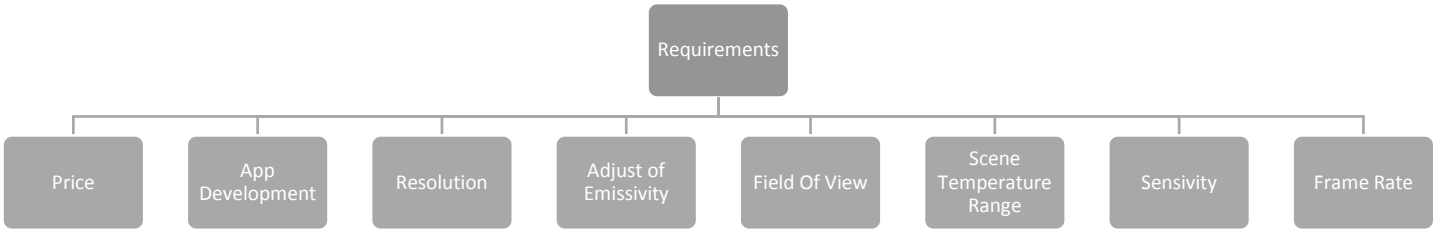

Figure 24. Requirements for purchase the thermographic camera.

The requirement that most delimited the election of the thermographic camera was the price. This project has as purpose, create a low cost method to document the heritage of the Valencian Silo-Yard. In addition, the objective of this project needed the possibility of developing different applications using the thermographic camera, so the thermographic camera had to have easy access software that allows its development.

Due to the requirement of a possible app development, the target of the first commercial search was the market of thermographic cameras connected to smartphones. With this requirements the models chosen were the following:

- Flir One
- SeekThermal
- SeekThermal XR
- Therm-App
- Therm-App Hz

3.2.1 Flir One

FLIR ONE is lightweight, easy to connect and easy to use. Explore the world around you in ways you never thought possible, with no additional cords, cases, devices or screens necessary. Connect your FLIR ONE to your smartphone or tablet to transform it into a thermal camera. What will you do with your new super power? With this advertisement Flir Systems[23] is selling the Flir One, with a price of 243€, the main characteristics of the Flir One are the following:

[23] FLIR Systems is the world's largest commercial company specializing in the design and production of thermal imaging cameras, components and imaging sensors. Based in Wilsonville, Oregon, United States, and founded in 1978. The company makes thermal cameras and components for a wide variety of commercial and government applications. FLIR is a component of the S&P 500 index with annual revenues in excess of $1.5 billion annually as of 2014.

Figure 25. Flir One camera.

Resolution	160x120
Adjust of Emissivity	-
Field of View	46°
Scene Temperature Range	-20°C to 120°C
Operating Temperature	0°C to 35°C
Weight	78 grams
Dimensions	72mm x 26mm x 18mm
Battery Capacity	350 mAh
Visible Camera	VGA
Sensivity	0.1°C
Charging Method	Micro-USB
Device Compatibility	Android devices with OTG connector

Table 1. Flir One characteristics

This camera could be bought in Android or iOS version. Both versions have an App called *Flir One App* which enable the smartphone to take pictures and video or create panoramas with the thermographic camera. Moreover this app enables the user to change the colour palettes of the visualization, measure the temperature of an object, select a correct emissivity, and save the location of the captured images if a GPS signal is available.

3.2.2 SeekThermal

Thermal imaging provides useful insight into the detection of energy loss in homes, commercial buildings, and industrial facilities. Inspection with thermal imaging detects energy loss caused by air leaks, missing or damaged insulation, inefficient HVAC systems, and poor construction. Finding and assessing these problems requires a thermal imager to identify hot and cold spots. SeekThermal thermal imaging cameras enable contractors to conduct building and home inspections quickly and accurately, without the need to crawl through attics and crawlspaces or punch holes in walls to find air leaks, thermal bypasses, and insulation gaps. This is the billboard from Seek Thermal[24].

The SeekThermal camera has a price of 270€. The housing is made of magnesium and the lens has a 36 degree field of view.

Figure 26. SeekThermal

Resolution	206x156
Sensivity	0.1°C
Temperature Detection Range	-40°C to 300°C
Field Of View	Wide, 36° FOV
Distance	1.5m to 300m
Adjust of Emissivity	8 modes
Battery	Not required

Table 2. SeekThermal characteristics.

[24] SeekThermal was founded in Santa Barbara by industry pioneers who spent 40 years advancing the state of military and professional-grade thermal technologies, SeekThermal has developed a new breakthrough series of thermal imaging solutions, sensors and devices.

SeekThermal XR is the world's smallest thermal imager. Its highly portable design fits in your pocket for easy connect and detect convenience. The SeekThermal XR delivers powerful thermal imaging through its advanced 206x156 thermal sensor engineered with the same military-proven technology the pros use. Its 20-degree narrow field of view allows it to detect heat signatures up to 550 meters away between -40 and 300 degrees Celsius.

The SeekThermal and the SeekThermal XR have the same components and software, the unique difference between both cameras is a change in the lens, reducing the Field of View until 20° in the SeekThermal XR. This design change increases the price of the SeekThermal to 349€, 69€ more than the SeekThermal camera.

Figure 27. SeekThermal XR camera.

3.2.3 Therm-App

Therm-App[25] transforms Android smartphones into powerful thermal imaging devices. It combines the power of a fully functional thermal camera with the mobility, processing power, display capabilities and advanced features provided by smartphones today. Launched over a year ago, Therm-App gained outstanding success as the first Android thermal imaging camera and is still the highest resolution device of its kind.

The Therm-App camera is created for professional use, this camera is only available in the U.S.A., for this reason his original price of 939$ is increased by 60$, for the shipping cost, and also the extra cost of an export tax should be added. For this camera, four different lenses are provided, and one of its most important features is the centesimal adjust of the emissivity.

[25] Therm-App® is just one in a long line of innovations developed by Opgal Optronic Industries. Since its inception in 1983, Opgal has been at the forefront of developing high performance, versatile visualization hardware and software products for a variety of markets using its state-of-the-art thermal and other advanced electro-optical technologies.

Figure 28. Therm-App camera.

Resolution (pixels)	384x288
Adjust of Emissivity	centesimal
Field Of View	6.8mm lens (55° x 41°) 13mm lens (29°x 22°) 19mm lens (19°x14°) 35mm lens (11° x 8°)
Scene Temperature Range	-20°C to 50°C
Sensivity	NETD <0.07°C
Frame Rate	8.7Hz
Focus	Manual, 0.2m to infinity
Weight	138 grams
Size	55mm x 65mm x 40mm
Power Supply	No battery, 5V over USB OTG
Encapsulation	IP54

Table 3. Therm-App characteristics.

The body of the Therm-App allows it to be used by any smartphone regardless of the position of the Micro-USB connection.

3.2.4 Therm-App Hz

Therm-App Hz is a high-end thermal imaging device for security, safety and other night / outdoor applications. Through its higher 25 Hz frame rate, Therm-App Hz delivers smooth thermal images, especially when the user or the targets observed are on the move, using a variety of interchangeable lenses ranging from 6.8mm to 35mm.

The Therm-App Hz has the same specifications as the Therm-App with the difference of an increase in the frame rate until 25Hz which enables an improvement in moviemaking. This improvement increases the price to 1550$, increased by 60$ for the shipping cost, plus the tax charged for exporting from U.S.A. to Europe.

3.2.5 Global comparison and choice

	Flir One	Seek Thermal	Seek Thermal XR	Therm-App	Therm-App Hz
Price	243 €	299 €	349 €	939$ + 60$ shipping + tax exporting	1550$ + 60$ shipping + tax exporting
Resolution (pixels)	160x120	206x156	206x156	384x288	384x288
Adjust of Emissivity	-	8 modes	8 modes	centesimal	centesimal
Field Of View	46°	36°	20°	6.8mm lens (55° x 41°) 13mm lens (29°x 22°) 19mm lens (19°x14°) 35mm lens (11° x 8°)	6.8mm lens (55° x 41°) 13mm lens (29°x 22°) 19mm lens (19°x14°) 35mm lens (11° x 8°)
Scene Temperature Range	-20°C to 120°C	-40°C to 300°C	-40°C to 300°C	-20°C to 50°C	-20°C to 50°C
Sensivity	0.1°C	0.1°C	0.1°C	NETD <0.07°C	NETD <0.07°C
Frame Rate	9Hz	9Hz	8.7Hz	8.7Hz	25Hz

Table 4. Global comparison.

In the previous table are marked some of the most important characteristics of the different cameras. All these cameras have common things as the Android OS or the need of an OTG USB connector in the smartphone.

The Flir One has the lowest price and offers no professional features with its low resolution 160x120px and without the possibility of adjusting the emissivity in the official App. On the other hand, in addition to its low cost has the biggest Field Of View and it has a VGA camera in the visible spectrum combined with the thermal infrared spectrum from the thermal sensor. It also stands out for having the biggest community developers for thermal cameras.

The SeekThermal and SeekThermal XR cameras increase its resolution until 206x156px, reducing the Field Of View.

The Therm-App and Therm-App Hz cameras are in the range of the professional cameras, with a cost five times more than the Flir One, and offer almost three times more resolution, four different lenses and a centesimal adjust of the emissivity. The unique disadvantage is the high cost of acquisition, added with the tax for exporting and the shipping time.

Considering all these grounds, the chosen camera was the Flir One due to the low price, in accordance with the low cost spirit of the project, the great Field Of View and the big developer community. Another of the most important section is the existence of a SDK[26] from Flir to develop Android applications.

Figure 29. Flir One unboxing.

3.2.6 Smartphone

[26] A software development kit (SDK or "devkit") is typically a set of software development tools that allows the creation of applications for a certain software package, software framework, hardware platform, computer system, video game console, operating system, or similar development platform.

Figure 30. Motorola Moto G.

The Flir One was used in this project together with a Motorola Moto G smartphone (first generation) with a camera of 5 MP, f/2.4, autofocus and LED flash. This smartphone has an USB OTG connector, allowing the use of the Flir One.

It takes images at a maximum resolution of 2592x1944 pixels. It has a built-in HDR mode, which can even be set to activate automatically in certain shooting conditions.

The available advanced settings include HDR, touch capture, panorama, geo-tagging, widescreen mode, and shutter sound.

In this smartphone colours are under saturated and there is very little noise, but that's due to the overly aggressive noise reduction, which eradicates a fair amount of the fine detail - a watercolour painting effect is visible whenever the user shoots grass, foliage or similar textures.

The camera of this smartphone (5MP) improves the visible VGA (0.3MP) camera of the Flir One. In other project, with better smartphones, the difference could be more significant. For this reason the main objective of this project was to take advantage of the smartphone sensor in order to create a 3D model in which the thermal images from the Flir One were projected, obtaining a thermal 3D model with the geometry of the visible smartphone sensor.

3.3 Creation of App for Flir One camera

After the selection of the Flir One camera as the camera for this project, it can be seen that the official application "Flir One for Android", which can be found in the Play Store of Android, it would not fulfil the requirements for this project, take photos at same time using the visible camera of the smartphone and the thermal camera of the Flir One.

The purpose of this project "Thermal Characterization of the Valencian Silo-Yard" needed to take photos in the visible spectrum with good quality, and additionally take photos in the thermal infrared spectrum. For this reason it was mandatory to create an application in the Android operating system able to do this job. In addition, different features were created to facilitate the data collection.

The HSKA Flir one App was developed using Android Studio. Android Studio is the official integrated development environment (IDE)[27] for Android platform development. Based on JetBrains' IntelliJ IDEA software, Android Studio is designed specifically for Android development. It is available for download on Windows, Mac OS X and Linux.

Android Studio has the following features:

- Gradle-based build support.
- Android-specific refactoring and quick fixes.
- Lint tools to catch performance, usability, version compatibility and other problems.
- ProGuard integration and app-signing capabilities.
- Template-based wizards to create common Android designs and components.
- A rich layout editor that allows users to drag-and-drop UI components, option to preview layouts on multiple screen configurations.
- Support for building Android Wear apps
- Built-in support for Google Cloud Platform, enabling integration with Google Cloud Messaging and App Engine.

All projects in Android have the same folder structure (Cruz Zapata, 2015):

- module-name/
  - build/

    Contains build outputs.
  - libs/

    Contains private libraries.
  - src/

    Contains all code and resource files for the module in the following subdirectories:
    - androidTest/

[27] An integrated development environment (IDE) is a software application that provides comprehensive facilities to computer programmers for software development.

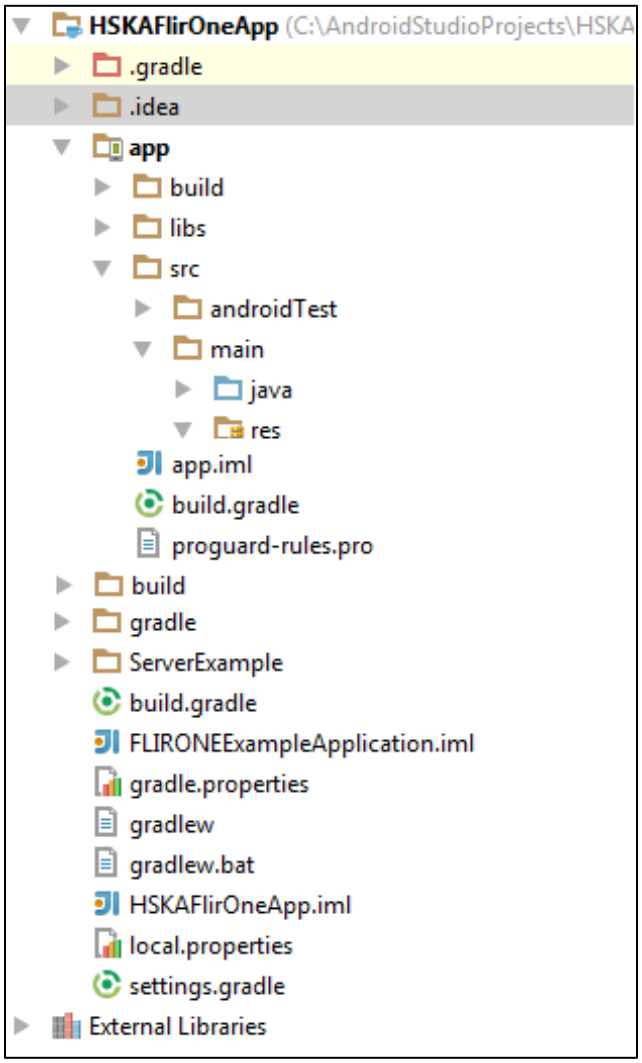

Figure 31. Folder structure of the HSKA Flir One App.

Contains code for instrumentation tests that run on an Android device.

- main/

  Contains the "main" sourceset files: the Android code and resources shared by all build variants (files for other build variants reside in sibling directories, such as src/debug/ for the debug build type).

- AndroidManifest.xml

  Describes the nature of the application and each of its components.

- java/

  Contains Java code sources.

- jni/

  Contains native code using the Java Native Interface (JNI).

- gen/

  Contains the Java files generated by Android Studio, such as the R.java file and interfaces created from AIDL files.

- res/

  Contains application resources, such as drawable files, layout files, and UI string.

- assets/

  Contains file that should be compiled into an .apk file as-is. One can navigate this directory in the same way as a typical file system using URIs and read files as a stream of bytes using the AssetManager. For example, this is a good location for textures and game data.

- test/

  Contains code for local tests that run on the host JVM.

- build.gradle (module)

  This defines the module-specific build configurations.

- build.gradle (project)

  This defines the build configuration that apply to all modules. This file is integral to the project, so one should maintain them in revision control with all other source code.

Within each Android app module, files are shown in the following groups:

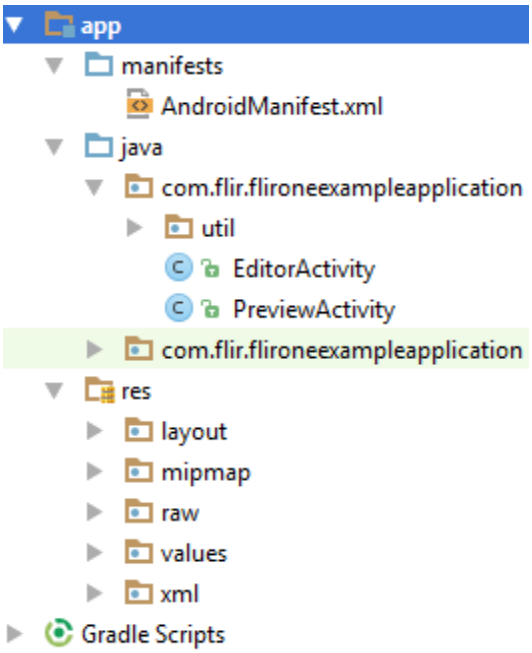

Figure 32. Android structure of the HSKA Flir One App.

- manifests

  Contains the AndroidManifest.xml file.
- java

  Contains the Java source code files, separated by package names, including JUnit test code.
- res

  Contains all non-code resources, such as XML layouts, UI strings, and bitmap images, divided into corresponding sub-directories.

3.3.1 *AndroidManifest.xml*

Every application must have an AndroidManifest.xml file (with precisely that name) in its root directory. The manifest file presents essential information about your app to the Android system, information the system must have before it can run any of the app's code. The AndroidManifest.xml of the HSKA Flir One App has special permission to write and read the external storage of the smartphone (SD Card) to save and use the different photos taken.

3.3.2 *EditorActivity.java*

In the EditorActivity.java file the images taken by the thermographic camera of the Flir One are processed to be shown into an ImageView object. In this file are defined actions of all buttons and link them with the different functions of the PreviewActivity.java.

3.3.3 *PreviewActivity.java*

The PreviewActivity.java develops different functions implemented in the code:

- Battery percentage of the Flir One camera. The camera battery has 350 mAh with an approximate duration of one hour of use.
- Force Tuning. The camera has a mechanical shutter inside that periodically activates and allows the thermal camera to do a calibration or image refresh. When the shutter activates, the image will freeze for a brief period. The purpose of the shutter is to allow the camera to provide an improved image. The FLIR ONE performs the tuning operation automatically on a periodic basis and this button allows the user to force the tuning (Figure 59).

- Rotation. This button allows to do a rotation of 180 degrees (Figure 58).
- Change View. This button allows one to change the visualization of the thermographic view using different palettes:
    - Thermal Linear Flux14Bit Image. Thermal view of the thermographic camera taking images of 14 bits (Figure 36).
    - Thermal Image. Thermal view (Figures 37 to 45).
    - Blended MSXImage. Blended of the thermographic camera and the visible camera of the Flir One (Figures 46 to 54).
    - Visual JPEGImage. View of the visible camera cropped to the Field Of View of the thermographic camera. The visible camera has a Field Of View bigger than the thermographic camera (Figure 55).
    - Visual Image. Original image of the visible camera (Figure 56).
    - Thermal Radiometric Kelvin Image. Visualization of the thermographic with a Kelvin scale (Figure 57).
- Toggle Sim. Simulator of the Flir One camera to test the proper functionality of all the functions implemented (Figure 60).
- Take a Picture. This function takes photos of three different images (Figures 61 and 62):
    - Visible photo of the smartphone camera, to obtain better resolution than the photos from the VGA camera of the Flir One.
    - Visible photo of the VGA camera from the Flir One camera.
    - Thermal photo from the thermographic Flir One camera.

3.3.4 Activity_preview.xml

The activity_preview.xml file is the main layout of the HSKA Flir One App. This layout defines the visual structure for a user interface, such as the UI for an activity or app widget.

In this interface the user can find all the features implemented in the different java files. This GUI[28] provides a dynamic component to the application, because prioritizes the thermal view, instead of the different buttons. If the user does not touch the screen the different buttons disappear and only the photos from the selected view are displayed, activating the activity_editor.xml

3.3.5 Activity_editor.xml

This layout displays the signal from the camera with the selected view.

[28] A graphical user interface (GUI), is a type of user interface that allows users to interact with electronic devices through graphical icons and visual indicators such as secondary notation, instead of text-based user interfaces, typed command labels or text navigation.

Figure 33. Activity_preview.xml, main layout of the HSKA Flir One App.

3.3.6 Ic_launcher.png

Finally, an icon to identify the HSKA Flir One App was created. This logo is a thermal representation of a cap of silo with the Hochschule Karlsruhe – Technik und Wirtschaft logo as mask.

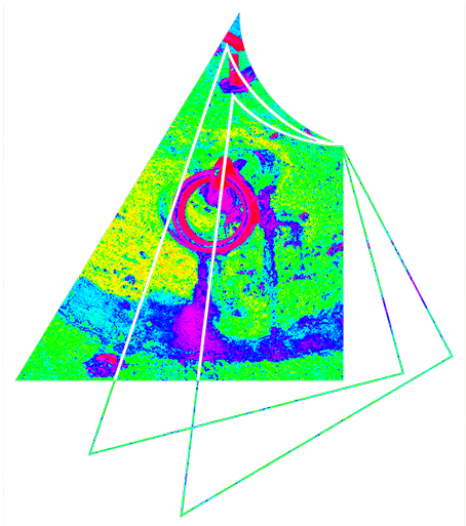

Figure 34. HSKA Flir One App logo.

3.4 HSKA Flir One App

The HSKA Flir One App was designed thinking of an intuitive use for the different features. This app needs the Flir One camera connected to use all the features, but it a video demo to test all the features without connecting the camera to the smartphone is implemented.

When the Flir One is connected the App automatically shows the view *Thermal Linear Flux14Bit Image*, and by pressing the *Change View* button the user could change the visualization to five different modes. In the thermal modes (Thermal Image and Blended MSXImage) the user could change the palettes of colour of the thermal representation.

Figure 35. Visualization views.

Figure 36. Thermal Linear Flux 14Bit Image.

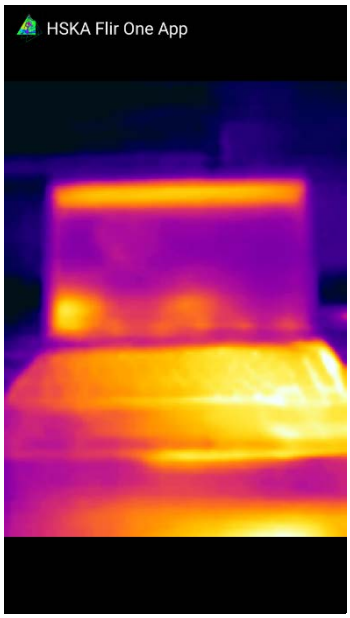

Figure 37. Thermal image with iron palette.

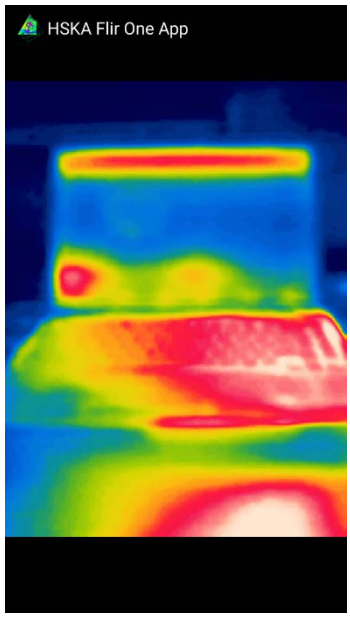

Figure 38. Thermal image with rainbow palette.

Pressing the take photo button at any time will automatically save a photo from the smartphone camera and simultaneously another photo from the Flir One. When the user takes a photo the App launches an intent to the Android OS (Figure 61), and for this reason if the user wants an instant result, the user needs to have installed previously an Android app capable of this. In this project the external App used was “InstaCamera”. Once the visible photo from the smartphone is taken, the Flir One takes a thermal image and saves it in .RAW format with *14 bits* (Figure 62), to extract the maximum resolution and information of the thermal shot. Then this image must be processed.

The .RAW file is saved in the *Pictures* folder of Android, but the OS cannot read or write .RAW files natively. If the user wants to view the .RAW file taken, another application to handle these files such as RawDroid would be required. In this project all the treatment of the data will be performed in a computer under Windows OS.

Figure 39. Thermal image with gray palette.

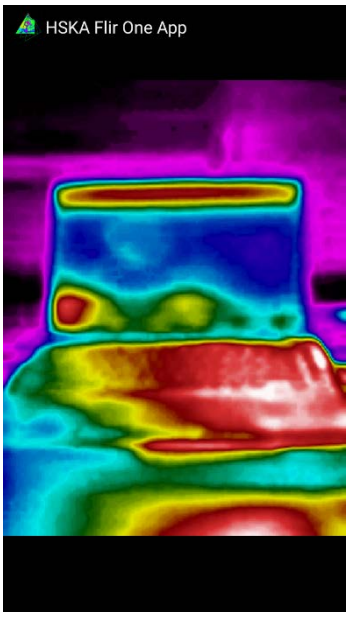

Figure 40. Thermal image with contrast palette.

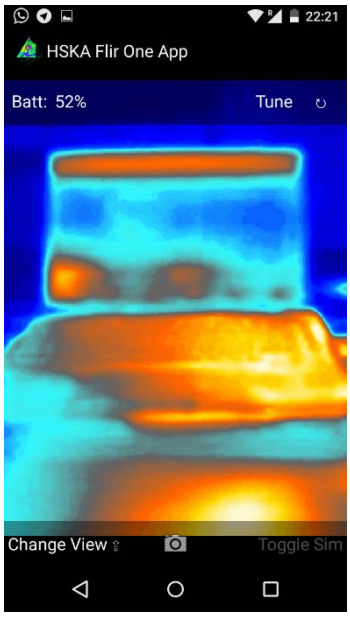

Figure 41. Thermal image with artic palette.

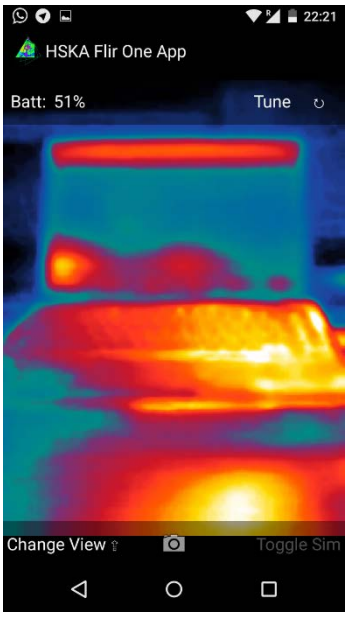

Figure 42. Thermal image with lava palette.

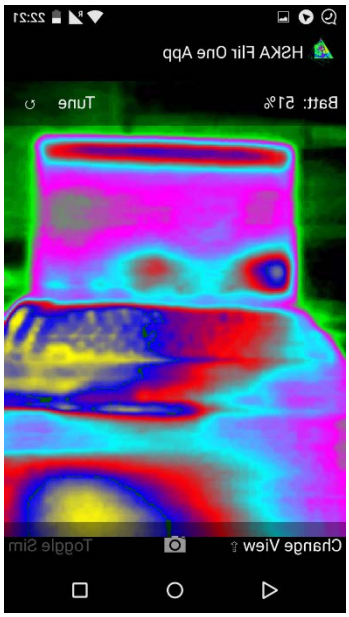

Figure 43. Thermal image with wheel palette.

Figure 44. Thermal image with coldest palette.

Figure 45. Thermal image with hottest palette.

Figure 46. Blended MSXImage with iron palette.

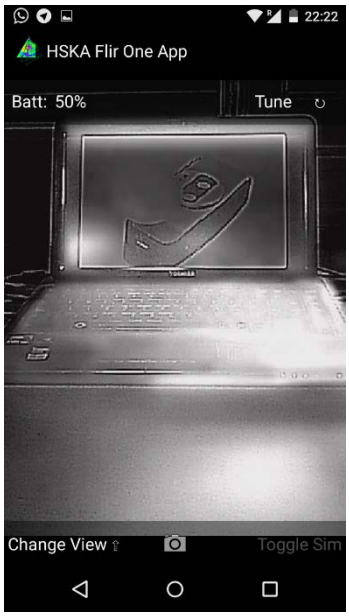

Figure 47. Blended MSXImage with gray palette.

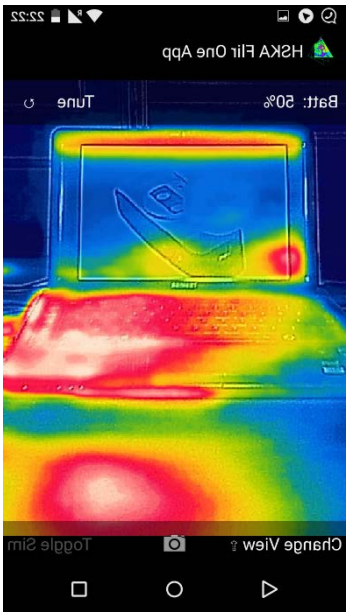

Figure 48. Blended MSXImage with rainbow palette.

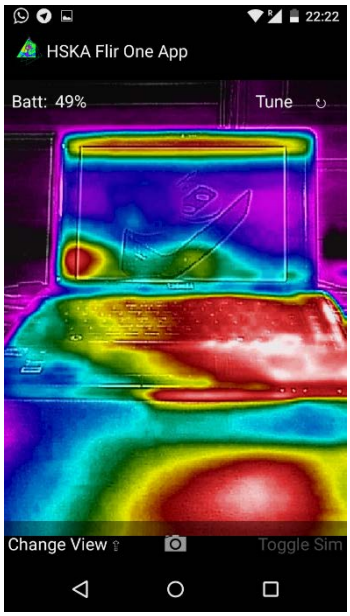

Figure 49. Blended MSXImage with contrast palette.

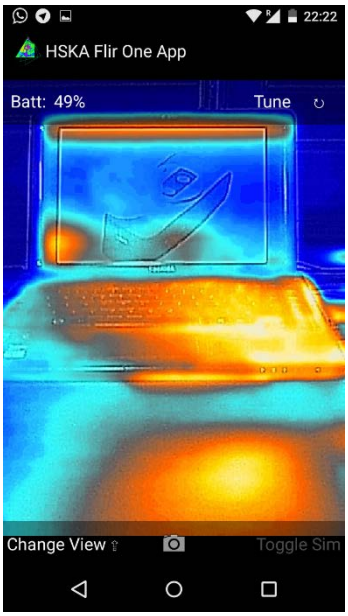

Figure 50. Blended MSXImage with artic palette.

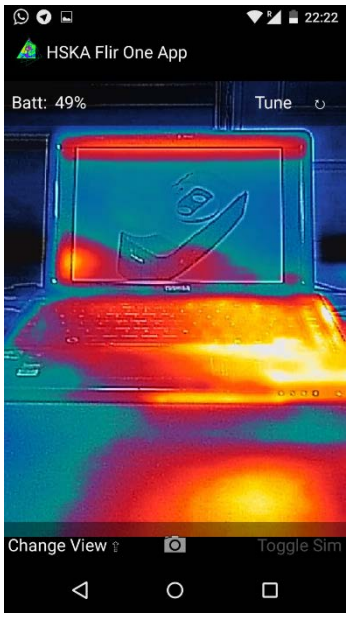

Figure 51. Blended MSXImage with lava palette.

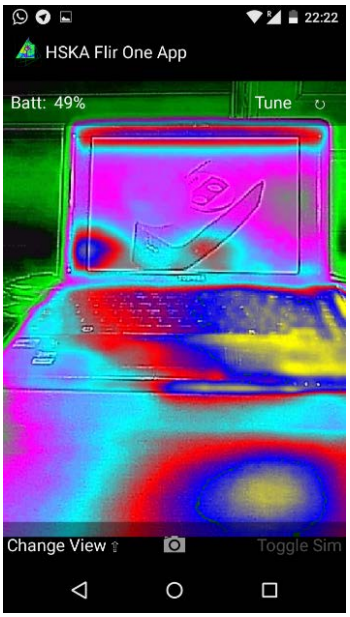

Figure 52. Blended MSXImage with wheel palette.

Figure 53. Blended MSXImage with coldest palette.

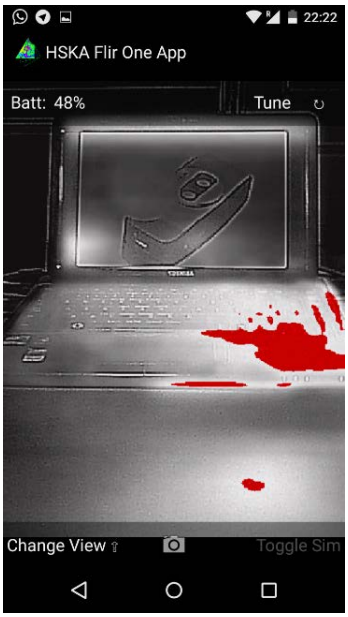

Figure 54. Blended MSXImage with hottest palette.

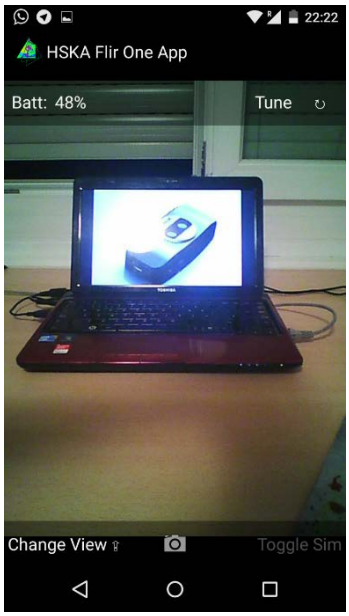

Figure 55. Visual JPEGImage.

Figure 56. Visual Image.

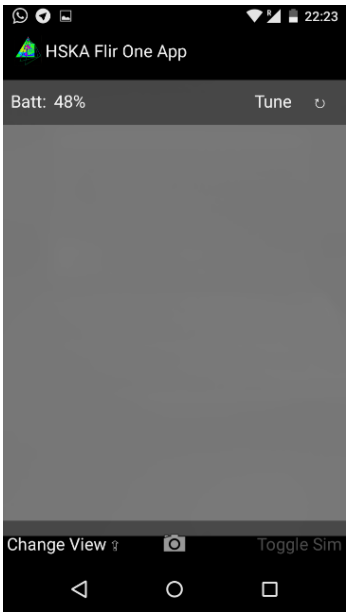

Figure 57. Thermal Radiometric Kelvin Image.

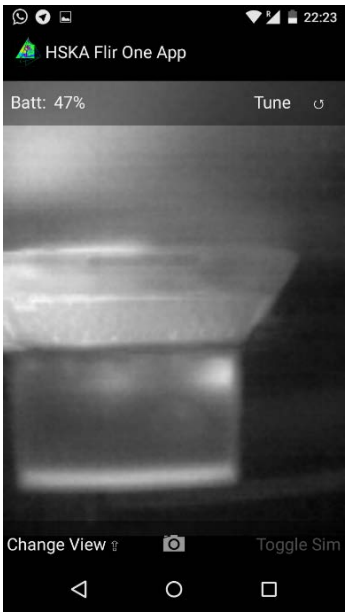

Figure 58. Rotation using the Flir One camera.

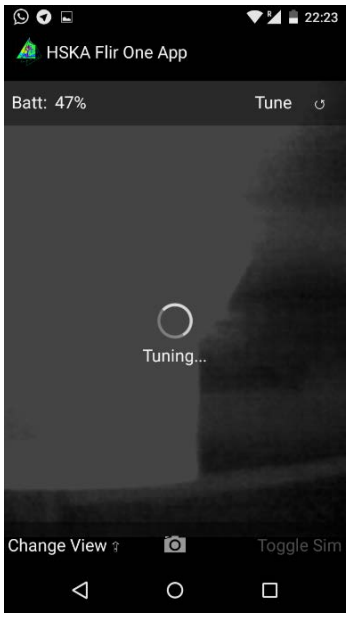

Figure 59. Forcing tuning.

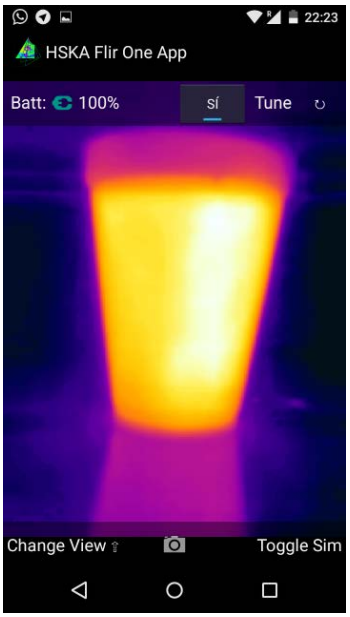

Figure 60. Thermal Image of the demo mode.

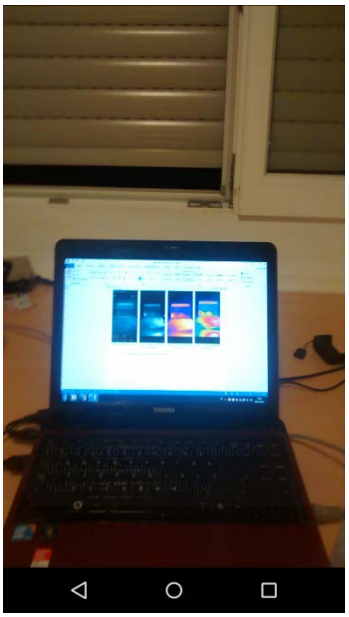

Figure 61. Pressing the *"Take a Photo"* button, visible image.

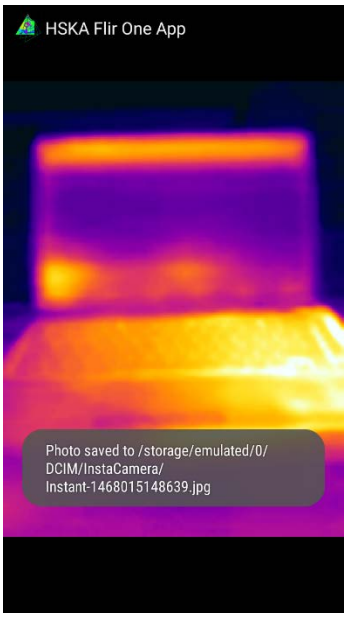

Figure 62. Pressing the "Take a Photo" button, thermal image.

The visible image taken by the smartphone camera could be visualize in the Android Gallery. This image is saved into the InstaCamera App folder of the SD card of the smartphone.

3.5 Data Acquisition

The data acquisition occurred between the 11th to 15th April in the Valencian Silo-Yard, located in Burjassot. The thermography data acquisition was split in 7 parts during the campaign, in addition to supporting tasks of other groups.

3.5.1 April, Monday 11th, first day of campaign

On 11th April in the morning the first step of the surveying network was scheduled, and in the afternoon the first data acquisition for the thermography was planned.

Figure 63. First meeting around the Silo-Yard.

This schedule was changing throughout the day, in the morning a touchdown around the Silo-Yard was performed, explaining the planning to be followed during the campaign.

Figure 64. Touchdown around the Silo-Yard.

Furthermore, the groups 1 and 2 (Table 6) would be responsible for the transportation of equipment and materials each day from the Silo-Yard to the *Casa de Cultura*[29] *de Burjassot,* because this place had an insurance to protect the instruments.

Figure 65. Instruments into the *Embarronat*[7] south.

In the afternoon the planning also changed, the whole afternoon was dedicated to planning the data acquisition of the laser scanner, thermography and terrestrial photogrammetry (Figure 66).

Figure 66. Planning the placement of targets for thermography in the silo 2 with the professor Vassilios Tsioukas.

This fact delayed the original planning. The original planning is shown in the next figure.

[29] The *Casa de Cultura* (in English cultural center) is a complex that promotes culture and arts. Cultural centers can be neighborhood community arts organizations, private facilities, government-sponsored, or activist-run. The cultural center of Burjassot is a government-sponsored center.

UNIVERSITAT POLITÈCNICA DE VALÈNCIA

Thermal Characterization of the Valencian Silo-Yard

Hochschule Karlsruhe Technik und Wirtschaft
UNIVERSITY OF APPLIED SCIENCES

	Group	M	Group	T	Group	W	Group	Th
Morning		Study site presentation		Task assigment and organization		Task assigment and organization		Task assigment and organization
		Task assigment and organization						
	1 - 8 15 16	**Surveying network** 1. Connection to the national geodetic network 2. Local network inside silos 3. Targets inside silos (Almost all students working together in WP surveying network)	7/8 2/6	**Surveying network Network measurements** 1. Planning UAV+Photogrammetry with groups 2. Targets for UAV+Photogrammetry	7/8 2/6	**Surveying network - network adjustment** Delimitation of working areas for GPR and Thermography: 1. Walls 2. Silo-yard	7/8	**Surveying network - CP for photogrammetry and Laserscanning**
			5/17	**UAV** marking Control Points (CP), flight for roofs, Silo-yard, Walls, Building facades	13	**Geophysics** GPR in walls	2/6 9?	**Laser scanning** Walls and surrounding, Silo-yard, 1 silo isolated
			4 15? 16?	**Terrestrial photogrammetry** Embarronat loggia San Roque square/main access/chapel facade	1/3 13?	**Thermography** Taking photos in silo-yard	4 5?	**Terrestrial photogrammetry** Data acquisition inside buildings (optional)
			16/17 15?	**Geophysics** GPR silo 2	5	**UAV** Data review and data acquisition in case it hasn't been finished	16 5?	**Geophysics** GPR inside buildings (optional)
			1/3	**Thermography** Taking photos in silo 3	4	**Terrestrial photogrammetry** Data review and data acquisition in case it hasn't been finished	1/3 9?	**Thermography** Taking photos inside buildings (optional)
Afternoon	7/8 2/6 9/10?	**Surveying network** Local network surrounding	7/8 2/6 9/10?	**Surveying network measurements**	2/6 910?	**Laser scanning + Surveying network** Planning for laser scanning data acquisition	2/6 910?	**Laser scanning** Walls and surrounding, Silo-yard, 1 silo isolated Prepare presentation
	15 16/17?	**Geophysics** GPR silo 1	16/ 13/15	**Geophysics** GPR silo 3	7/8	**Surveying network - CP for photogrammetry and Laserscanning**	7/8	**Surveying network** Prepare presentation
	1/3 9/110?	**Thermography** Taking photos in silo 2	1/3 9/10? 11/13?	**Thermography** Taking photos in silo 1	15 12?	**Geophysics** GPR in silo-yard	16/15	**Geophysics** Prepare presentation
			5 15?	**UAV** Silo lid in detail	1/3 9/10/11?	**Thermography** Taking photos in walls	1/3 9/10/11?	**Thermography** Prepare presentation
	5 17?	**UAV** Planning for data acquisition	4/11 12?	**Terrestrial photogrammetry** Silo lid in detail Building facades	5 12?	**UAV** Data review and data acquisition in case it hasn't been finished	5 15?	**UAV** Prepare presentation
	4 16?	**Terrestrial photogrammetry** Planning for data acquisition			4/11	**Terrestrial photogrammetry** Data review and data acquisition in case it hasn't been finished	4/11 12?	**Terrestrial photogrammetry** Prepare presentation
				Assembling and dismantling mobile scaffold		Dismantling mobile scaffold		

	Group	F
Morning		Task assigment and organization
	2/6	**Laser scanning** 6 silos Data review
	1 - 8 16 13?	**Presentations** Result review Comments
		Quality and satisfaction survey
Afternoon		Result review Comments Discussion (In case of being necessary)

Table 5. Friday's timetable.

1	Juan Pedro Carbonell
2	David Montalvá
3	David Arenas
4	Ahmed Ali Hadaby Alamen
5	Vasileios ALEXANDRIDIS
6	Irini Soubry
7	Felix Ambs
8	Stephanie Lackner
9	Gema Zarrías Martos
10	David Ferrer Calatayud
11	Ester Alegre Torres
12	María José Casamayor Polo
13	Ignacio Dies Guillen
14	Tereza Ivaylova Ilieva
15	Nuria Juan Moraleda
16	Eduardo Tormo Polo
17	Francisco Moya Dolz

Table 6. Working groups.

3.5.2 April, Tuesday 12th, second day of campaign

On Tuesday morning it was planned to start with the thermography of the Silo 1 and recover the time, trying to do the thermography of the Silo 2 that should have been done on Monday afternoon. However, there was a problem with some locked tribrachs, this problem delayed the start of the surveying network, because the team could not mount the tribrachs in the surveyor's tripods.

Due to this problem, different groups tried to unlock them with different screwdrivers, but finally the groups had to go to the instrumentation laboratory of the UPV to unlock the tribrachs.

Figure 67. Trying to unlock the tribrachs.

During the afternoon the first targets were placed on the surface of the silos one, two and three, using ladders and a scaffold.

Figure 68. Placing targets in the silo 2.

These different problems delayed the start time of the thermography data acquisition in two days from the planned schedule.

3.5.3 April, Wednesday 13th, third day of campaign

During the third day of the campaign the surveying network measurements started, and the different groups were split to ensure that the different tripods placed were not moved by people.

At the end of the afternoon, lighting needed to heat the surface of the silos was taken. The lightning is composed of four bulb lights each of 1250W. The use of this lighting causes an increase in the temperature by radiation, heating up the surface of the silos to detect changes of materials thanks to the thermal inertia of the materials. For example, concrete has slow change in temperature while metals have a quick change. The existence of air gaps between outer skin and the rest cause an increase in the temperature, so with the thermographic cameras the building pathology can be detected.

Throughout this afternoon more targets and the lighting were placed without have more time to start the acquisition of data.

3.5.4 April, Thursday 14th, fourth day of campaign

On the fourth day of the campaign the data acquisition started, during this day the HSKA Flir One App was modified to take photos with the mode Blended MSXImage of the Flir One.

Figure 69. Data acquisition in the silo 1.

Figure 70. Data acquisition in the silo 3.

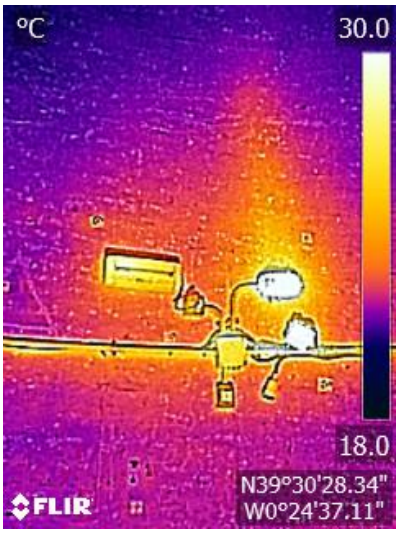

Figure 71. Thermal image from the silo 3.

During this day, photos of silos one, two and three were taken. These photos were taken trying to create an appropriate capturing scenario, making photos in circles trying to maximize the photographed area due to the small space to make the shots, with a 60% of overlap.

3.5.5 April, Friday 15th, fifth day of campaign

On the last day of the campaign, photographs were taken using the HSKA Flir One App to save visible images from the smartphone camera and thermal images from the thermographic sensor from the Flir One. Photos were taken from silos 1 and 3, because in silo 2 the brick coating, that is particular to this silo (Figure 68), prevented any use of the thermal image, obtaining similar temperatures in the surface.

During the data collection one must take into account the fast rate of change of the temperature, because the silos are being constantly heated with the lightning and a delay in the data capture could cause the temperature change of an area.

Figure 72. Photo of the silo 3 took with the smartphone camera.

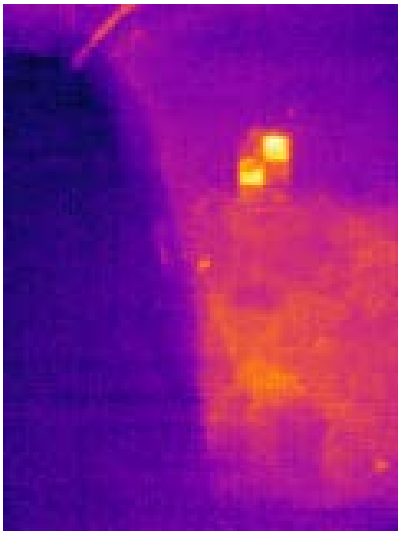

Figure 73. Photo of the silo 3 took with the thermographic sensor of the Flir One camera.

On the final morning, all the groups did a small presentation about a result review, some comments and a final discussion. These presentations were exposed during the afternoon.

Figure 74. Exposition of the presentation.

With this exposition a week of cooperation ended. During this week, we tried in the best way possible to help all participating groups, sharing an international experience in a real project, showing our different geomatics projects in the preservation of historical heritage and knowing professionals and friends with whom to collaborate in the future. With all our efforts, the aim is to make "Responsibility for Cultural Heritage" an excellent project.

3.6 Data Processing

The captured thermal images should be treated before starting with the analysis and modelling. Depending on the type of data collection the treatment will be different, for this reason two workflows were created. The first workflow was made for the treatment of the Blended MSX Image, and the second for the treatment of the visible photos from the smartphone and the thermal image from the thermographic sensor of the Flir One camera.

3.6.1 Treatment of the Blended MSX images

During the entire campaign, 977 Blended MSX images were taken using the combination between the thermographic and the visible sensors of the Flir One camera. All these images have a size of 364mb on the hard disk.

The first step was to know the type of metadata saved from the Flir software in the creation of the Blended MSX image. In this step the software ExifTool[30] (Mounce, 2013) was used with this command to extract all the metadata in a text file:

```
C:\Users\Juan Pedro\Desktop\Thesis\ExifTool>exiftool flir.jpg > metadata.txt
```

The folder ExifTool contained the file exiftool.exe and an image called “flir.jpg” from the data collection into the Silos. The text file created contained this information:

ExifTool Version Number : 10.15
File Name : flir.jpg
File Size : 406 kB
File Modification Date/Time : 2016:04:14 13:18:11+02:00
File Access Date/Time : 2016:07:12 10:34:47+02:00
File Creation Date/Time : 2016:07:12 10:34:47+02:00
File Permissions : rw-rw-rw-
File Type : JPEG
File Type Extension : jpg
MIME Type : image/jpeg
JFIF Version : 1.01
Exif Byte Order : Little-endian (Intel, II)
Make : FLIR Systems AB
Orientation : Horizontal (normal)
X Resolution : 72
Y Resolution : 72
Resolution Unit : inches
Software : HSKA Flir One App
Modify Date : 2016:04:14 13:18:10
Y Cb Cr Positioning : Centered
Exif Version : 0220
Create Date : 2016:04:14 13:18:10
Components Configuration : -, Cr, Cb, Y
Subject Distance : 1 m
Focal Length : 3.2 mm
Image Temperature Max : 213
Image Temperature Min : 213
Flashpix Version : 0100
Reflected Apparent Temperature : 20.0 C
Atmospheric Temperature : 20.0 C
IR Window Temperature : 20.0 C
IR Window Transmission : 1.00
Relative Humidity : 50.0 %
Planck R1 : 18160.975
Planck B : 1455.8
Planck F : 1
Atmospheric Trans Alpha 1 : 0.006569
Atmospheric Trans Alpha 2 : 0.012620
Atmospheric Trans Beta 1 : -0.002276
Atmospheric Trans Beta 2 : -0.006670
Atmospheric Trans X : 1.900000
Camera Temperature Range Max : 120.0 C
Camera Temperature Range Min : -40.0 C
Camera Software : 1.0.0
Lens Model : FOL2
Field Of View : 35.4 deg
Planck O : -1436
Planck R2 : 0.01255503
Raw Value Median : 12252
Raw Value Range : 1152
Date/Time Original : 2016:04:14 13:18:10.778+02:00
Focus Step Count : 0
Focus Distance : 2.0 m
Palette Colors : 224
Above Color : 170 128 128
Below Color : 50 128 128

[30] ExifTool is a platform-independent Perl library plus a command-line application for reading, writing and editing meta information in a wide variety of files.

Color Space : sRGB
Exif Image Width : 480
Exif Image Height : 640
Digital Zoom Ratio : 1
Image Unique ID : 9520A720B7A44C927B4E0692F226159F
GPS Version ID : 2.2.0.0
GPS Latitude Ref : North
GPS Longitude Ref : West
GPS Altitude Ref : Above Sea Level
Compression : JPEG (old-style)
Thumbnail Offset : 2016
Thumbnail Length : 1669
Embedded Image Width : 480
Embedded Image Height : 640
Embedded Image Type : JPG
Embedded Image : (Binary data 50075 bytes, use -b option to extract)
Emissivity : 0.95
GPS Map Datum : WGS84
GPS Latitude : 39 deg 30' 28.32" N
GPS Longitude : 0 deg 24' 37.08" W
GPS Position : 39 deg 30' 28.32" N, 0 deg 24' 37.08" W
Focal Length : 3.2 mm
Thumbnail Image : (Binary data 1669 bytes, use -b option to extract)
Object Distance : 1.00 m
Color Components : 3
Y Cb Cr Sub Sampling : YCbCr4:2:0 (2 2)
Overflow Color : 67 216 98
Underflow Color : 41 110 240
Isotherm 1 Color : 100 128 128
Isotherm 2 Color : 100 110 240
Palette Method : 0
Palette Stretch : 0
Palette File Name : iron.pal
Palette Name : Iron
Palette : (Binary data 672 bytes, use -b option to extract)
Raw Thermal Image Width : 240
Raw Thermal Image Height : 320
Raw Thermal Image Type : PNG
Raw Thermal Image : (Binary data 54413 bytes, use -b option to extract)
Real 2 IR : 1.41189825534821
Offset X : -8
Offset Y : +8
PiP X1 : 0
PiP X2 : 239
PiP Y1 : 0
PiP Y2 : 319
Image Size : 480x640
Megapixels : 0.307
Peak Spectral Sensitivity : 9.9 um
Image Width : 480
Image Height : 640
Encoding Process : Baseline DCT, Huffman coding
Bits Per Sample : 8

In this metadata file different information such as the resolution of the thermal sensor (X and Y resolution), the resolution of the visible sensor (Embedded Image Width and Height), GPS information of the smartphone and the distance between the visible sensor and the thermal sensor in the Flir one was saved (Real 2 IR).

The parameters that show the range of temperature in the metadata of each photo are the following:

FLIR PaletteInfo Tags

Index1	Tag Name	Writable
0	PaletteColors	N
6	AboveColor	N
9	BelowColor	N
12	OverflowColor	N
15	UnderflowColor	N
18	Isotherm1Color	N
21	Isotherm2Color	N
26	PaletteMethod	N
27	PaletteStretch	N
48	PaletteFileName	N
80	PaletteName	N
112	Palette	N

Figure 75. Flir PaletteInfo Tags from ExifTool::TagNames of Flir cameras.

To do the treatment of this type of data the software used was Flir Tools, which enables one to modify the different parameters of temperature to set the same range of temperatures in all the images thereby allowing the creation of a 3D model of the silos.

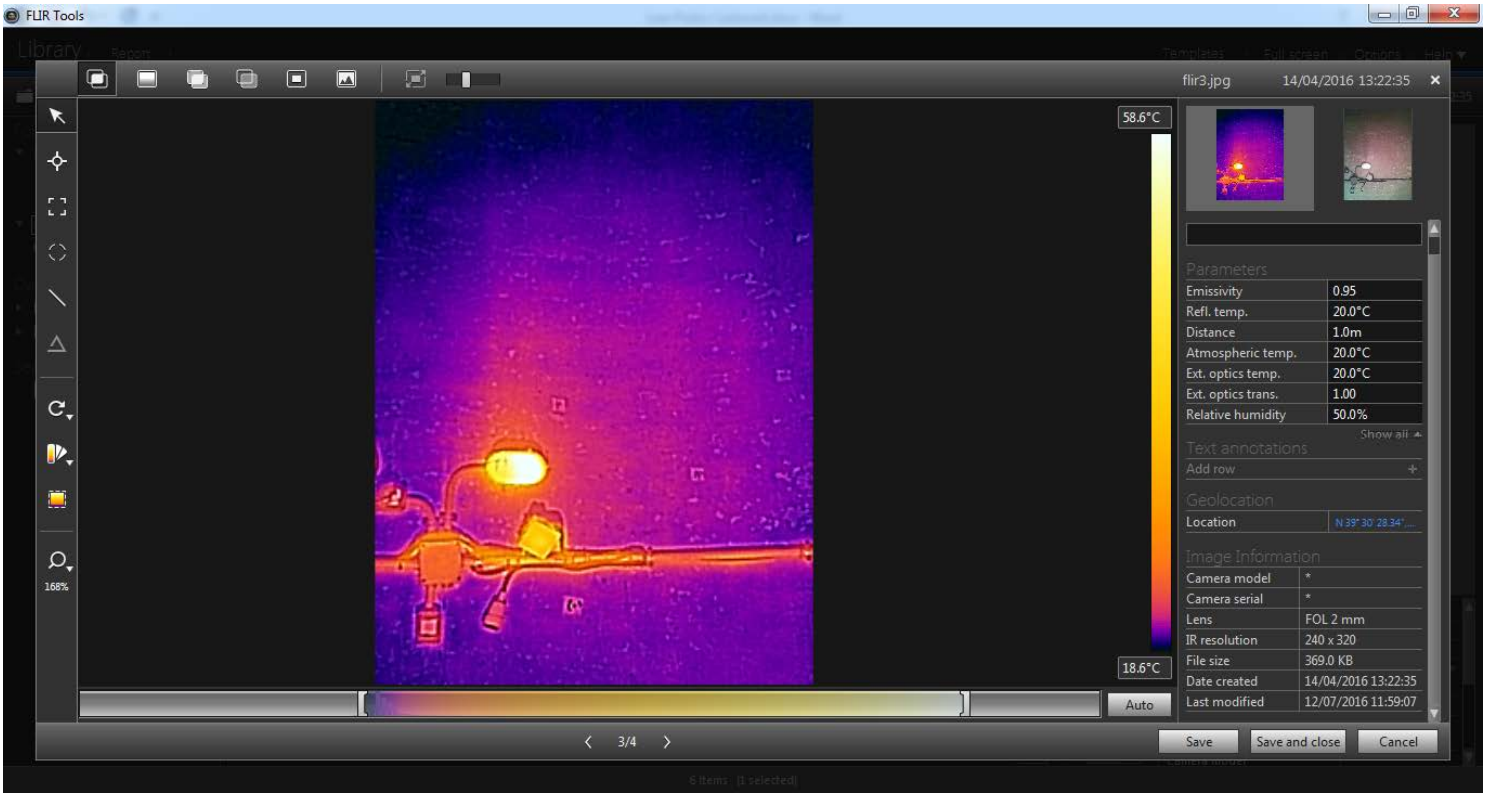

Figure 76. Screenshot of Flir Tools software.

This software enables one to change different parameters such as the emissivity of the object to calculate the real temperature, the reflected temperature, distance to the object, atmospheric temperature or the relative humidity. The objective of this project was to detect the difference of temperature of each material, for this reason, this parameters were not used because it was not the aim of this project to know the real temperature of a given material into the silo.

The user can choose between different visualizations of the image as Thermal MSX, Thermal, Thermal Fusion, Thermal Blending, Picture In Picture or Digital Camera. In addition to changing the palette like in the HSKA Flir One App, this software includes a feature to generate reports automatically with the most important information of each photo.

To change the range of temperatures the user has to change the number of degrees in the right bar of the image (Figure 77). For this project the temperature chosen was the range of 18º to 30º, considering the range temperature from the 977 images of the three different silos. Each image has a different default range temperature, so it is mandatory to perform an equalization of the range temperature of all the photos.

Figure 77. Changing the range of temperature of a MSX Blended Image.

In the next figures are shown different pictures without doing the equalization of temperature range. The figure 78 shows as objects that have the same temperature are not represented with the same digital value making impossible a match between photos.

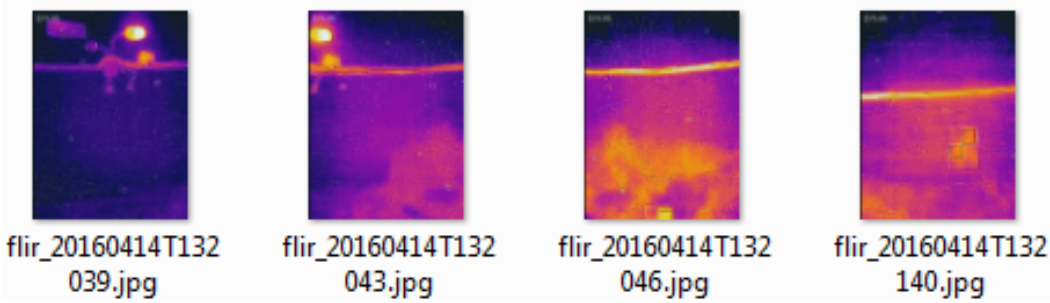

Figure 78. Images without equalize the temperature range.

Doing this process is displayed, as there is continuity in the temperatures of the different elements, displaying the same colour at the same temperature, allowing the union of textures in a 3D model. The figure 79 shows the result of the process of equalization, in all pictures the same digital value of a pixel is represented with the same colour, in other words all images have the same digital value for the same temperature.

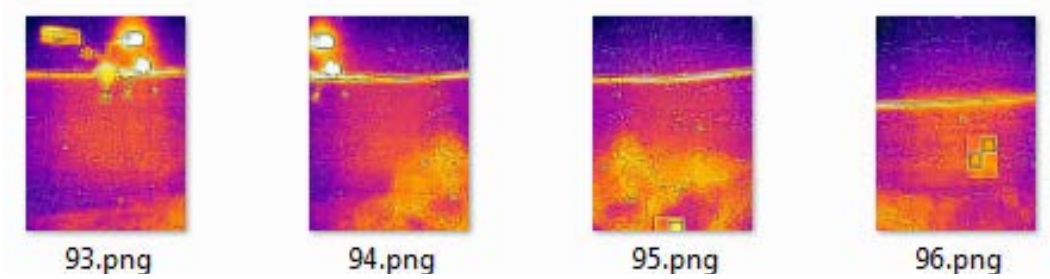

Figure 79. Images with the temperature range equalized.

3.6.2 Treatment of the thermal images

The treatment of the thermal images was done with the software ImageMagick[31], version 6.9.3.-Q16, and ExifTool. ImageMagick and ExifTool work using a command-line interface, thanks to this feature it was possible to implement the automation of transforming the .RAW files taken with the HSKA Flir One App to a .PNG file with a determinate range of temperatures.

During the campaign 84 photos of the silo 1 and 83 of the silo 3 were taken. This means, 167 visible photos of the smartphone camera and 167 thermal photos of the Flir One.

The photos from the smartphone do not need any type of treatment, but the .RAW images need a specific treatment to transform an image in the infrared spectrum to another in the visible, in addition to equalizing the range of temperatures.

These .RAW files were taken with the Thermal Linear Flux14Bit Image mode, the difference with another image file is the number of tonal values that can be recorded. An image recorded in 14 bits (16,384 tonal values per channel) offers a number of advantages, not the least of which is helping to ensure smooth gradations of tone and colour within the image, even with the application of strong adjustments to the image. The bit depth is doubled for a 16-bit-per-channel image relative to an 8-bit-per-channel image, this means the actual file size will be double. Increasing the bit-per-channel of an image, the size will increase, but the low resolution of the Flir One causes that the size of a file is 160x120x2=38.400 Byte, a size unimportant for the storage capacity of a smartphone.

The treatment was split in 3 parts:

- Transformation .RAW to .png.
- Temperature normalization.
- Colouring .png files.

3.6.2.1 Transformation .RAW to .png

To do this a process was created called "*1.BatRAWtoPNG.bat*" that contain the next code:

```
for /l %%x in (1, 1, 167) do (
	echo %%x
	convert -size 120x160  -depth 16 gray:%%x.raw %%x.png
	convert %%x.png -auto-level %%x.png
)
```

This code consists in a loop that converts, using ImageMagick, the .RAW files with name numbered from 1 to 167, to .png files. To execute this line it was necessary to introduce the options size and depth of the original .RAW image. The Figure 81 shows a .png file created after this first line of code, in this figure image is observed as the histogram does not behave in an ideal way.

[31] ImageMagick® is a software suite to create, edit, compose, or convert bitmap images. It can read and write images in a variety of formats including PNG, JPEG, JPEG-2000, GIF, TIFF, DPX, EXR, WebP, Postscript, PDF, and SVG. Use ImageMagick to resize, flip, mirror, rotate, distort, shear and transform images, adjust image colors or apply various special effects. The version needed to execute this project is the Q16 to do the treatment of 16 bits images.

The options –level and –auto of ImageMagick resolve this problem of changing the brightness of the image by applying the correct values to the histogram expanding 16 Bit to visible range (Figure 81). With 16 Bit convert (Q16) we can simply stretch the brightness from 16*256=4096 to 238*256=60928.

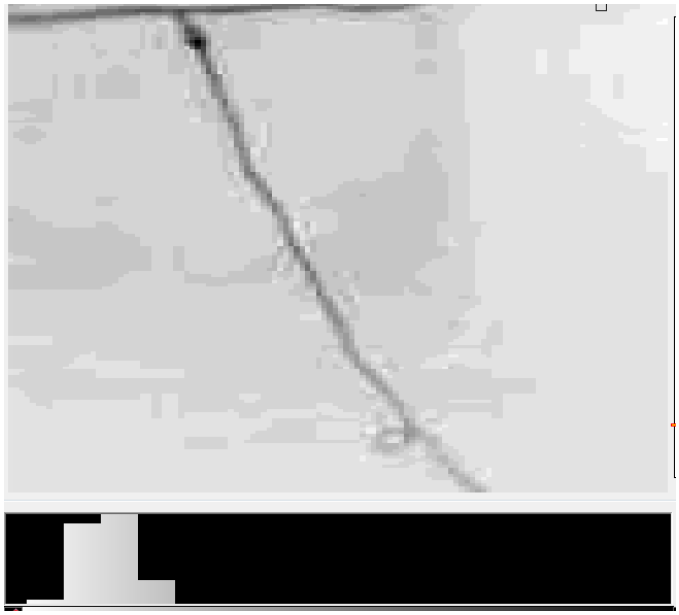

Figure 80. .RAW file transform to .png.

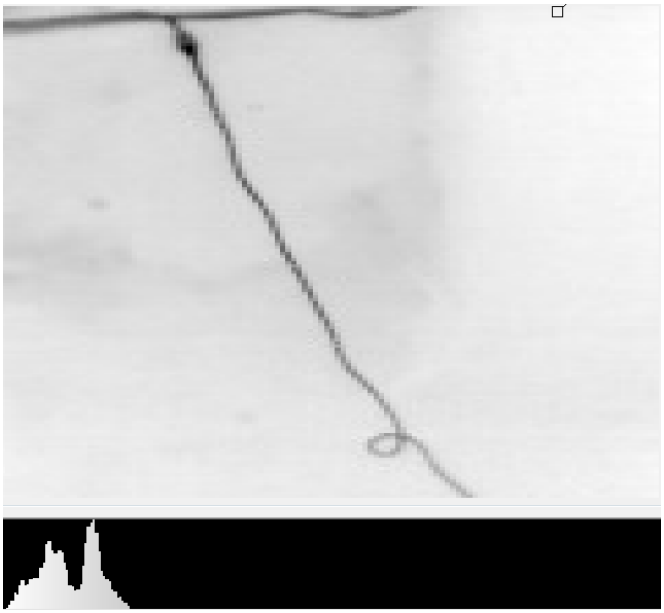

Figure 81. Histogram correction.

3.6.2.2 Temperature normalization

The next step is the normalization of the values of temperature to get a regular range of temperature of all the images. This step increases the size of the file. To execute this step it is necessary to install *Gawk* for Windows and introduce the path of the installation into the path of the system.

In order to find a correct range of temperatures for the representation the user needs to execute this line:

```
identify -verbose *r.png | grep -n5 statist | grep -e "max\|min" | sort -k3 -n | awk
"{ if (NR ==1) print} END {print}"
```

Obtaining this result:

```
17-      min: 11548 (0.176211)
1976-      max: 18040 (0.275273)
```

This values are necessaries in the next code:

```
for /l %%x in (1, 1, 167) do (
      echo %%x
      convert %%x.png -resize 480x -sharpen 0x1 -level 11500,18100 %%x.png)
```

Once the code is executed, the images have the range of temperature equalized (Figure 82). Thus, an object with the same temperature, as the lamp in the figure 82, in an overlap area of two or more photos has the same digital value of its pixels in all the photos.

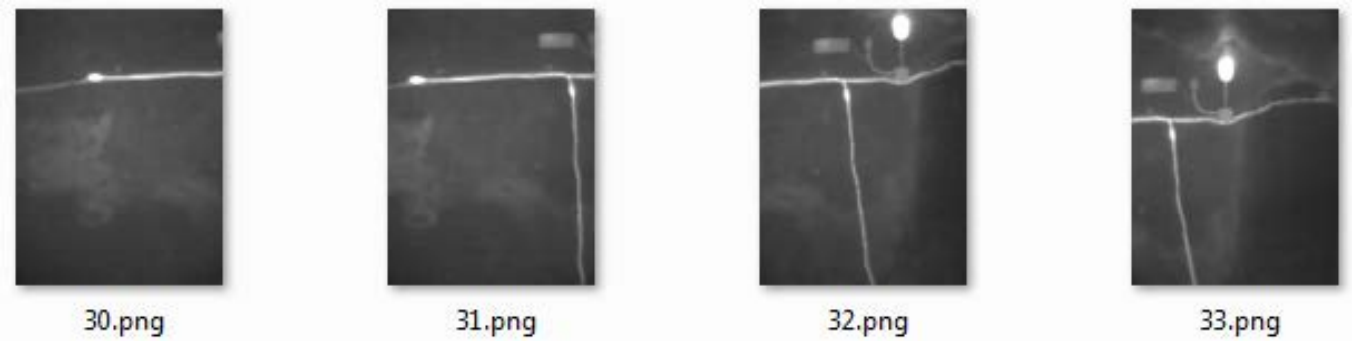

Figure 82. Thermal images with the same range of temperature.

3.6.2.3 Colouring .png files

In the last step another file .bat called "*2.BatColoringPNG.bat*" that contains this code was created:

```
exiftool FLIR0080.jpg -b -Palette > pal.raw
convert -size 224X1 -depth 8 YCbCr:pal.raw -separate -swap 1,2 -set colorspace YCbCr -combine -
        colorspace sRGB pal.png

for /l %%x in (1, 1, 167) do (
        echo %%x
        convert %%x.png pal.png -clut Coloring%%x.png
        convert -size 224X1 -depth 8 YCbCr:pal.raw -separate -swap 1,2 -set colorspace
                YCbCr -combine -colorspace sRGB -auto-level pals.png
        convert %%x.png pals.png -clut ColorBetter%%x.png
)
```

To apply a colour palette to the different images a colour table is necessary. This colour table was extract in this project from a test image (called "*FLIR0080.jpg*") of the Flir Tools software. This action is performed with the Exiftool software, creating a .RAW image of the palette.

The next step is to convert this .RAW file to .png, swapping the color space to YCbCr[32]. After this process the colour table can be visualized.

Figure 83. Color table.

[32] YCbCr is a family of color spaces used as a part of the color image pipeline in video and digital photography systems. Y' is the luma component and CB and CR are the blue-difference and red-difference chroma components. Y' (with prime) is distinguished from Y, which is luminance, meaning that light intensity is nonlinearly encoded based on gamma corrected RGB primaries.

Then, a loop was created to apply the colour to the radiometric image with a colour lookup table. (Figure 84). To improve the visualization one step was added to expand video pal colour table from [16,235] to [0,255] with -auto-level (Figure 85).

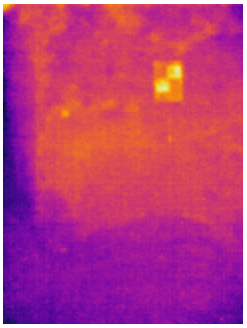

Figure 84. Image with colours.

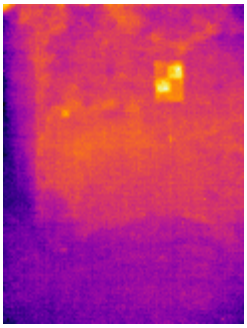

Figure 85. Improving the colours.

Finally, we can visualize the final results for the treatment of the thermal images:

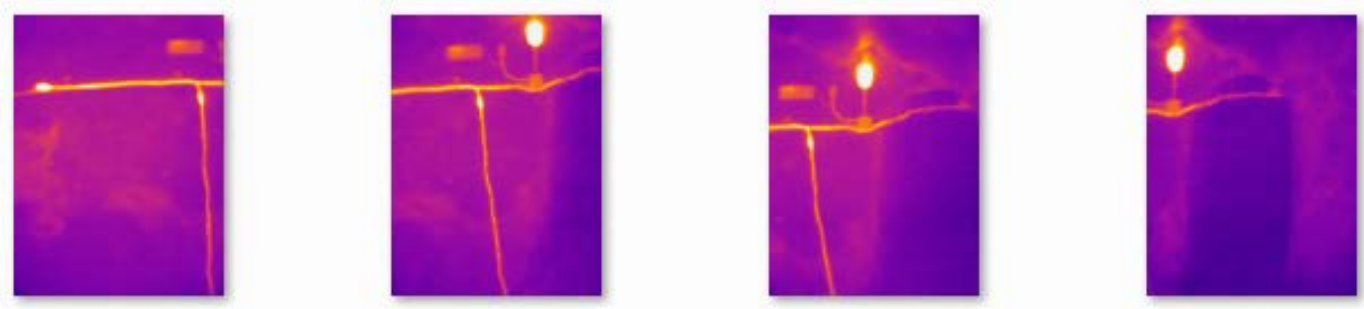

Figure 86. Thermal images with the range of temperature equalized and coloured.

Once the treatment process of the thermal image is completed, it is interesting to make a comparison with the photographs taken at same time with the smartphone camera using the HSKA Flir One App.

Figure 87. Visible images of Figure 87.

3.7 Creation of 3D Models

The creation of 3D models is split in two sections, from all raw data collected in silos:

- Creation of 3D model from laser scanner point clouds. This model was created in order to connect the silos with the tunnels constructed in the Spanish Civil War.
- Creation of 3D models from the HSKA Flir One App. From the raw data collected using the HSKA Flir One App different models were created:
  - Creation of 3D models from the visible images of the smartphone. Using the smartphone camera photos two 3D models were created, one of silo 1 and another of silo 3.
  - Creation of 3D models from MSX thermal images of the Flir One. With the MSX thermal images 3D models of the silos 1, 2 and 3 were created.
  - Creation of 3D models from RAW thermal images of the Flir One. Lastly, from the RAW thermal images models of silos 1 and 2 were performed.

Once the models have been created, from them a comparison of results will be performed. The laser scanner point clouds are courtesy of the groups 2, 5 and 6 (Table 6).

3.7.1 Creation of 3D model from laser scanner point clouds

The area of data collection for the thermal acquisition was the three first silos of the Valencian Silo-Yard in Burjassot, for this reason the area required for the laser scanner is the area of these silos. The different teams have given all the point clouds into the silos, so the first step is the visualization of all the point clouds and choose the point clouds that make up these three silos.

3.7.1.1 Registration

The process of registration of the point clouds was done with Faro Scene, the first step was to load all the scans to visualize it, in the figure 88 is shown the first scan loaded.

Figure 88. Visualization of the Scan "Silos000" in Faro Scene.

Once all the scans were displayed, the scans that included the three silos wew the scans "Silos011" to "Silos021", eleven point clouds with a size of 1.09GB. Then two clusters[33] were created to split the registration process. In this way it is possible to do individuals registration of areas, dividing the process for the computer. In this project two different areas to allow the visualization and registration on all this point clouds were created. To create a cluster the user only has to do a right button click in the main folder of the Workspace, and follow the path New/Cluster. To add point clouds to the Cluster the user only has to drag and drop them into the Cluster.

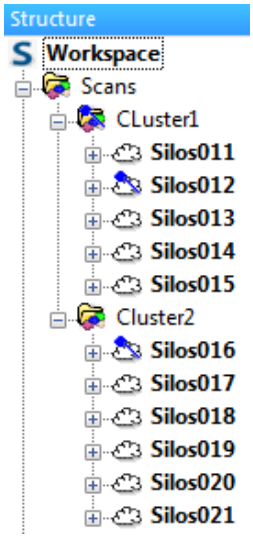

Figure 89. Structure in Faro Scene.

Once the clusters were created, the next step was to find the targets placed in the scene to connect the different point clouds. These targets were checkerboards of paper and spheres of polyethylene.

Faro Scene has a feature to auto detect most targets, pressing the right button of the mouse into a point cloud in the Structure and following this path, Operations / Find Objects / Checkerboards for the checkerboards and Operations / Find Objects / Spheres for the spheres. This process is repeated in all the point clouds and was mandatory to check the view of each point cloud to make sure that all the objects were found.

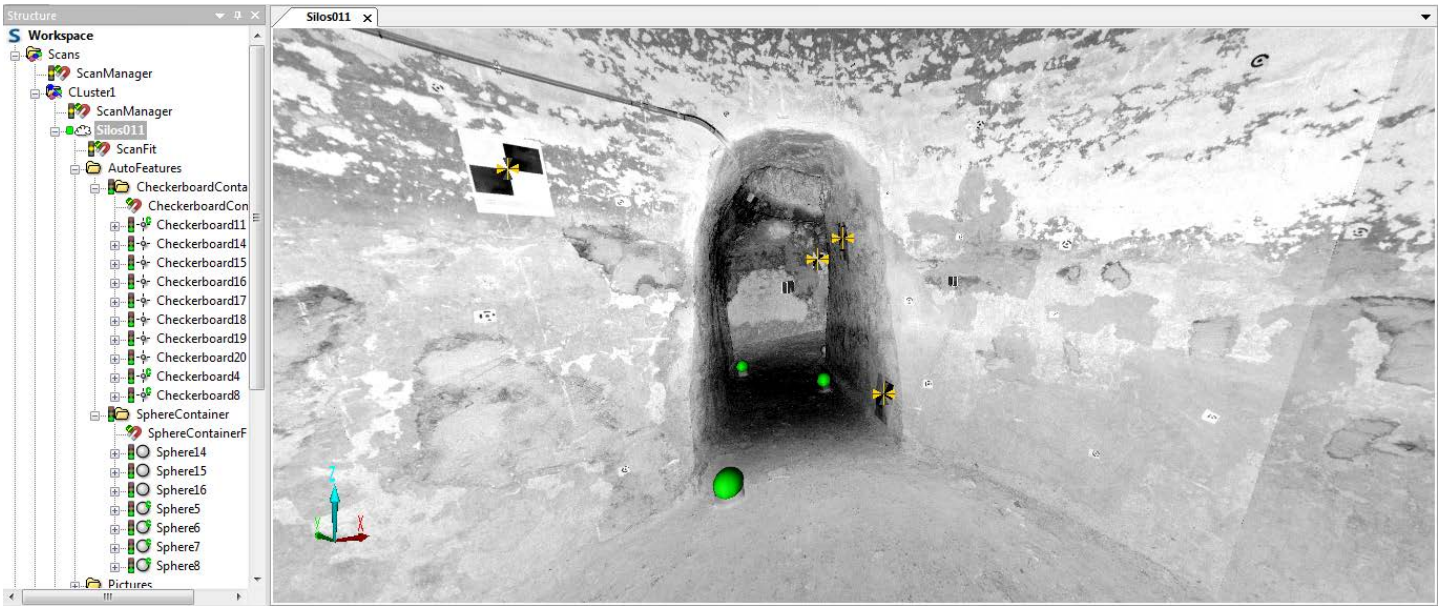

Figure 90. Review of the autodetected objects.

After the location of all the objects was found, the place of scans was performed. In that case it was done in three steps.

1. Place scans for the first cluster. To place scans the user has to follow this path, clicking with the right button in a cluster, Operations / Registration / Place Scans.

[33] A cluster usually collects scans which somehow belong together, for example scans which were recorded on the same floor of a building, or scans which were taken in the same room.

When the user presses the *Place Scans* feature different options are shown. For this project the chosen options are the following:

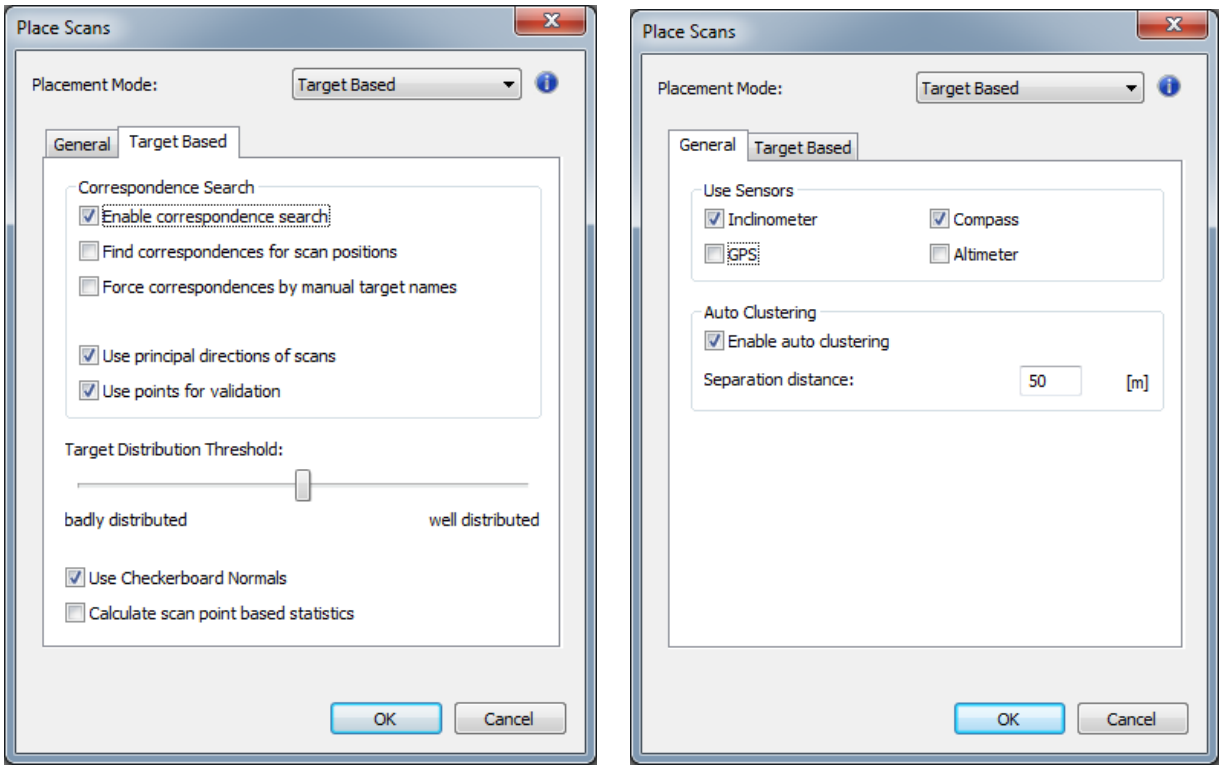

Figure 91. Place Scans options.

After this operation the silos 3 and 2 can be visualized (Figure 92).

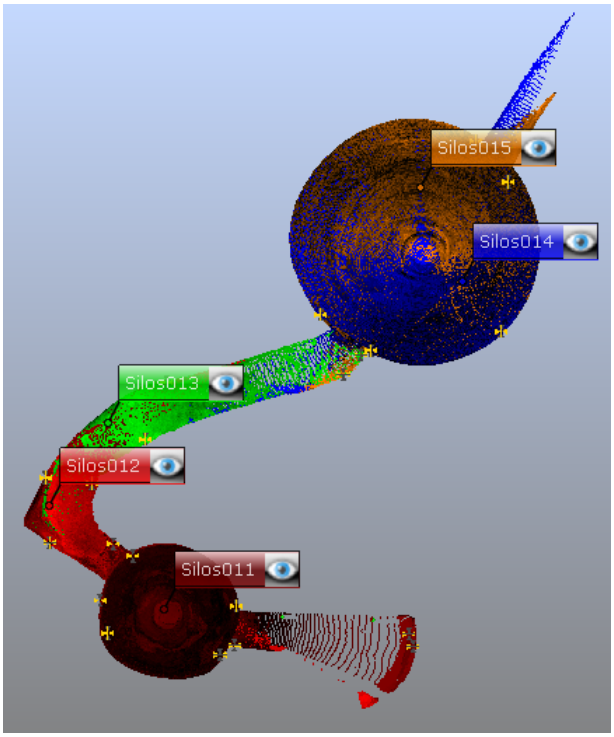

Figure 92. Point clouds of the silos 2 (top) and 3 (down).

2. Place scans for the second cluster, with the same methodology applied in the first step (Figure 93).
3. Finally the same method is used to join both scans, clicking in the main folder in that case and doing a registration between clusters (Figure 94).

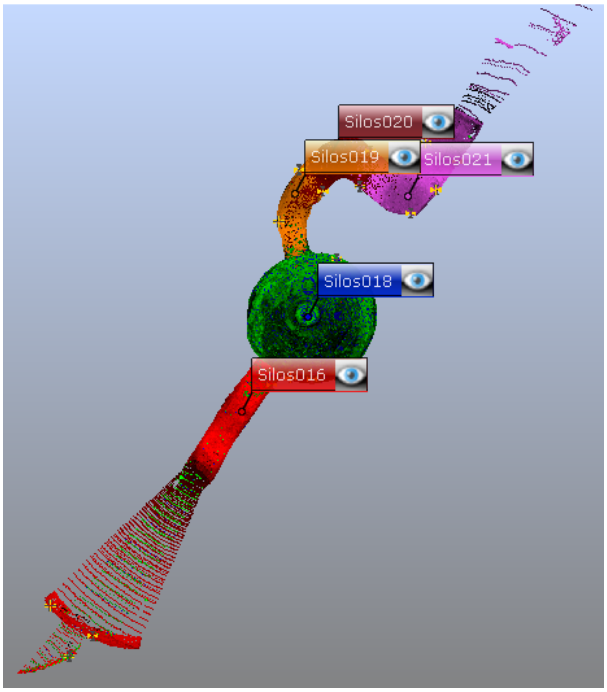

Figure 93. Point clouds of the silo 1.

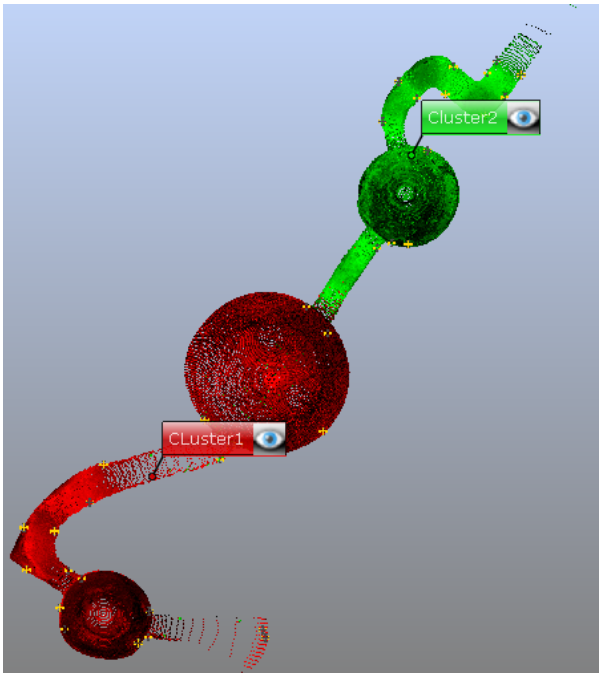

Figure 94. Visualization of the complete registration of the silos 1 (down), 2 (center) and 3 (top).

The registration report is shown in Annex 3, thanks to it some information could be extracted, such as the mean error of 0.0046m, with a standard deviation of 0.0082m, a minimum of 0.0000m, and a maximum of 0.0319m. These statistics indicate that the point cloud registration is optimal.

3.7.1.2 Size reduction

After the registration process the point clouds were exported to a .PTX file including the eleven point clouds. These point clouds have a size of 12.957.433 KB, due to the size of this file, the treatment becomes very complex. To fix the problem the first step was to perform a process of subsample. This process was done using the software CloudCompare.

To subsample the point clouds the user has to import the .PTX file in CloudCompare and access the subsample tool via the “Edit/Subsample” menu. Several subsampling methods are available (random, spatial and octree[34]-based). In this project the octree-based method was used. The 'octree' mode lets the user select a level of subdivision of the octree at which the cloud will be 'simplified'. In each cell of the octree, the nearest point to the octree cell center is kept. In this project the subdivision level was 10 (Figure 95).

[34] An octree is a tree data structure in which each internal node has exactly eight children. Octrees are most often used to partition a three dimensional space by recursively subdividing it into eight octants. Octrees are the three-dimensional analog of quadtrees.

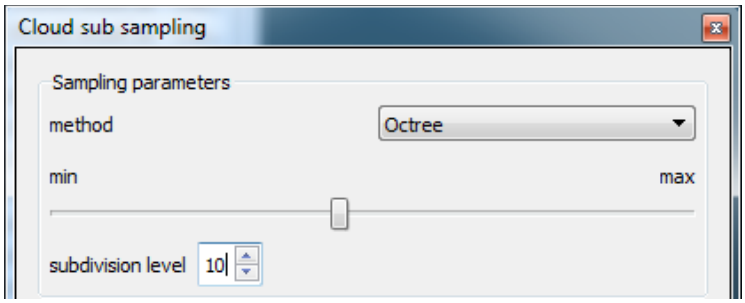

Figure 95. Cloud sub sampling.

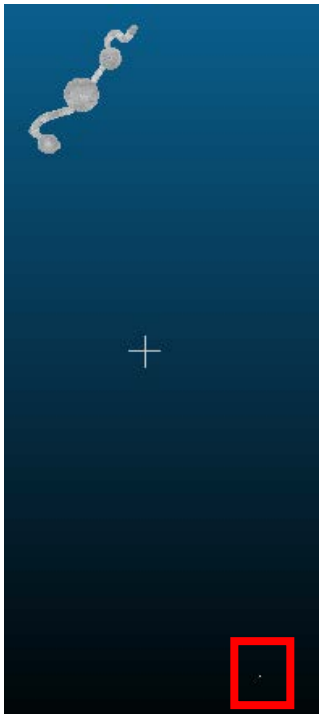

Figure 96. Outliers in the point cloud "Silos020".

During this process different outliers were detected in the point cloud called “Silo020”. For this reason it was necessary to use the tool “Cross Section”. This tool allows the user to define a clipping box around a given cloud. The box extents and orientation can be adjusted in order to segment the cloud for instance.

Once the clipping box was chosen, the button “Export selection as a new point cloud” was pressed.

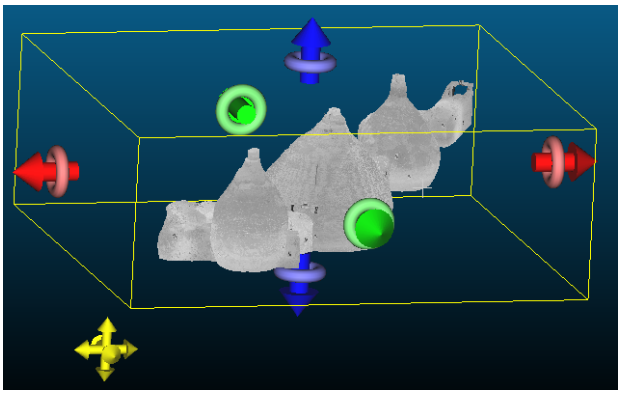

Figure 97. Clipping box.

The last process before the exportation was the merge of the 11 point clouds with the tool “Merge multiple clouds”.

Finally the point clouds were exported to a .e57 file having a size of 197.022 KB. This means that the size was reduced by a percentage of 98.48%.

3.7.1.3 Creation of the mesh

The mesh creation was done using the software 3DReshaper. The first step was to create a rough mesh using the tool “3D Mesh”, setting 0.06m for the average triangle size and keeping the default parameters for holes detection. After the rough mesh process, the silos can be represented using the option “Flat + Wire” to visualize the triangles created (Figure 98). The first rough mesh is composed of regular triangles, covering the entire surface of the point cloud. In the next steps, this mesh was refined in order to add the details present in the cloud.

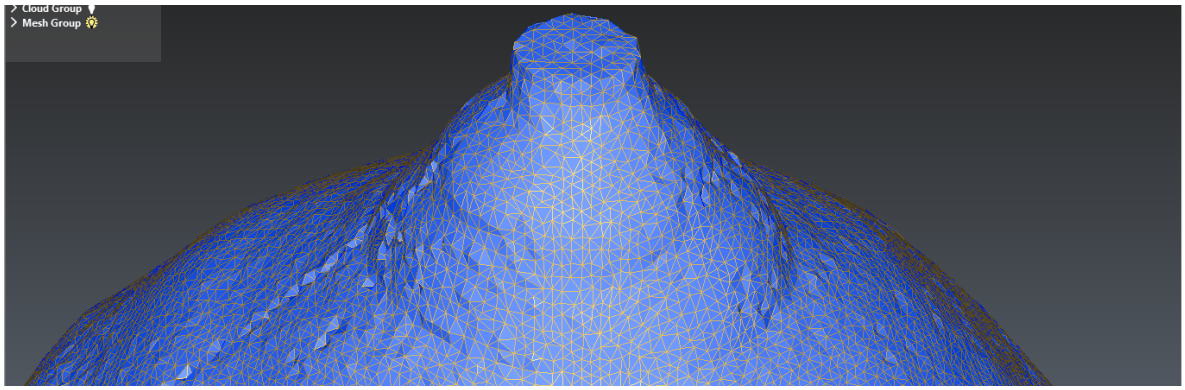

Figure 98. Rough mesh.

The next mesh was done using the tool “Refine Mesh, from a point cloud”, to activate this tool the user must select the point cloud and the mesh created in the previous step. This tool was executed using the method “Take points of the cloud” with a “Deviation error with best points only” of 0.001 and a “Outlier point distance” of 0.01. This function adds real points from the cloud inside the mesh, and the smaller the deviation error is, the more details that appear in the mesh.

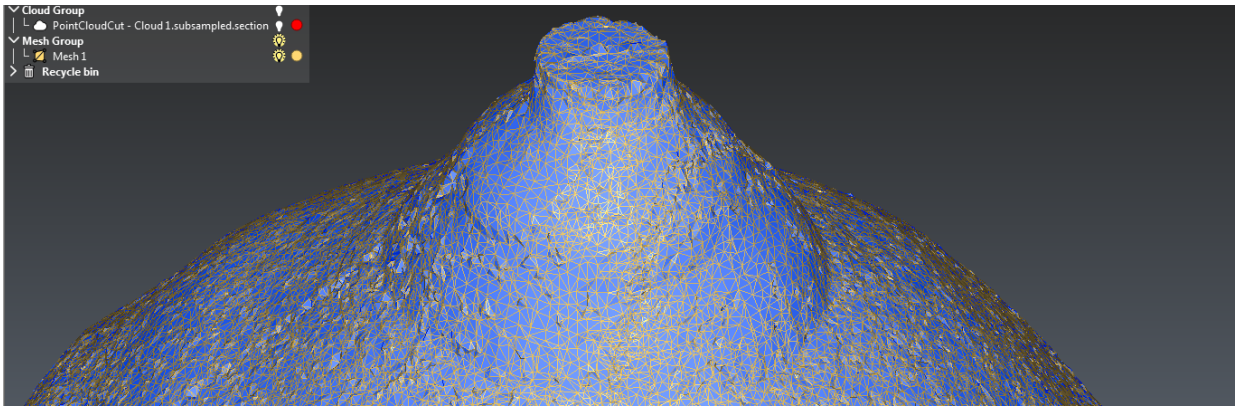

Figure 99. Mesh refined.

Figure 99 shows as this step creates more detail, but as the real points have been added to the mesh, its aspect is quite noisy. To solve this problem, a second refinement was done using again the tool “Refine Mesh, from a point cloud”. In that case the method used was “Interpolate new points” with a “Deviation error with best points” of 0.0005, a “Minimum triangle size” of 0.001 and an “Outlier point distance” of 0.001, activating the option “Local reorganization”.

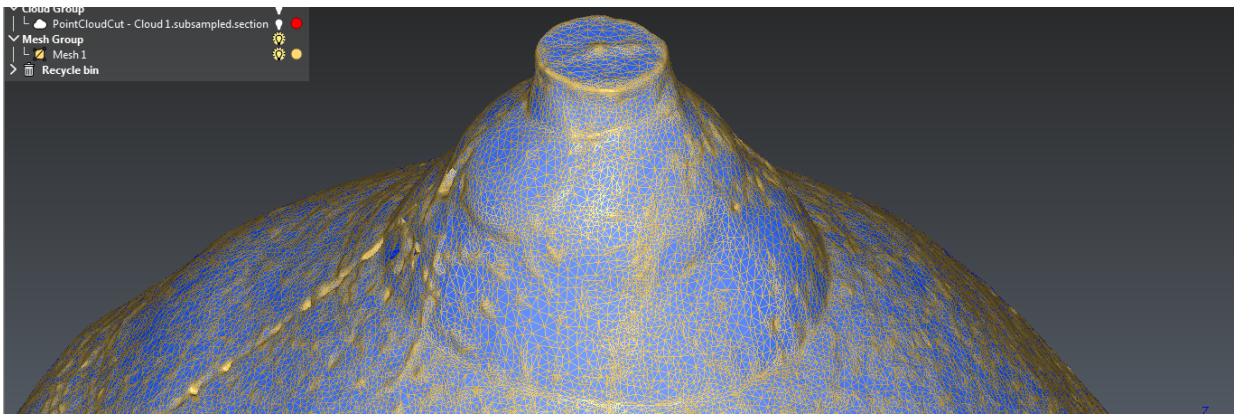

Figure 100. Second refine of the mesh.

The lack of data in the point cloud created different holes in the mesh, to fix them a process of "Fill holes" was performed. These small holes were selected automatically by the software and using the default options for the curvature filling, these holes were closed, creating a continuous surface, but without fill the holes of entrance and exit of the tunnel. After this step it was exported to a .OBJ file in order to import it into the visualization of the project.

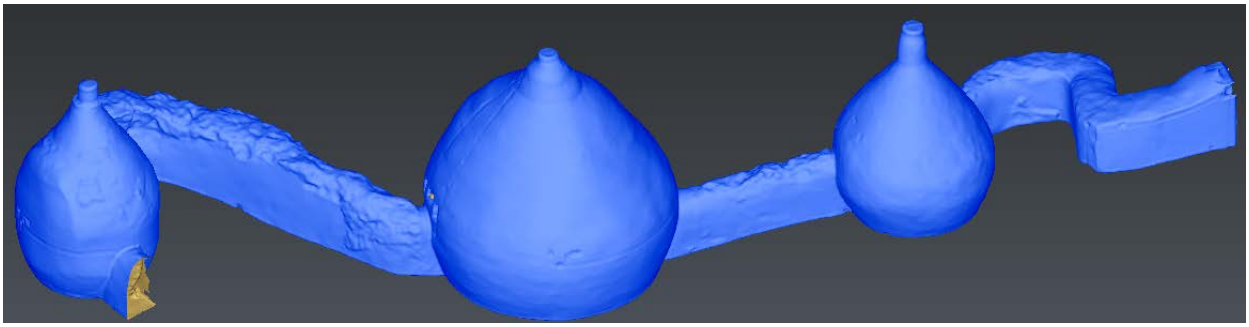

Figure 101. View of the final mesh.

3.7.2 Creation of 3D models from the HSKA Flir One App

During the campaign in Burjassot different types of photos were taken using the HSKA Flir One App. This types of photos were the following:

- Visible images from the smartphone camera.
- MSX thermal images from the Flir One.
- RAW thermal images from the Flir One.

These different photos have been used to create different 3D models in order to perform different models with multispectral information, besides to compare the geometric errors obtained in the models using the smartphone visible camera or the Flir One thermal camera. The visible images would be the geometric reference, due to the higher resolution of the sensor. Another 3D model was created with the MSX thermal images in order to know the reliability of the models created only using the Flir One Camera. Finally, the RAW thermal images were used to project them on the 3D model built from the visible images of the smartphone camera, obtaining a multispectral texture with the geometry of a smartphone camera with higher resolution than the Flir One.

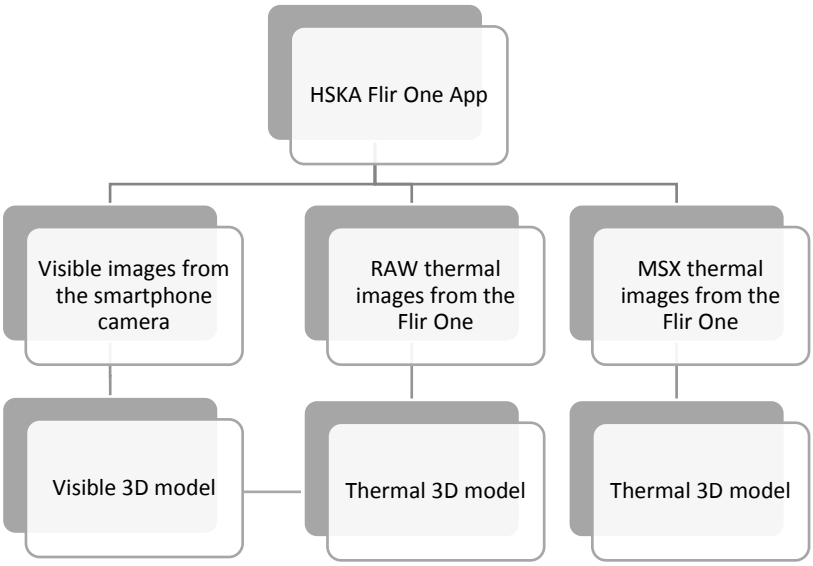

Figure 102. Diagram of the 3D models created from the HSKA Flir One App data.

3.7.2.1 Creation of 3D model from the visible images of the smartphone

To make the whole process of creation of the 3D models from the smartphone the software Agisoft PhotoScan was used. Agisoft PhotoScan is an advanced image-based 3D modelling solution aimed at creating 3D content from still images. Based on the latest multi-view 3D reconstruction technology, it operates with arbitrary images and is efficient in both controlled and uncontrolled conditions. Photos can be taken from any position, providing that the object to be reconstructed is visible on at least two photos.

The first step was the calibration of the camera using the software Agisoft Lens that estimates both internal and external camera orientation parameters, including nonlinear radial distortions. Using the screen of a personal computer different photos were taken with different angles.

Figure 103. Different photos of the camera calibration.

The camera calibration file was exported to a .xml file, this file was imported to the camera calibration menu of PhotoScan in order to use the camera calibration in all the processes of generation of the 3D model.

3.7.2.1.1 Visible 3D model of the silo 1

PhotoScan allows one to perform a general workflow creating batch processes to automate the task of creation of 3D models. The workflow used to create the 3D model of the silo 1 started by adding the 84 photos taken in the silo 1. Then, the creation of the batch process was made, this feature is found via Workflow/Batch Process. In this workflow the first step was the option “Align Photos”, once photos are loaded into PhotoScan, they need to be aligned. At this stage PhotoScan finds the camera position for each photo and builds a point cloud model, in the settings the accuracy value was changed to “Highest” value, in order to improve the camera position estimation. The values of the option “Key point limit”, upper limit of feature points on every image to be taken into account during current processing stage, and the option “Tie point limit”, upper limit of matching points for every image, were the default values.

Settings:

Property	Value
General	
Accuracy	Highest
Pair preselection	Disabled
Advanced	
Key point limit	40000
Tie point limit	4000
Constrain features by mask	No

Figure 104. Align Photos settings.

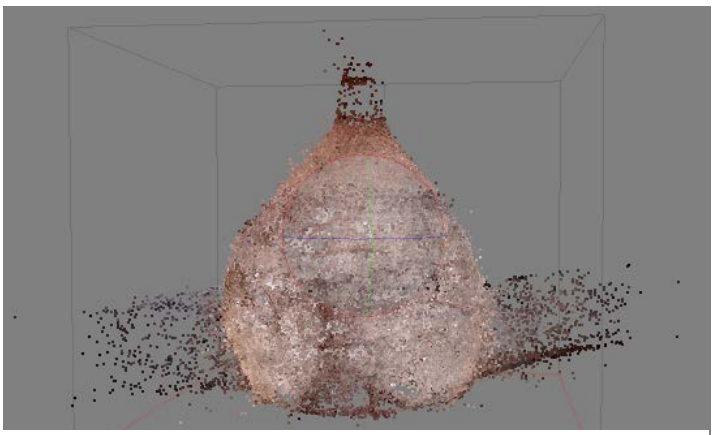

Figure 105. Tie points of the silo 1.

After this process the tie points are created, during the align process 79.583 points were created.

The next job added to the batch process was the tool "Build Dense Cloud". Based on the estimated camera positions the program calculates depth information for each camera to be combined into a single dense point cloud. PhotoScan tends to produce extra dense point clouds, which are of almost the same density. In that case, the quality of this process was increase to "Ultra high". The "Depth filtering" option is used because at the stage of dense point cloud generation reconstruction PhotoScan calculates depth maps for every image. Due to some factors, like noisy or badly focused images, there can be some outliers among the points. In that case, the "Aggressive" depth filtering mode was chosen to sort out most of the outliers.

Settings:

Property	Value
General	
Quality	Ultra high
Advanced	
Depth filtering	Aggressive
Reuse depth maps	No

Figure 106. Build Dense Cloud settings.

In this process the point cloud was increased up to 21.071.447 points.

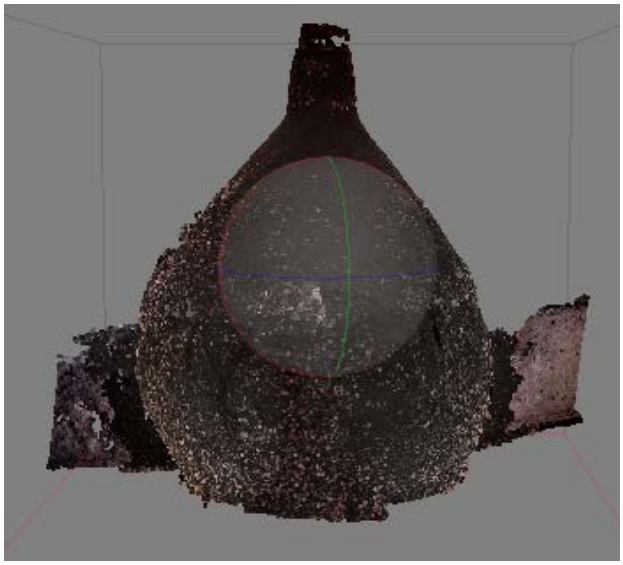

Figure 107. Dense cloud of the silo 1.

After the "Build Dense Cloud" process, the next process executed was the "Build Mesh". The mesh is a collection of vertices, edges and faces that defines the shape of a polyhedral object in 3D computer graphics and solid modelling. In the settings window the face count was changed to "High" in order to increase the maximum number of polygons in the final mesh. The surface type was "Arbitrary" and the source data was from the dense cloud created in the last step.

Settings:

Property	Value
General	
Surface type	Arbitrary
Source data	Dense cloud
Face count	High
Custom face count	200000
Advanced	
Interpolation	Enabled (default)
Point classes	All

Figure 108. Mesh settings.

This mesh was smoothed using the "Smooth Mesh" tool with a parameter of 3 passes. After that, a process of close holes was performed in order to close small holes created by lack of information, this step used a level of 95 in order to close most holes without affect to the ground or the tunnel which must remain as a hole, the figure 109 shows the model without holes. The final process of the batch was "Build texture", following the default settings obtaining the figure 110.

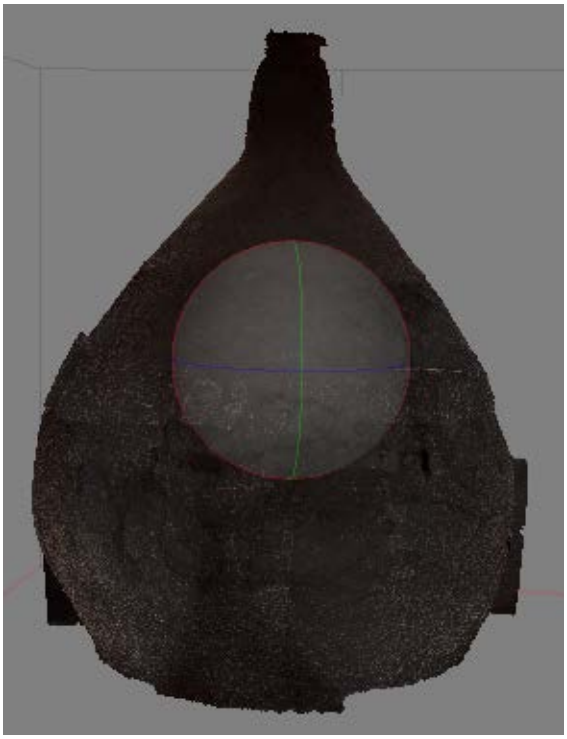

Figure 109. 3D model of the silo 1.

Figure 110. Model 3D textured of the silo 1.

Once the textured model was created, the process of inserting different marks with known coordinates in order to position and scale the model was done. The coordinates were extracted from the different point clouds registered (Part 3.7.1.1) knowing that positioning errors of the points from laser scanner registration were accumulated to errors of 3D models created. This process was done with the software Cyclone due to its fast process of point cloud loading.

In this process the coordinates were taken from the laser scanner targets, taking 3 coordinates per target.

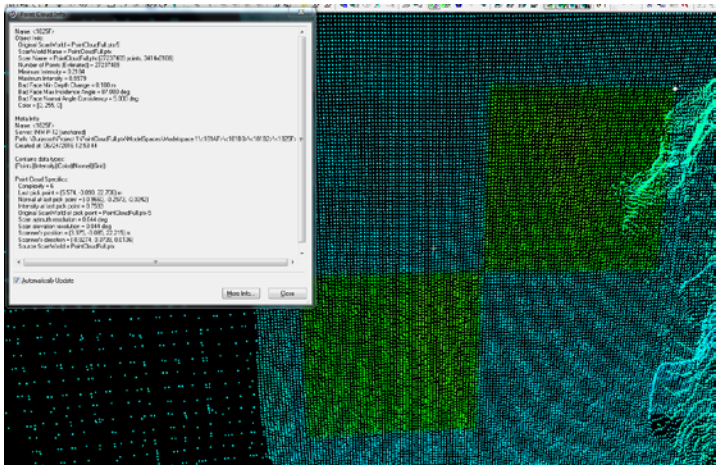

Figure 111. Point coordinates in Cyclone.

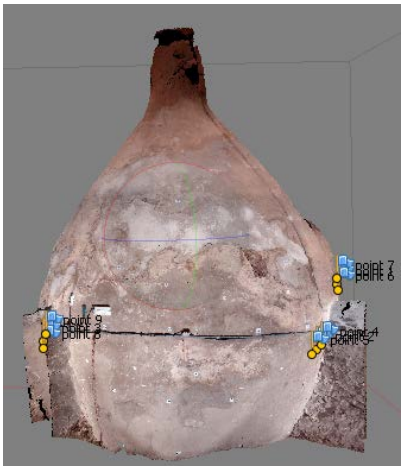

Figure 112. Location of marks.

Once the model is scaled, the user can see the errors made in the model. These error are visualized in the next table. The mean error in meters in the marks position is 0.019m, an optimal result knowing the characteristics of the smartphone camera.

Markers	X (m)	Y (m)	Z (m)	Accuracy (m)	Projections	Error (pix)	Error (m)
point 3	18.071000	17.802000	21.829000	**0.005000**	6	0.028	0.006493
point 2	17.204000	13.572000	21.506000	**0.005000**	5	0.036	0.027904
point 4	17.110000	13.546000	21.592000	**0.005000**	5	0.037	0.020990
point 5	17.292000	13.627000	21.422000	**0.005000**	5	0.037	0.021222
point 8	17.976000	17.821000	21.733000	**0.005000**	6	0.037	0.005449
point 9	18.159000	17.773000	21.926000	**0.005000**	6	0.043	0.011252
point 1	16.461000	13.633000	22.621000	**0.005000**	6	0.049	0.019541
point 7	16.382000	13.681000	22.716000	**0.005000**	4	0.075	0.030222
point 6	16.544000	13.578000	22.524000	**0.005000**	6	0.083	0.015118
Total Error						**0.050**	**0.019413**

Table 7. Errors in the visible model of the silo 1.

Lastly, the 3D model was exported with its textures as Wavefront OBJ (.obj file). The textures were exported in JPEG. The model created can be visualized in a plane in annex I (Visible orthophoto of the Silo No. 1)

Ultimately with the 3D model exported is possible to build a comparison with the mesh made using the point cloud. This comparison was performed using the software CloudCompare. The next figure shows a colored silo with the distance error between the both models, this comparison was possible because the relative coordinates added to the model of the smartphone were extracted from the point cloud.

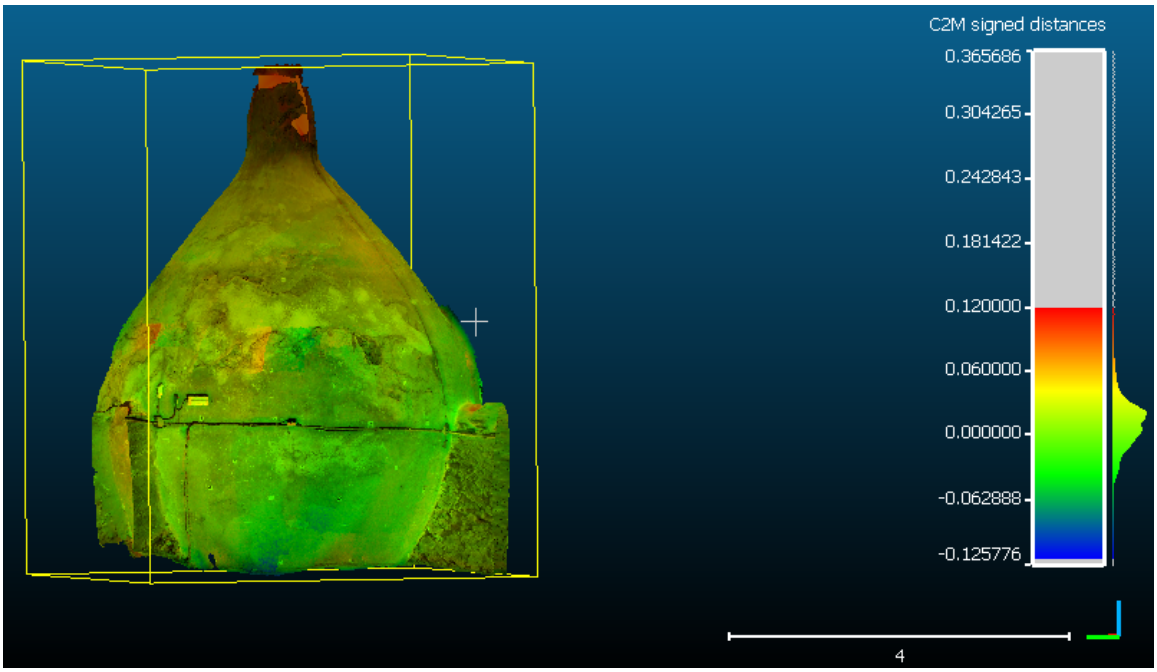

Figure 113. Comparison between the visible 3D model and the point cloud 3D model of silo 1.

In this comparison the maximum error is located in the cap of the silo for the lack of overlap, but it is possible to fit a Gaussian distribution in order to know the mean error and the standard deviation of

the distances between the two meshes. The mean was 0.009280 meters and the standard deviation 0.027801 meters with 1 σ, 68.27% of the values (Figure 114).

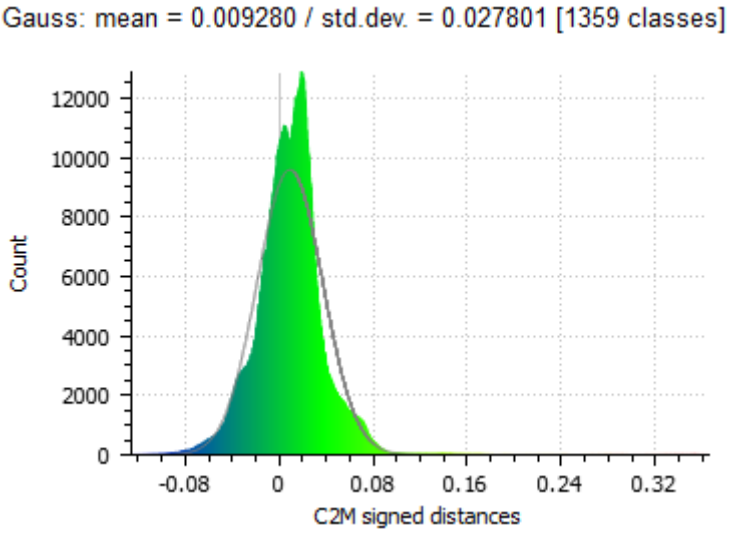

Figure 114. Distributtion fitting of the errors between the point cloud model and the smartphone camera model of silo 1.

3.7.2.1.2 Visible 3D model of the silo 3

In silo 3 the same process was performed with 83 photos, obtaining a first point cloud with 72.085 points. The "Dense cloud" process increased the point cloud until 21.226.246 points. This model has an error of 0.008m, an optimal result for a camera of 5 megapixel of resolution.

Markers	X (m)	Y (m)	Z (m)	Accuracy (m)	Projections	Error (pix)	Error (m)
point 1	5.081000	-4.440000	22.250000	0.005000	8	0.012	0.005649
point 8	1.821000	-3.876000	21.705000	0.005000	3	0.024	0.008473
point 10	1.533000	-2.830000	22.554000	0.005000	7	0.024	0.002841
point 2	5.130000	-4.357000	22.158000	0.005000	8	0.025	0.002744
point 3	5.023000	-4.520000	22.345000	0.005000	7	0.031	0.006617
point 4	5.558000	-2.995000	22.610000	0.005000	7	0.033	0.003000
point 5	5.574000	-3.090000	22.706000	0.005000	9	0.034	0.008787
point 7	1.760000	-3.791000	21.793000	0.005000	3	0.036	0.006928
point 6	5.541000	-2.900000	22.516000	0.005000	8	0.045	0.004066
point 12	1.548000	-2.734000	22.649000	0.005000	7	0.051	0.003327
point 9	1.694000	-3.709000	21.877000	0.005000	3	0.058	0.019791
point 11	1.515000	-2.926000	22.458000	0.005000	6	0.068	0.012423
Total Error						**0.039**	**0.008519**

Table 8. Errors in the visible model of the silo 3.

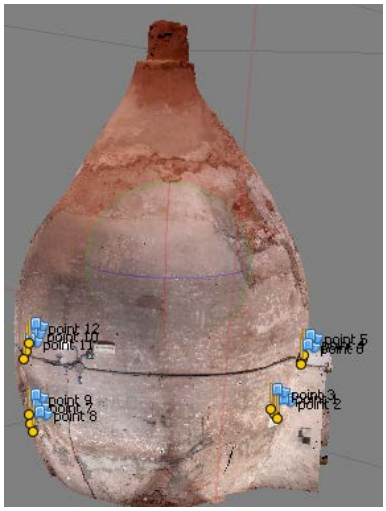

Figure 115. 3D model of the silo 3.

The final orthophoto could be visualized in the Annex I (Visible orthophoto of the Silo No. 3).

The comparison between the point cloud and the model created is similar to the silo 1, where the bigger errors are located in the cap of the silo.

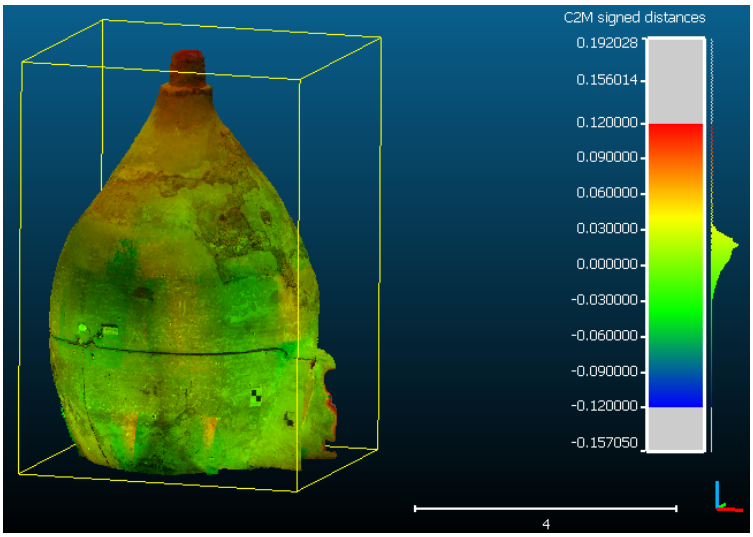

Figure 116. Comparison between the visible 3D model and the point cloud mesh of silo 3.

In that case the mean was 0.009462 meters and the standard deviation was 0.022226 meters (68%). The mean increased respect the silo 1 but the standard deviation decreased (Figure 117).

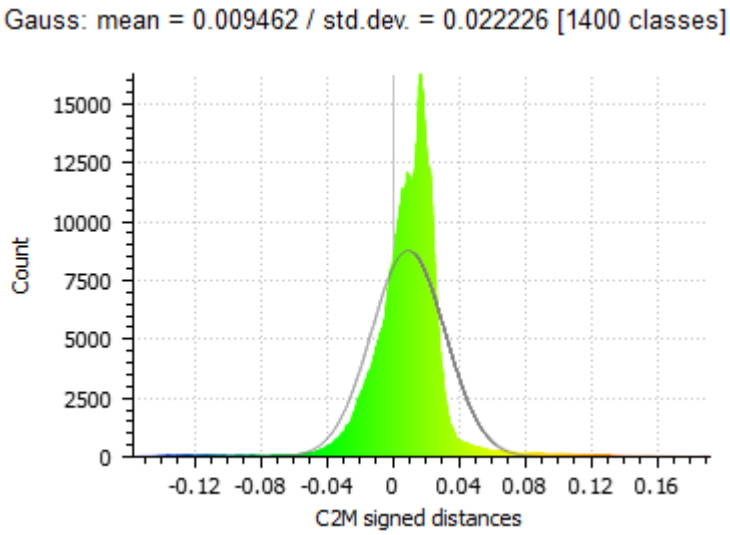

Figure 117. Distributtion fitting of the errors between the point cloud mesh and the smartphone camera model of silo 3.

3.7.2.2 Creation of 3D model from MSX thermal images of the Flir One

The same process was followed to create the 3D models of the thermal images with a change, due to the impossibility of calibrating the thermal camera this step was passed. The main idea of this project was to calibrate the thermographic camera using a 3D grid printed using a 3D printer following the PhotoModeler pattern with an A4 size and minimum thickness to reduce the possible shadows (0.5mm), this grid has holes instead of targets, the calibration process to follow was heating the pattern and placing it on a cold surface, the contrast of heat would detect the targets to calibrate the thermal camera. But finally, the breakdown of the 3D printer of the Universitat Politècnica de València prevented the creation of the calibration grid.

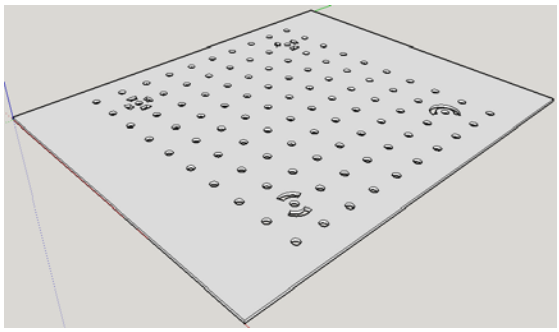

Figure 118. Calibration grid.

Other solutions were referred as heat a sheet of paper with the grid printed, but the low resolution of the thermal sensor of the Flir One prevented to make a correct calibration of the camera because the different software used did not detect the targets of the calibration grid.

3.7.2.2.1 Thermal 3D model of the silo 1

To create the thermal model of silo 1, 334 photos were taken with the HSKA Flir One App, obtaining a first point cloud with 79.093 points. The "Dense cloud" process increased the point cloud until 4.306.694 points. In the next figure the model is shown with a color table range of 18°C to 30°C. In that case the model has an error of 0.025m, this error increases with respect to the visible models due to the low resolution of the Flir One.

Markers	X (m)	Y (m)	Z (m)	Error (pix)	Error (m)
point 5	17.292000	13.627000	21.422000	0.000	0.004858
point 3	18.071000	17.802000	21.829000	0.011	0.004511
point 1	16.461000	13.633000	22.621000	0.012	0.014664
point 9	18.159000	17.773000	21.926000	0.013	0.007854
point 8	17.976000	17.821000	21.733000	0.015	0.006162
point 7	16.382000	13.681000	22.716000	0.021	0.019332
point 6	16.544000	13.578000	22.524000	0.029	0.018047
point 4	17.110000	13.546000	21.592000	0.062	0.038707
point 2	17.204000	13.572000	21.506000	0.063	0.055195
Total Error				**0.031**	**0.024951**

Table 9. Errors in the thermal model of the silo 1.

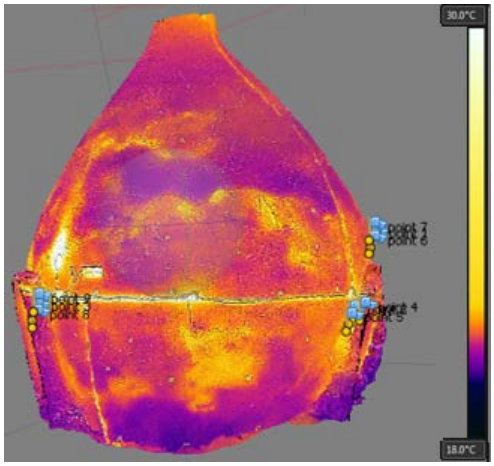

Figure 119. Thermal 3D model of the silo 1.

In the comparison with the laser scanner mesh the thermal 3D model gets bigger distance that the visible 3D models created with the smartphone camera, predictably by the resolution of the sensor. The errors obtained in the different markers located in PhotoScan suggest a worst geometrical accuracy, and the comparison certifies it, obtaining the same range of maximum errors ±12cm but with a mean range higher than the visible models.

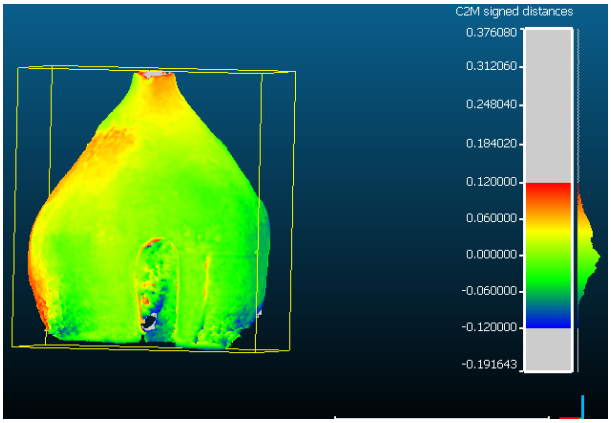

Figure 120. Comparison between the thermal 3D model and the point cloud mesh of silo 1.

This model has a mean of 0.010355 meters and a standard deviation of 0.047080 meters (68%). Comparing with the visible smartphone model the mean error and standard deviation increase, this error would decrease in case of use a better smartphone camera, confirming the main idea of this project, to project thermal images on the model created with the camera smartphone in order to get the better model geometry with a thermal texture.

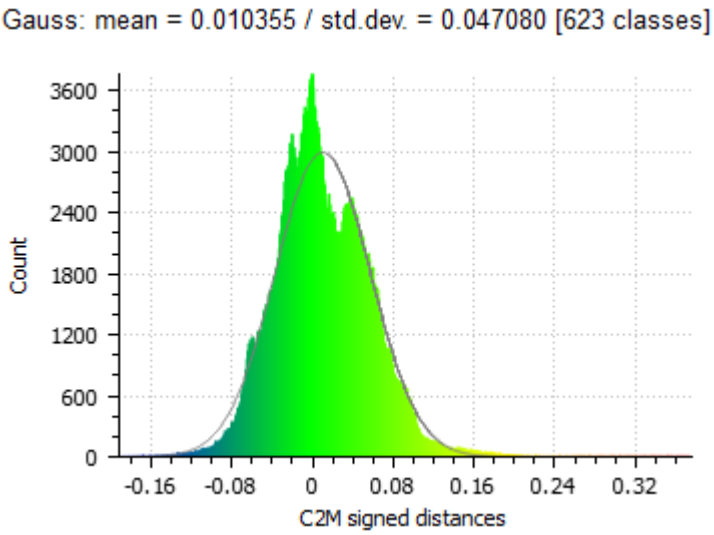

Figure 121. Distributtion fitting of the errors between the point cloud mesh and the Flir One camera model of silo 1.

The final orthophoto could be visualized in the Annex I (Thermal orthophoto of the Silo No. 1).

3.7.2.2.2 Thermal 3D model of the silo 2

In silo 2, 187 photos were taken obtaining a first point cloud with 107.220 points. The “Dense cloud” process increased the point cloud until 4.020.443 points. In that case the model has an error of 0.017m (Table 10).

Markers	X (m)	Y (m)	Z (m)	Error (pix)	Error (m)
point 5	13.380000	5.133000	21.111000	0.007	0.005785
point 2	8.040000	5.625000	21.113000	0.009	0.008985
point 14	12.543000	10.811000	20.833000	0.010	0.020408
point 10	7.978000	5.703000	21.207000	0.010	0.022429
point 9	8.105000	5.564000	21.019000	0.011	0.017569
point 6	13.438000	5.214000	21.010000	0.012	0.015392
point 3	12.629000	10.769000	20.925000	0.012	0.004968
point 8	9.439000	4.592000	20.675000	0.013	0.028179
point 11	13.322000	5.062000	21.197000	0.014	0.008182
point 15	12.709000	10.733000	21.013000	0.016	0.011755
point 7	9.631000	4.559000	20.497000	0.023	0.020755
point 1	9.533000	4.580000	20.590000	0.027	0.024868
Total Error				**0.015**	**0.017446**

Table 10. Errors in the thermal model of the silo 2.

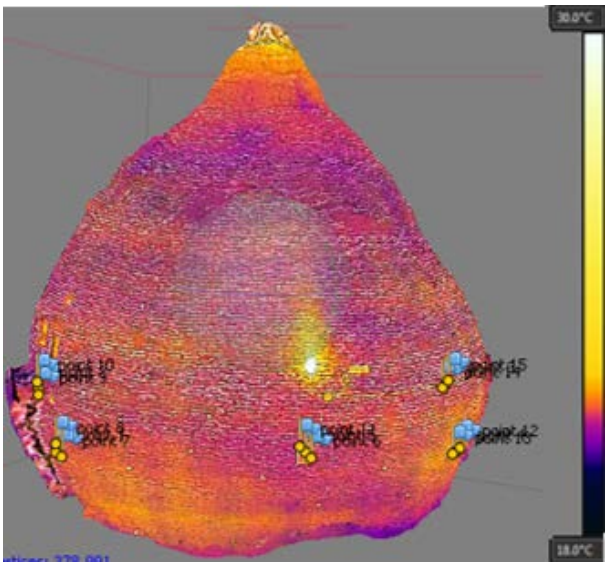

Figure 122. Thermal 3D model of the silo 2.

The errors are similar than the model 1. But it is necessary to perform a distances analysis.

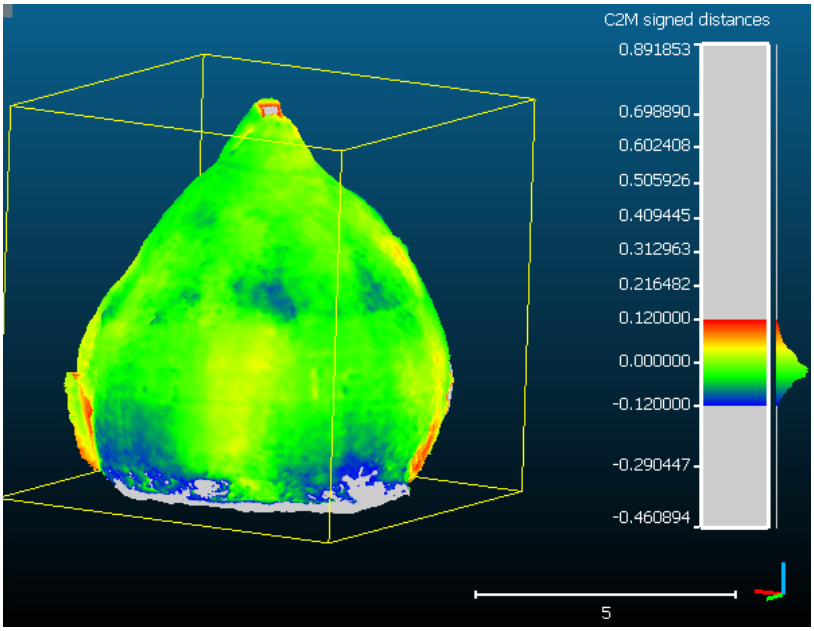

Figure 123. Comparison between the thermal 3D model and the point cloud mesh of silo 2.

In that case the mean was -0.014524 meters and the standard deviation 0.063376 meters. This model has the worst errors due to the lack of photos and larger size of silo 2. In that case 187 photos were taken, meanwhile silos 1 and 3 were taken more than 300 photos in each one.

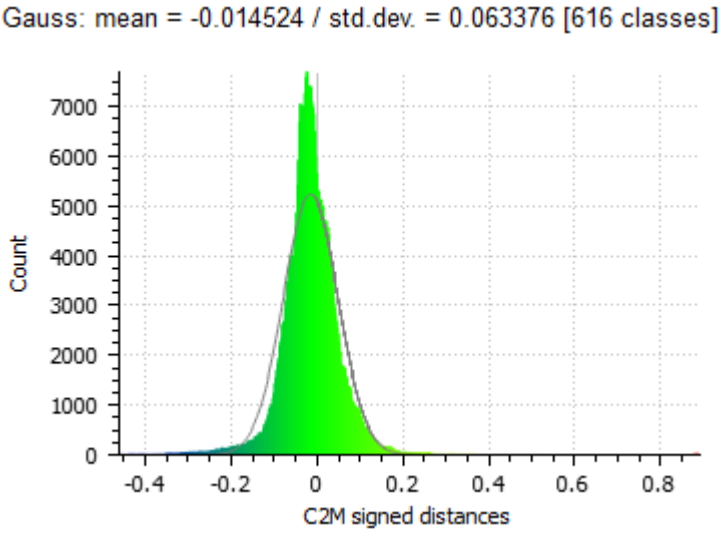

Figure 124. Distributtion fitting of the errors between the point cloud mesh and the Flir One camera model of silo 2.

3.7.2.2.3 Thermal 3D model of the silo 3

A total of 445 images were taken in silo 3, creating a first point cloud with 127.943 points. The “Dense cloud” process increased the point cloud until 5.585.339 points. In that case the model has an error of 0.010m, the best accuracy obtained in this project for a thermal model.

Markers	X (m)	Y (m)	Z (m)	Error (pix)	Error (m)
point 12	1.548000	-2.734000	22.649000	0.007	0.004126
point 10	1.533000	-2.830000	22.554000	0.008	0.005896
point 11	1.515000	-2.926000	22.458000	0.010	0.011811
point 9	1.694000	-3.709000	21.877000	0.010	0.011033
point 7	1.760000	-3.791000	21.793000	0.011	0.006193
point 4	5.558000	-2.995000	22.610000	0.012	0.009487
point 6	5.541000	-2.900000	22.516000	0.012	0.015399
point 1	5.081000	-4.440000	22.250000	0.013	0.009618
point 8	1.821000	-3.876000	21.705000	0.013	0.007873
point 5	5.574000	-3.090000	22.706000	0.014	0.007465
point 2	5.130000	-4.357000	22.158000	0.014	0.006265
point 3	5.023000	-4.520000	22.345000	0.015	0.018058
Total Error				**0.012**	**0.010223**

Table 11. Errors in the thermal model of the silo 3.

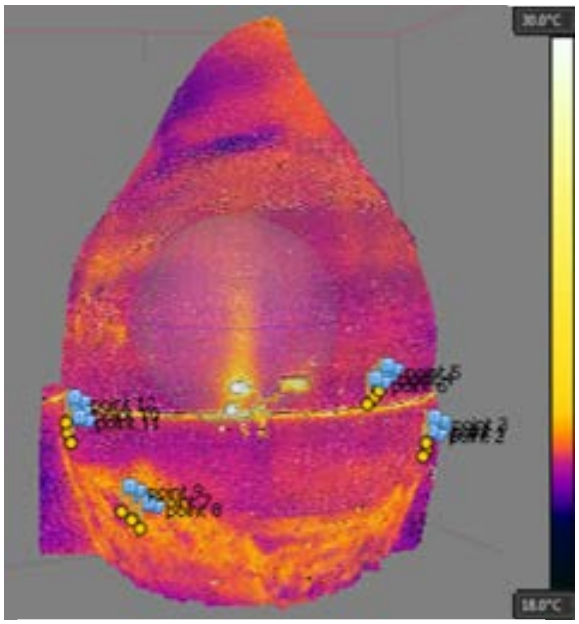

Figure 125. Thermal 3D model of the silo 3.

In this silo the results obtained for the thermal 3D model are similar that the comparison obtained in the silo 1. The final orthophoto could be visualized in the Annex I (Thermal orthophoto of the Silo No. 3).

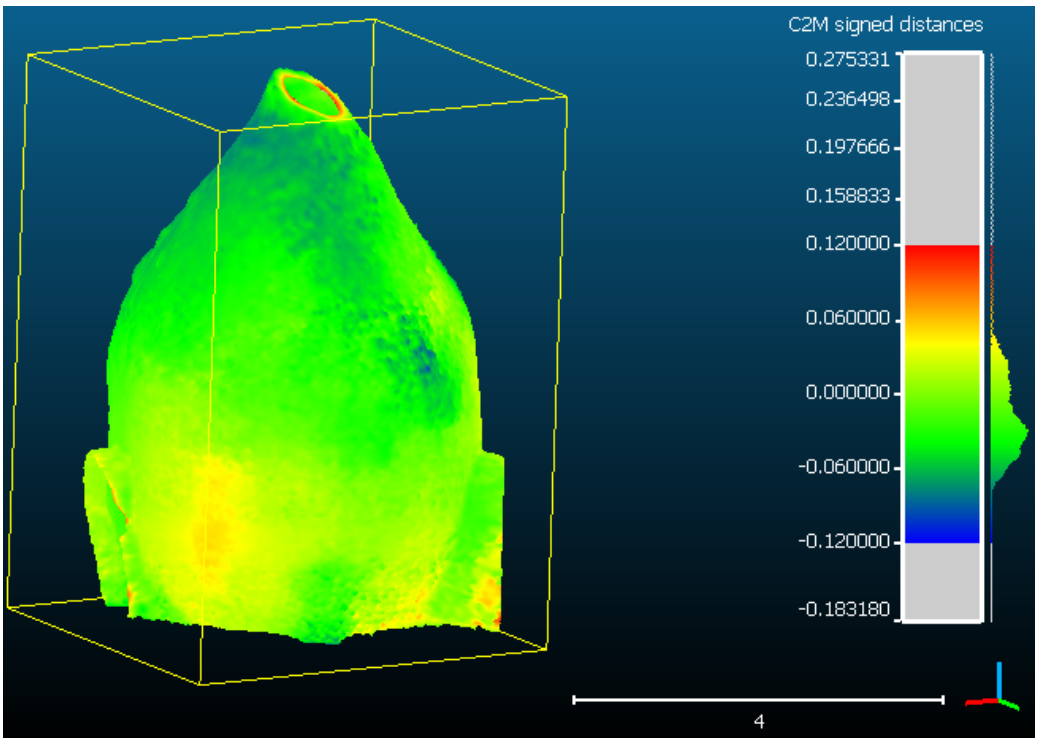

Figure 126. Comparison between the thermal 3D model and the point cloud mesh of silo 3.

In that case the mean was -0.018954 meters and the standard deviation 0.031786 meters (68%).

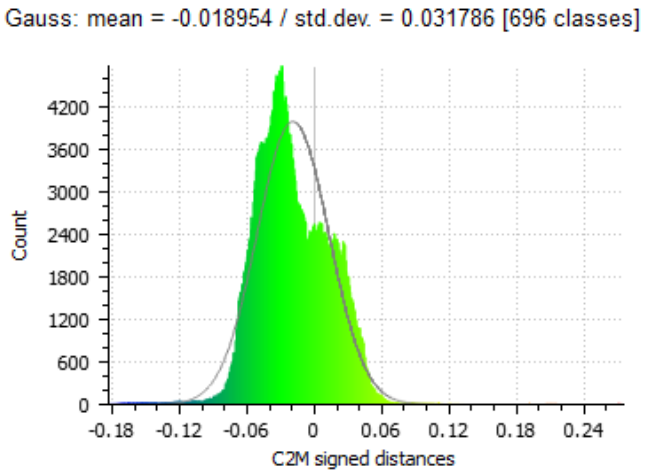

Figure 127. Distributtion fitting of the errors between the point cloud mesh and the Flir One camera model of silo 3.

With this last model the process of creation of 3D models is finished, all these models were exported to different .OBJ files in order to import them to the visualization of all the Silo-Yard.

3.7.2.3 Creation of 3D model from RAW thermal images of the Flir One

The images treated in the reference 3.6.2 were projected to the 3D model created using the smartphone camera. Following this method the 3D model has the best resolution from the smartphone photos with thermal information from the Flir One.

This process was performed with the software 3DReshaper, loading the visible 3D model and using the tool “Texture Mapping” from the Image tab. In this tool the user has to load the different photos to project on the model, in that case 84 for the silo 1. Once the images are loaded, the user must select couples of tie points on the mesh and on the picture, these tie points should be distributed over the entire picture. The next figure shows the process of matching, and the difficult to select correctly the target, for this reason is advisable the use of bigger targets than the used in this project, printing them with inverted colours in order to predominating the black colour with a fast thermal inertia and easier to differentiate.

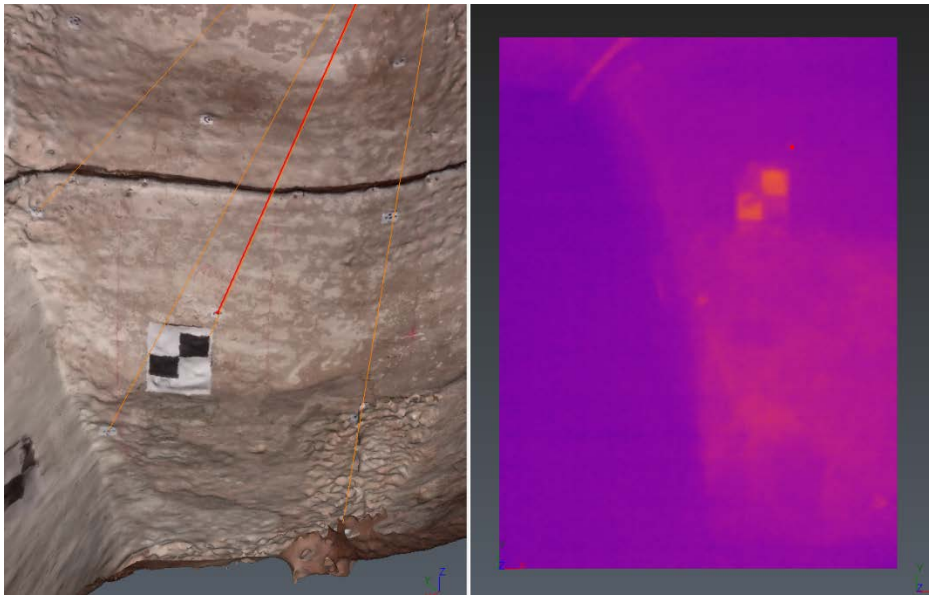

Figure 128. Selecting couples of points.

The position and orientation of the camera are computed dynamically while tie points are being added. During this process is necessary to export the reference points to a .txt file because if the "Preview" button is pressed appear an error, "*Warning! Some texture could not be applied because the camera definition could not be determined.*" This error is due to the existence of a preview texture, in that case the texture from the smartphones photos.

To fix this bug, the original texture must be removed, using the tool "Texture Material" and pressing the button "Remove texture". Once the texture is removed and returning to the "Texture Mapping" tool, the user has to reload the images and import all the reference points exported before.

Pressing the "Preview" button, the picture is applied on the mesh and pressing the "OK" button, the texture is saved.

During this process, several problems were found. The main problem was the matching process between the thermal photographs and the visible 3D model in the top part of the silo due to the lack of targets. The lack of a safe scaffolding and safety harness prevented the placement of targets in the tops of the silos.

This fact can be seen in the figure 129, where it is very difficult to locate the targets due to the absence of texture by the low resolution of the thermal sensor. This figure only has two targets identified with a red circle, this two couples of points are not enough to project correctly the thermal photo on the model.

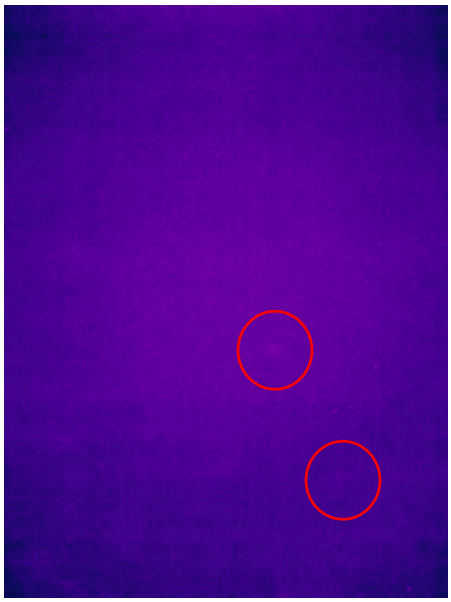

Figure 129. Thermal image of the top of the silo 1.

These problems affected negatively to the outcome 3D model, for this reason in the next projects must be necessary the use of high contrast targets (Annex 1), placing targets in all the object. The size of the targets would be increased if the object is more than 1.50 meters of the camera.

Therefore in this project the thermal characterization of the silos were performed using the 3D models obtained with the MSX images due to increase the texture. These images enables to create a thermal 3D model because MSX adds key details from the visible camera of the Flir One to the entire infrared image in real time, with these images is possible to see the structural features.

The next figures (figure 130 and figure 131) show the final orthophoto of the 3D thermal model created only with the .RAW thermal images, in these images is possible to see as the main problem was the lack of overlap between the different photos, it can be seen as the bottom of the silos have a correct textured but if the height is increased, the overlap problems are exacerbated.

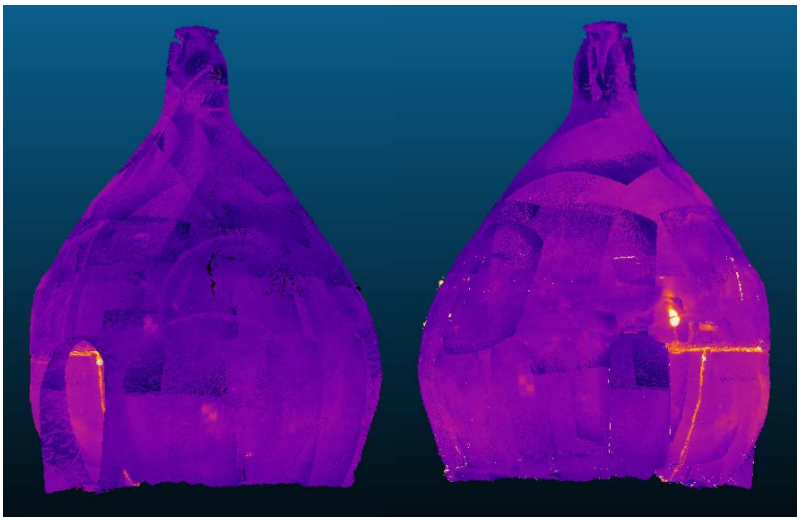

Figure 130. Silo 1 with thermal texture.

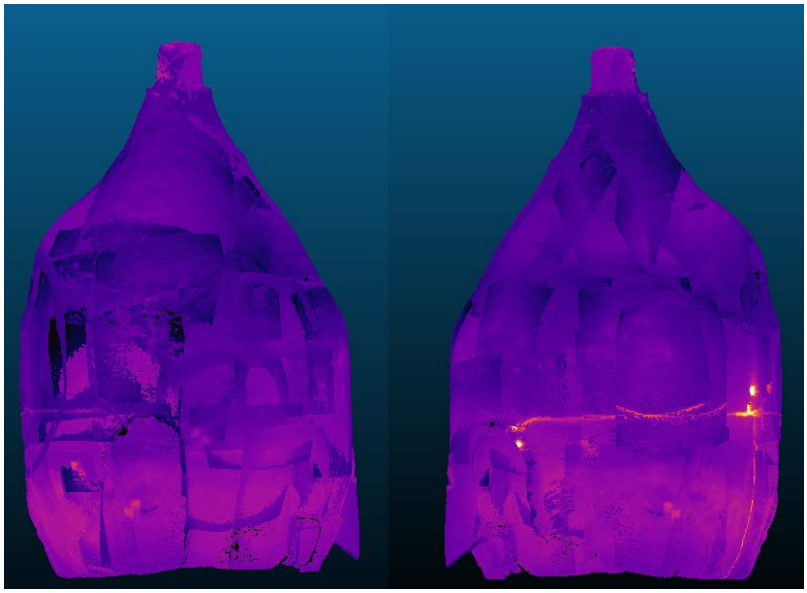

Figure 131. Silo 3 with thermal texture.

In view of the results of the .RAW thermal images can be obtained different conclusions. The first conclusion is placing the targets with a good geometric distribution, displaying at least five targets for photography in order to reduce the positioning error of the camera during the projection on the model. To facilitate this task, it is necessary improve the view of the targets, even the material of the targets using targets of iron or other material with a fast thermal inertia, if the targets are of paper a good solution is invert the colours using white targets with black paper or increase the size. Another solution could be the use of MSX images and project them on the 3D model obtained from the smartphone camera photographs. The side figure represented a high contrast target as proposed.

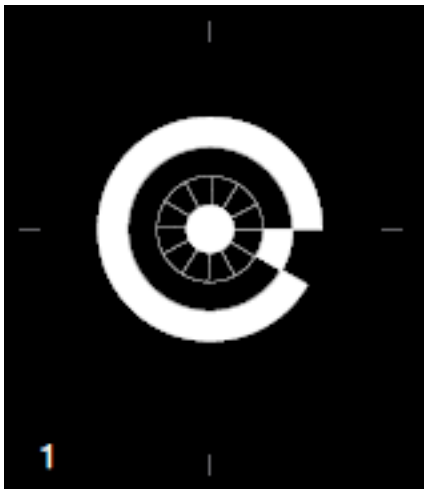

3.8 Thermal Characterization

After the 3D model creation the thermal characterization of the silos using the visible models from the smartphone camera and the MSX models from the Flir One could be performed.

3.8.1 Thermal characterization of the silo 1

The models performed in silo 1 in the visible and infrared spectrum allow one to detect different areas damaged and material changes of the silo. The figure 132 shows the orthophotos from the side view of silo 1. These profiles expose a correlation between the areas with pathologies in the visible image and the hottest areas in the thermal image.

These orthophotos could be visualized with more details in the Annex I, in the graphics "*Visible orthophoto of the Silo No. 1*" and "*Thermal orthophoto of the Silo No. 1*".

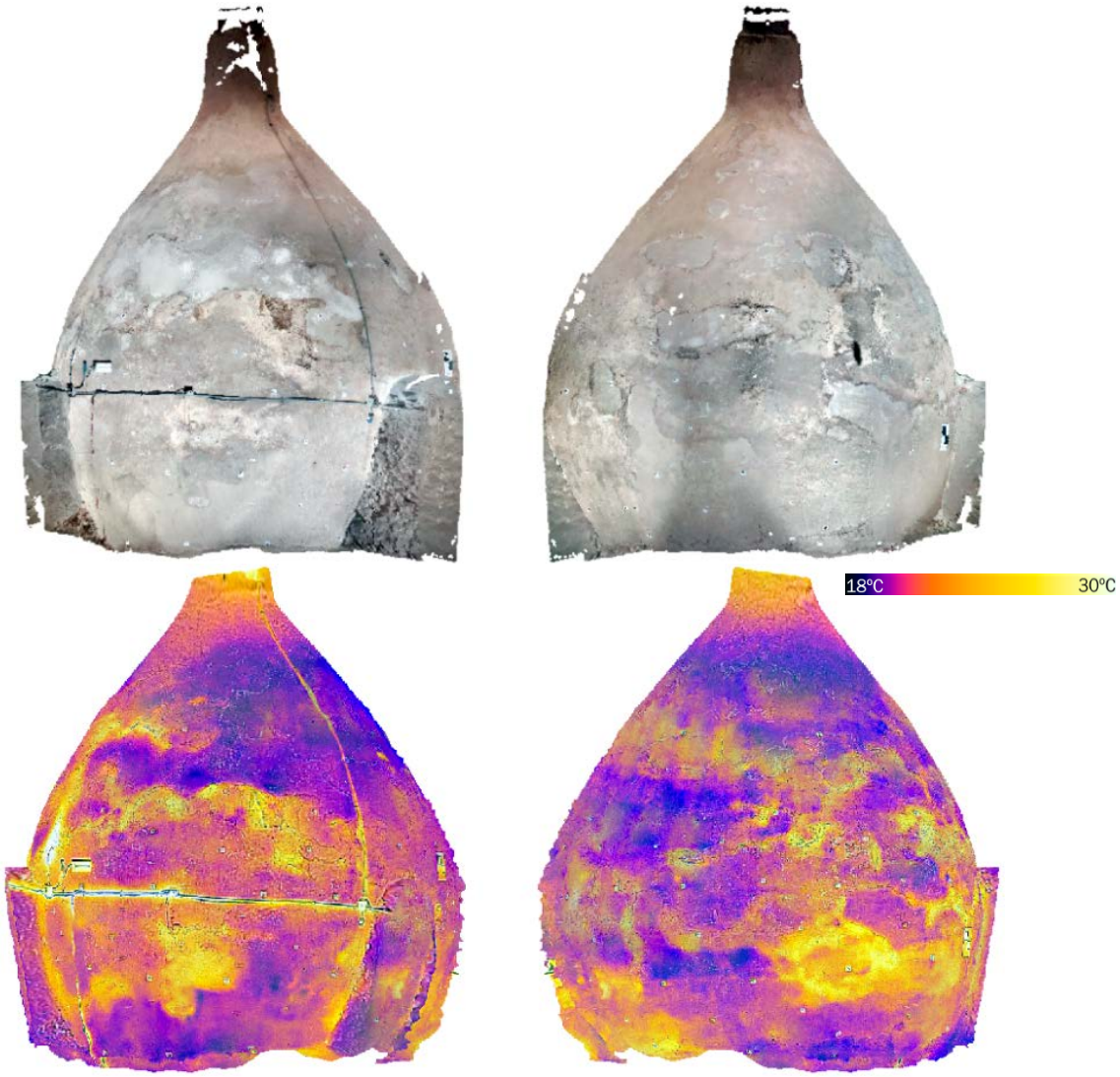

Figure 132. Visible and thermal orthophotos of the silo 1.

The existence of air gaps between the outer skin and the rest cause an increase in the temperature, also material changes are detected thanks to the thermal inertia of the materials.

An optimal geometry of the silos is essential to do a comparison between the visible and the thermal models. For this reason a comparison between the distances of the both meshes was done.

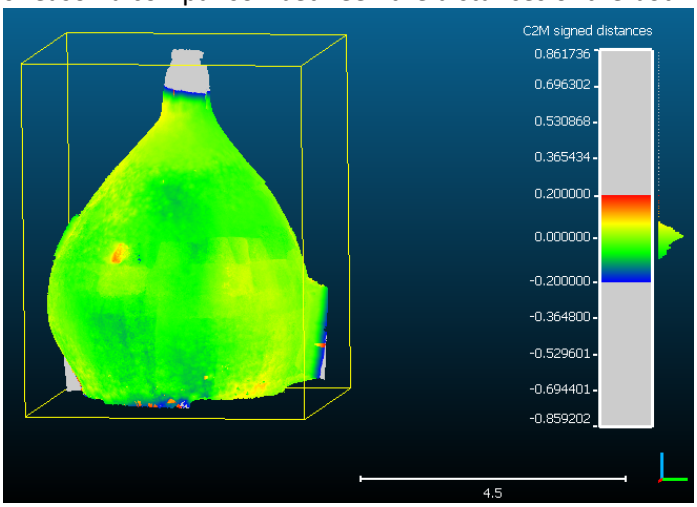

Figure 133. Comparison between the thermal and the visible meshes of the silo 1.

The figure 134 shows as the mean of the errors is -0.011731 meters and the standard deviation 0.089791 meters, these errors increase because in the cap of the silo and the tunnel the difference between the two models are bigger than ±0.20 meters (Figure 133).

An overlay from the thermal and the visible images allows one to see, as the change of temperatures of the thermal images matches with the different pathologies of the silo (Figure 135).

There are areas of interest in which it is necessary to undertake a detailed analysis. This

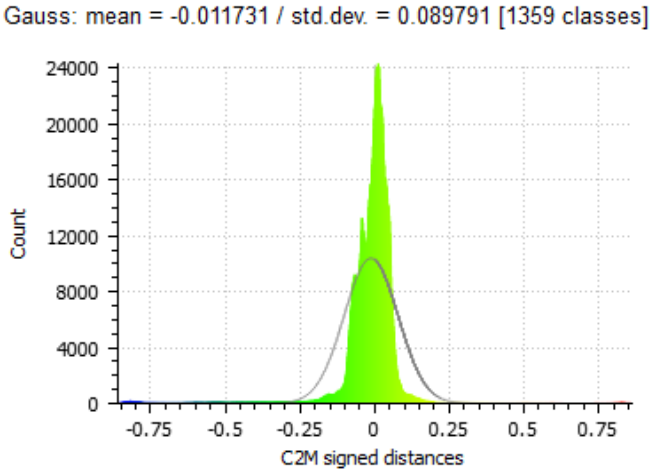

Figure 134. Distributtion fitting of the errors between the visible smartphone camera mesh and the Flir One camera model of silo 1.

analysis was performed in the central top part of the left side of silo 1 (Figure 136).

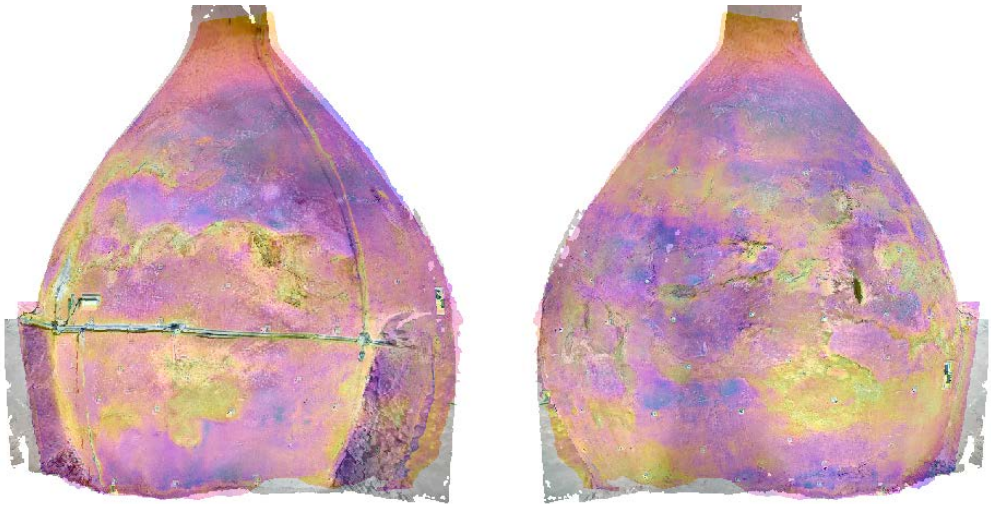

Figure 135. Visible and thermal images overlay of the silo 1.

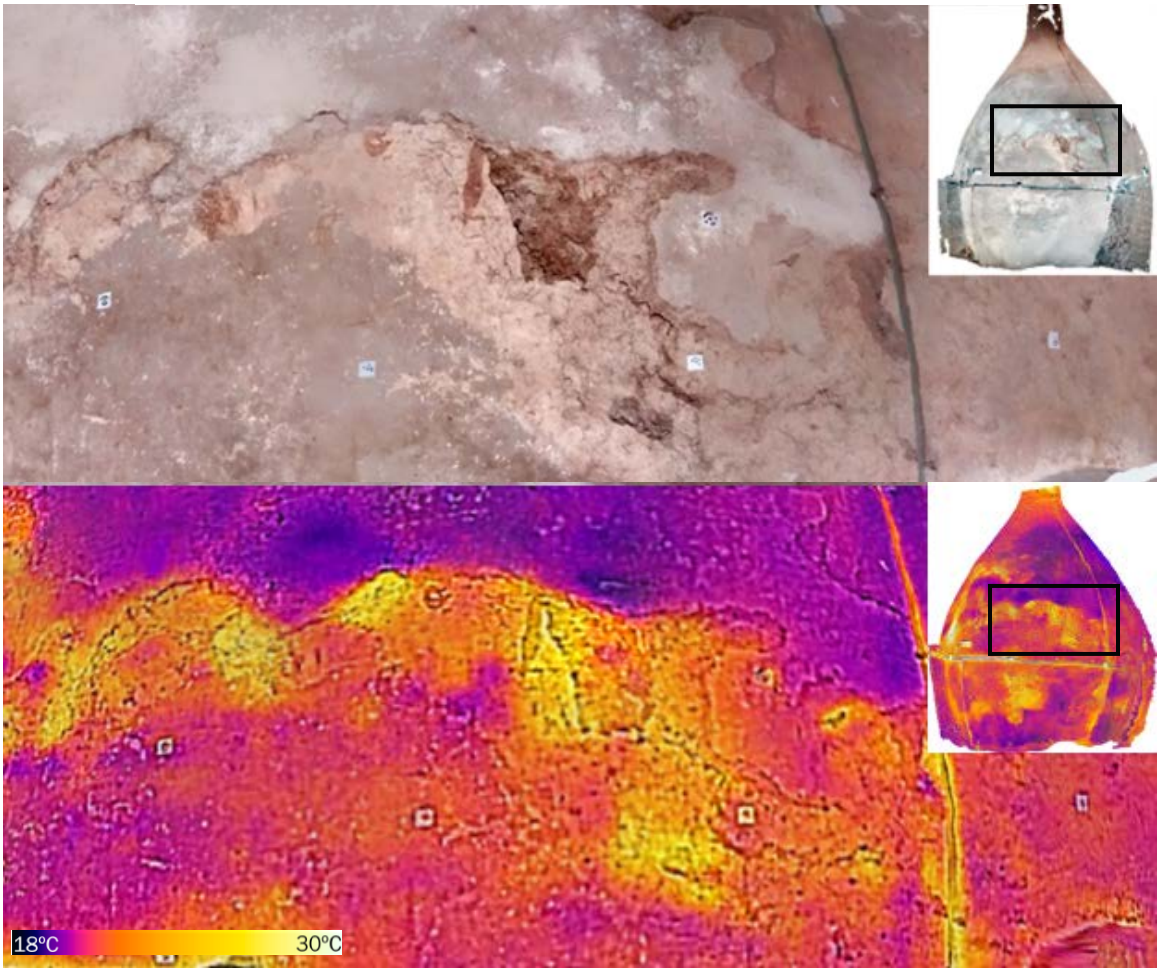

Figure 136. Detailed comparison of interest areas in the left side of the silo 1.

In this figure it is possible to differentiate three materials, each one with different thermal inertias. In the top left and top positions of the image the construction material of the silo is Portland cement used

in any reconstruction of the late 20th century. This material is detected thanks to its low thermal inertia, obtained in this area of the lower temperatures in the silo. In the center of the orthophoto is an area of plaster, in addition an area of air gaps exists between outer skin and the rest that it cause an increase of temperature. In the bottom and top right zones a layer of lime mortar from the original construction of the silo is found. This morphology and these three materials are in all silos that were visited, with the exception of silo 2.

Lime mortar is the material used in traditional building of the silos, before the invention of Portland cement and the modern building industry. Buildings originally built with lime mortar should be repaired with lime mortar but in the silos 3 different materials can be found in this zone causing that the materials do not adhere properly to the surface and end overthrowing. Furthermore, the original construction material of the silos, the lime mortar, is vapor permeable and allow buildings to breathe. This reduces the risk of trapped moisture and consequent damage to the building fabric. Porous and open textured materials such as lime plasters, help to stabilize the internal humidity of a building by absorbing and releasing moisture.

The most important reason to choose this material was that lime renders assist drying out by evaporation. High calcium lime renders allow evaporation and reduce the risk of trapped moisture and decay, solving the serious problem that is moisture for wheat and cereals. For these reasons it is necessary in a future reconstruction of the original surfaces the use of lime mortar to prevent pathologies in the complex of the Silos.

In the right side of the silo 1 the same pattern is repeated. In the center of the figure 137 is detected another air gap in the surface of the silo causing an increase of temperature in this area compared to other areas with consolidated materials with less thermal inertia. In addition, in the bottom right zone of the previous figure an area predictably burnt by the use of a torch is located, this pathology is differentiated by the thermal image obtaining a high temperature in this area.

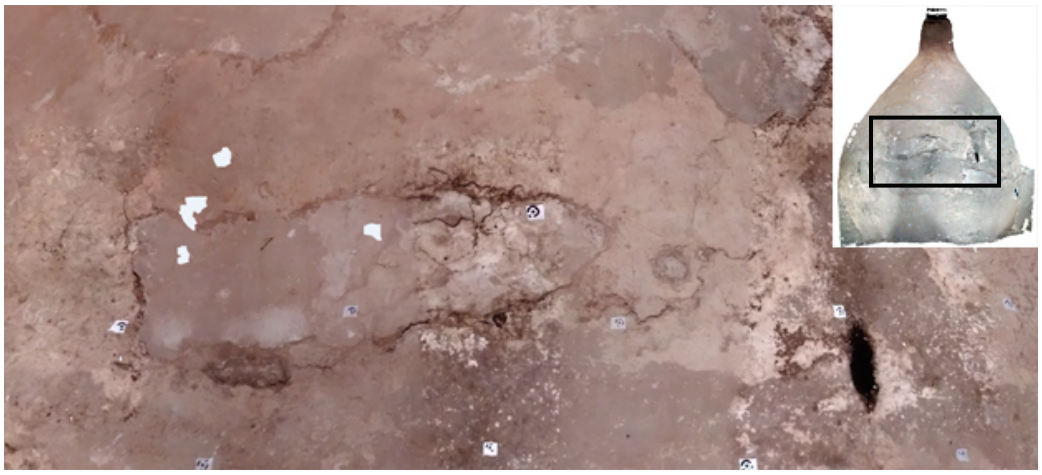

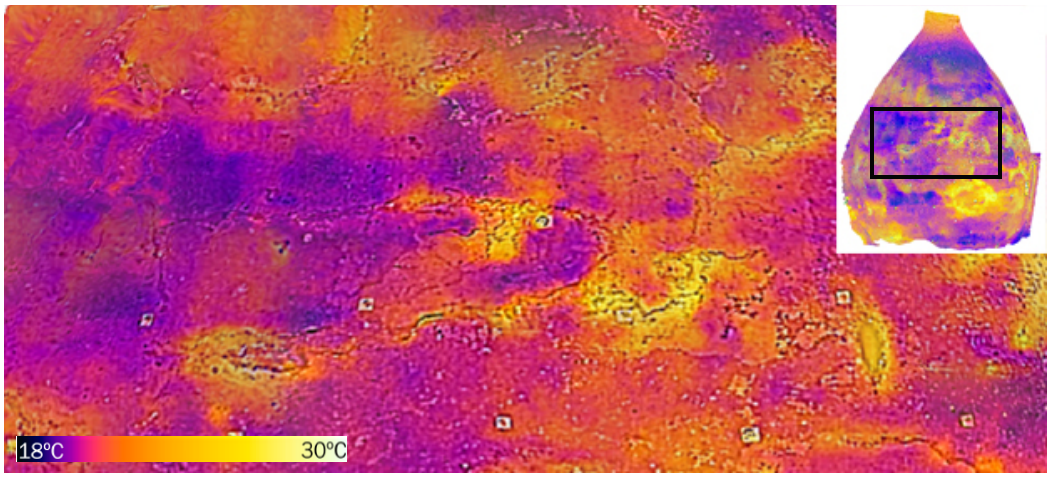

Figure 137. Detailed comparison of interest areas in the right side of the silo 1.

3.8.2 Thermal characterization of the silo 2

In 1980 silo 2 was modified with a solid brick coating (Generalitat Valenciana, 1983). This surface causes a regular response in the thermal spectrum. This coat of solid bricks has a thickness of about 20 centimeters, this coat has a very low thermal inertia, obtaining similar results in all the surface of this silo.

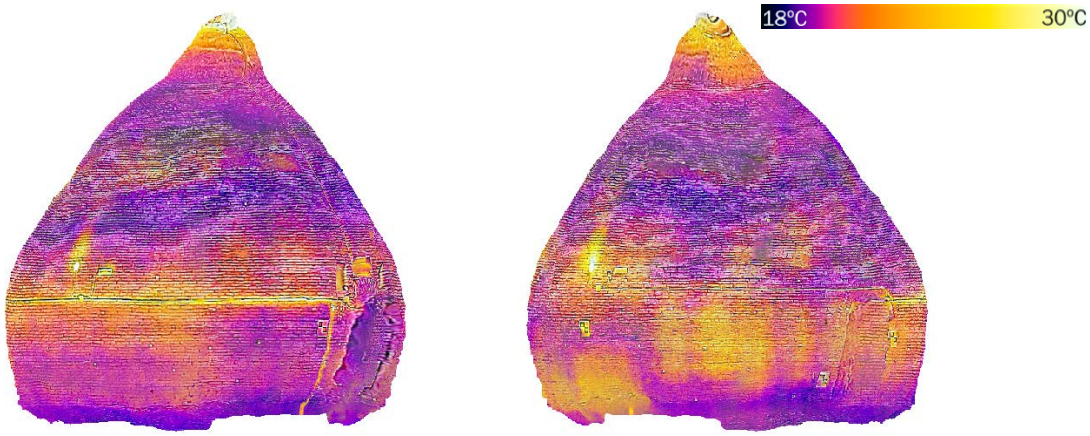

Figure 138. Thermal orthophoto of the silo 2.

3.8.3 Thermal characterization of the silo 3

Silo 3 has a similar morphology to silo 1. The next figure shows the orthophotos from the side view of silo 3.

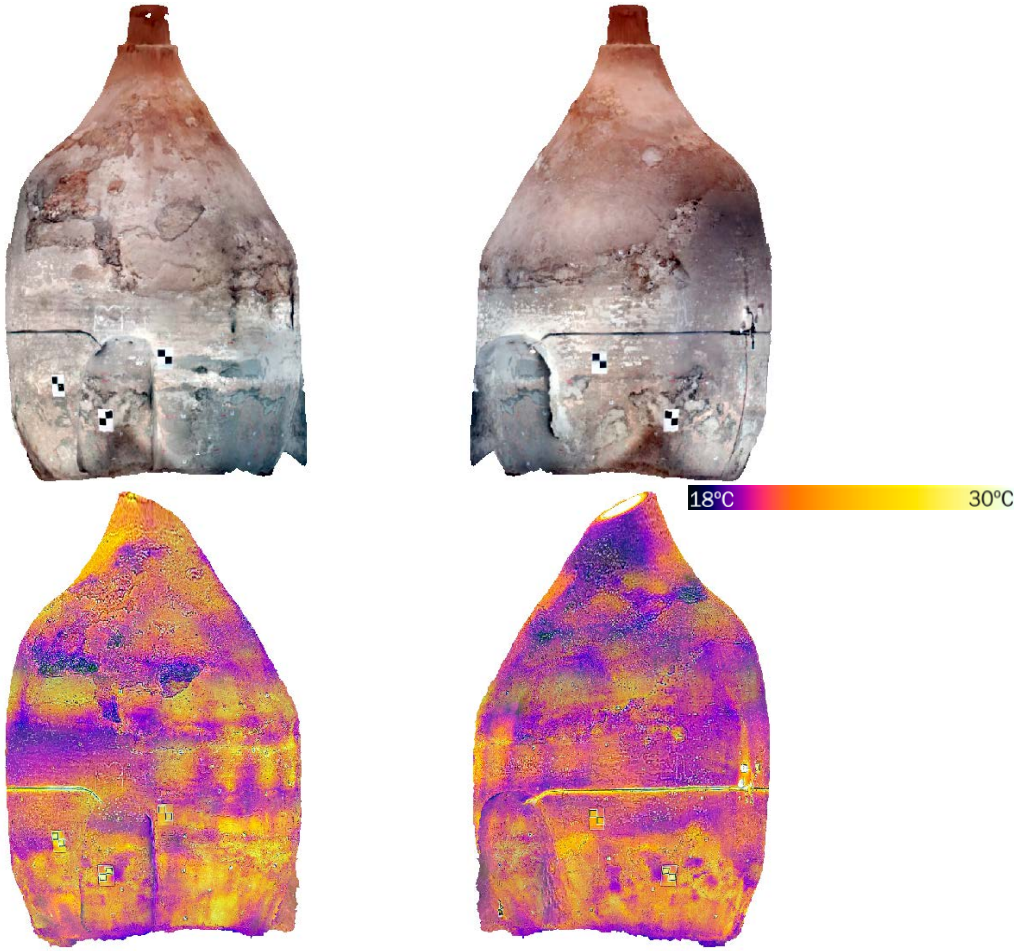

Figure 139. Visible and thermal orthophotos of the silo 3.

Using the software CloudCompare a distance comparison of the two meshes was performed as in the silo 1. CloudCompare will simply search the nearest triangle in the reference mesh. Meshes generally provide a side information thanks to the normal direction of the triangles. A wrong direction of the normals gets erroneous results, to prevent this the user can choose to either ignore the normal information or to invert it, and in that case the default options were selected because the triangles had normals properly directed.

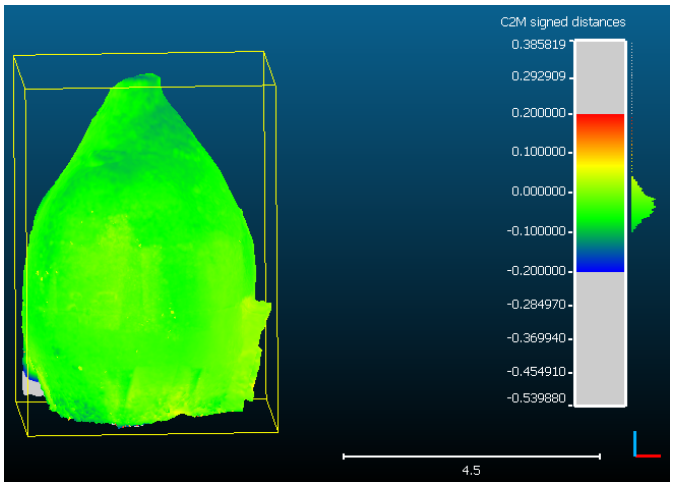

Figure 140. Comparison between the thermal and the visible meshes of the silo 3.

In this comparison similar results to silo 1 were obtained, finding that practically all the triangles are below 1 decimeter of difference.

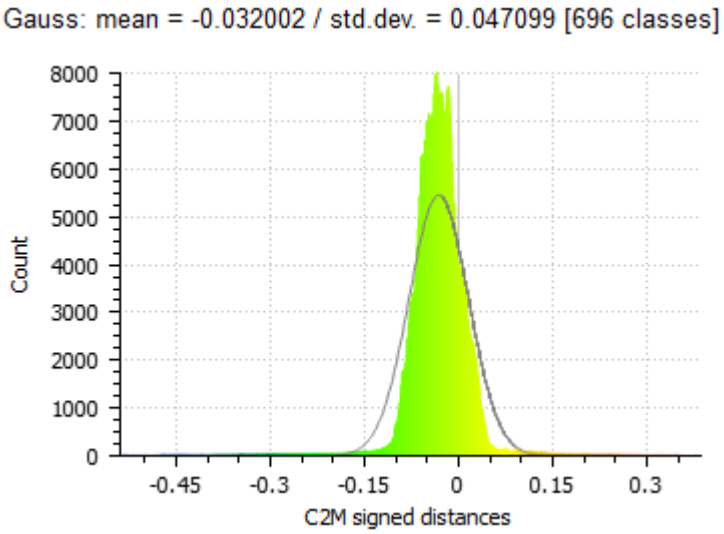

Figure 141. Distributtion fitting of the errors between the visible smartphone camera mesh and the Flir One camera model of silo 3.

In that case, the mean of errors was -0.032002 meters and the standard deviation was 0.047099 meters (68%), significantly the errors of this silo were lower than the errors of silo 1. The main reason was a reduction of the errors in the cap and the tunnel.

Making an overlay between the visible and the thermal orthophoto from the silo 3 can be viewed as the hot areas correspond to the most damaged areas of the silo.

The silo 3 has the worse condition of the three silos characterized, in this silo all the top part has spalling due to the filtration of rainwater through joints and gaps in the paving of the Silo-Yard.

Figure 142. Visible and thermal images overlay of the silo 3.

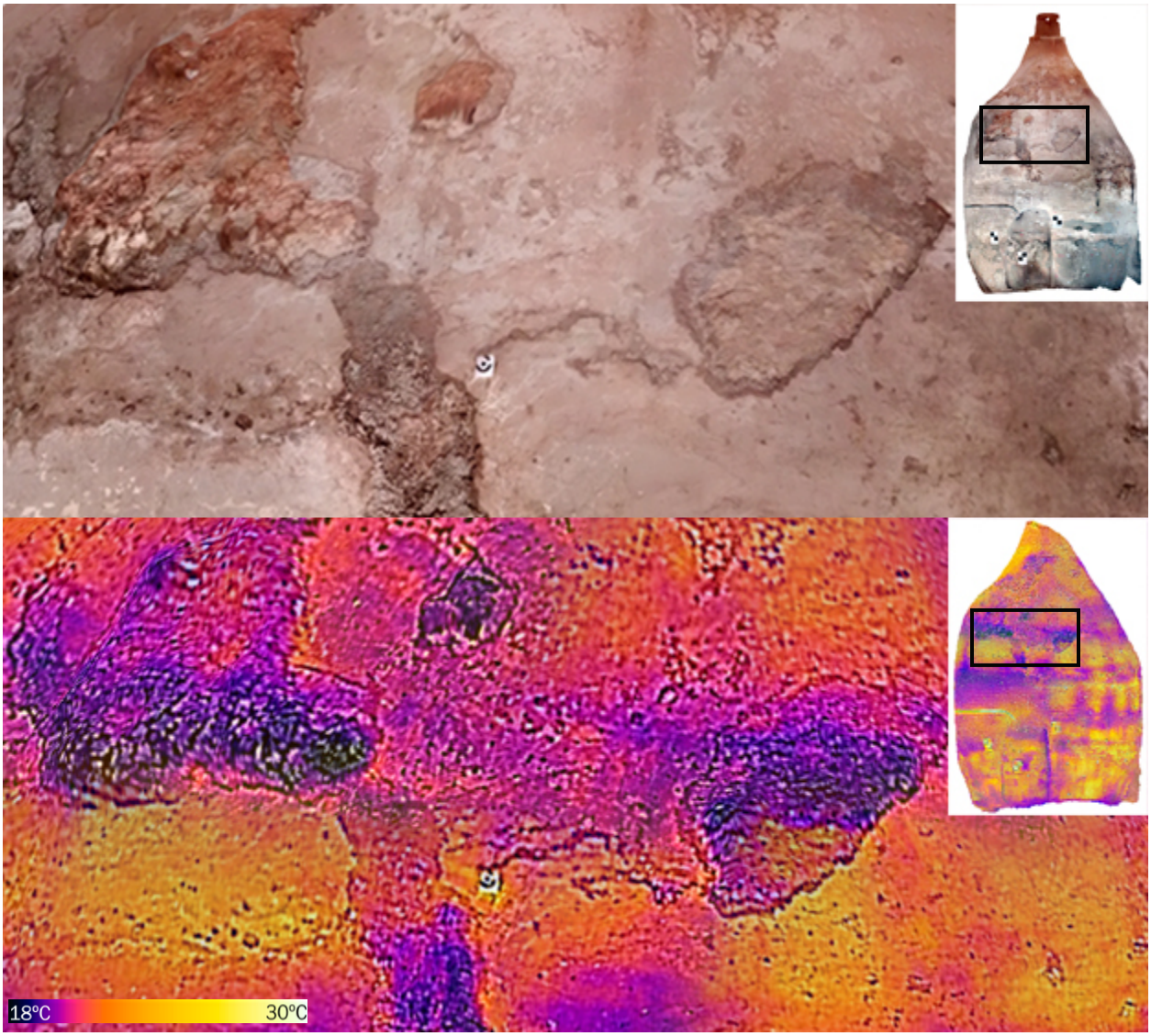

Figure 143. Detailed comparison of interest areas in the left side of the silo 3.

The figure 143 shows a comparison between the visible and the thermal images of the top left zone from silo 3. This figure illustrates different pathologies of the silo, and in the top left area the image shows the fall of the material allowing one to view the natural terrain in which the silos were constructed.

In this part the limestone is visible, and the thermal image detects this change of material thanks to its low thermal inertia. The comparison in the rest of the image shows that the thermal camera detects any changes in the different materials of this area.

In the right side of silo 3 (Figure 144) it is interesting to focus on the bottom part of the silo. In this comparison it shows as the thermal camera detects the most part of the change materials, but in that case in the center an area of plaster is located, and the thermal response is different, through being the same material. This fact may be due to a different thickness of the material, the beginning of a process of spalling or a change in the composition of the plaster. To know the reason why the thermal response is different in this area trial pits should be performed in order to identify the composition and structure of the subsurface.

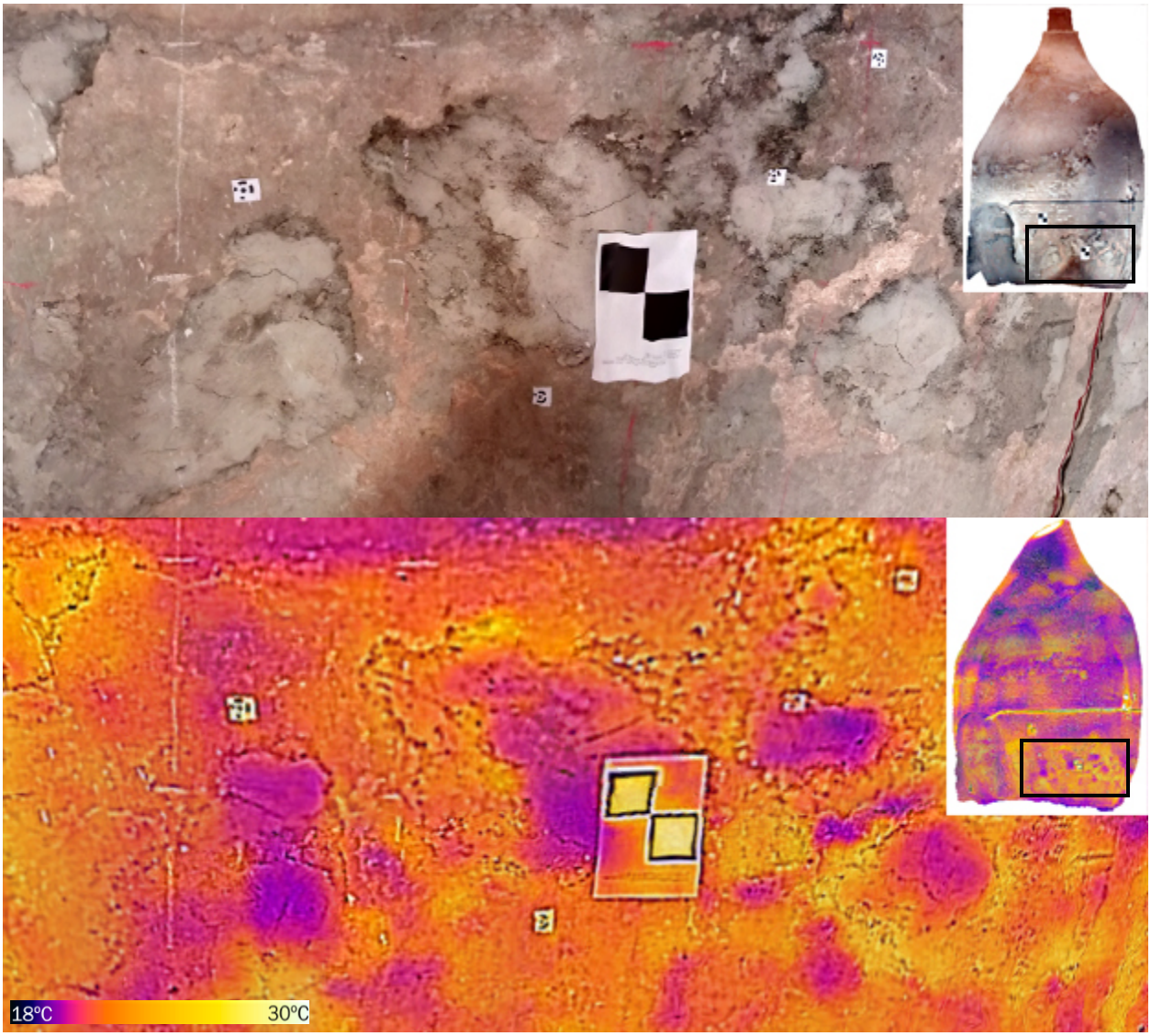

Figure 144. Detailed comparison of interest areas in the right side of the silo 3.

3.9 3D Visualization with Unity

The final objective of creating the different 3D models was achieved by creating a 3D visualization as a final product that collects all the work done. This 3D visualization was created using Unity. Unity is a cross-platform game engine developed by Unity Technologies and used to develop video games for PC, consoles, mobile devices and websites.

In this visualization different elements were added to create a realistic environment as the real landscape of the area of Burjassot or the buildings of the town in order to create a simulation as a virtual tour of the Silos of Burjassot.

3.9.1 Creation of the real landscape

To create a real landscape of the Burjassot area it is necessary to have an orthophoto and a DEM to project it on the terrain. The first step was to download these files from the *Centro Nacional de Información Geográfica*[35]*(CNIG)*. The information of the CNIG is divided in 1073 grids corresponding to the divisions made of the Spanish territory in the National Topographic Map with a scale of 1:50.000. The town of Burjassot is located in the grids number 696 and 722, requiring one to download the information from these two grids and join them.

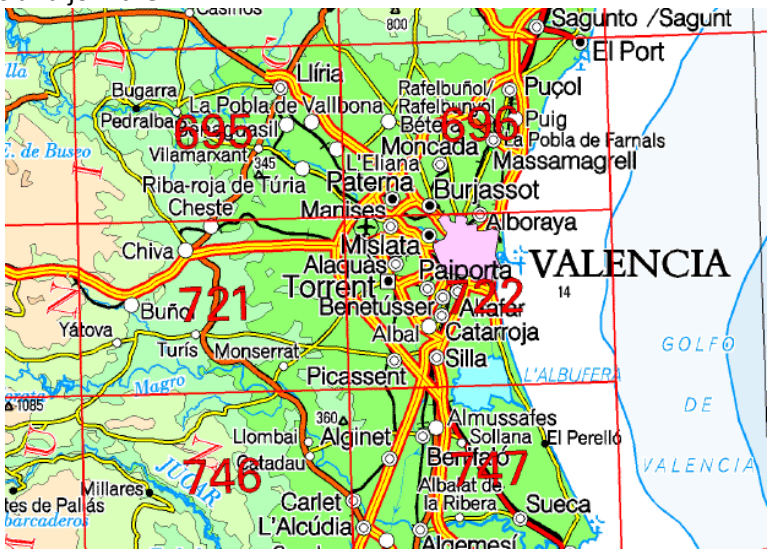

Figure 145. Numeration for Burjassot from the National Topographic Map with a scale of 1:50.000

The orthophoto was the most recent available in ECW format, geodetic reference system ETRS89 and UTM projection in its UTM zone accordingly with a resolution of 0.25m. The DEM has a resolution of 0.50m.

3.9.1.1 Workflow in ArcGis and Photoshop

Unity cannot read directly the information from these .ECW files for this reason it is necessary to do a treatment of the data. This treatment was performed using the software ArcGIS, due to the extensive workflow to perform, a model was created using the ModelBuilder tool from ArcMap (Figure 146).

[35]The *Centro Nacional de Información Geográfica* (in English, National Centre for Geographic Information) it is an autonomous organization of Spain belonging to the General State Administration and established in 1989. Its purpose is to produce, develop and distribute the work and publications of geographical character that requires the Spanish society.

Figure 146. ArcMap workflow to introduce the orthophoto and DEM to Unity.

The first step of this workflow was to determine the area of Burjassot, creating a square of the interest area. It was important to start clipping the area to reduce the workload of the computer. This area was used as feature mask data in the tool “Extract by mask” that it was executed in the four files, two orthophotos and two DEMs. The next step was to create a mosaic to join the two orthophotos and the two DEMs, using the tool “Mosaic to new raster”.

After obtaining the orthophoto and the DEM of the interest area, it was necessary to do a resample of the DEM file in order to convert the total number of cells in byte number, because Unity only works with cells in byte number. To do this job it the size of the raster in meters was measured, in that case the distance was 8824,713 meters, this number was divided by 256, the desired byte number, resulting 34,471, the size of the new cell. This number was introduced as X and Y in the tool "Resample" (Figure 147).

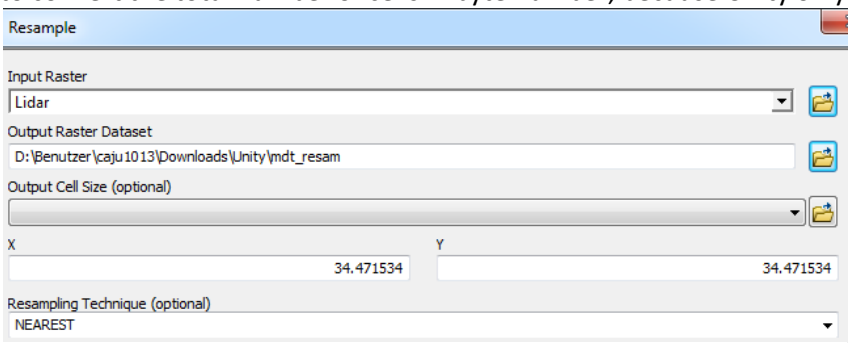

Figure 147. Resample of the DEM.

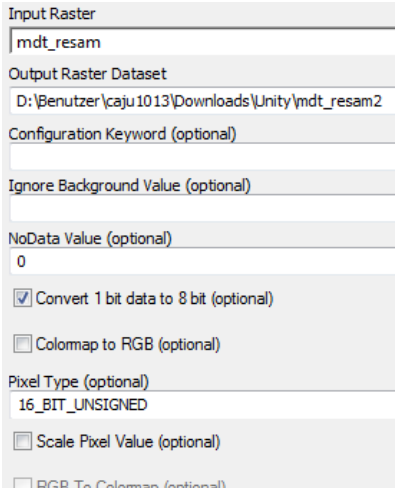

Figure 148. "Copy Raster" tool chosen options.

In order to calculate the height of the terrain in Unity a new raster was created and using the tool "Copy Raster" converting the output raster dataset of the previous step from 1 bit data to 8 bit with a pixel type of "16_BIT_UNSIGNED"(Figure 148). Then, a new raster was created using the same output raster dataset resulting from the "Resample" step, but in this case without converting 1 bit data to 8 bit.

Once both rasters were created, the real range from highest to lowest value of the heights of the both raster was taken. The range of the first raster is called x1, in this project has a value of 255, while the second raster create without converting 1 bit data to 8 bit has a range of 32398,42, this number is called x2. Then the division of x1/x2 was done, obtaining 0,00787. This number was multiplied with the whole, possible data range of a 16-bit unsigned integer, this means 65535 ($2^{16} - 1$). In this example z = 515,810m. This z will be the height of the terrain in Unity.

In that case the orthophotos downloaded from the CNIG[35] had a .ECW file format, and this file was converted to .PNG in order to enable the importation to Unity using the tool "Raster to other format". On the other hand, the DEM was converted to .TIFF, in order to import the file into Photoshop to create a .RAW file. The .RAW file is the only format that can be imported to Unity.

3.9.1.2 Workflow in Unity

Once these steps in ArcMap and Photoshop were completed, the .PNG file of the orthophoto and the .RAW of the DEM were imported to Unity. The first step in Unity was to create a new 3D project adding the assets "Characters" and "Environment". Once the project was created, the next step was to import the package "Terrain Composer" to generate and tweak the terrain. Pressing the button "Window" of the toolbar and choosing the tool "Terrain Composer" the user can create a new terrain.

Once the terrain was created it is necessary to modify the size, putting in the X and Z coordinates the numbers of bytes of the DEM, in that case 256 and in the Y coordinate the z value calculated previously, z = 515,810m, clicking the button "Create Terrain" the terrain was created. The next step is import a prefab called "*import_heightmap.prefab*", this prefab is located in the asset folder of the package Terrain Composer in the path Assets/TerrainComposer/Save/Layers/Preset, this prefab allow the user to import DEM files. Then, it is necessary to import the .RAW file pressing the right button of the mouse in

the Root menu. Once the DEM is loaded, pressing the button “Generate Map”, the DEM was loaded into the terrain (Figure 149).

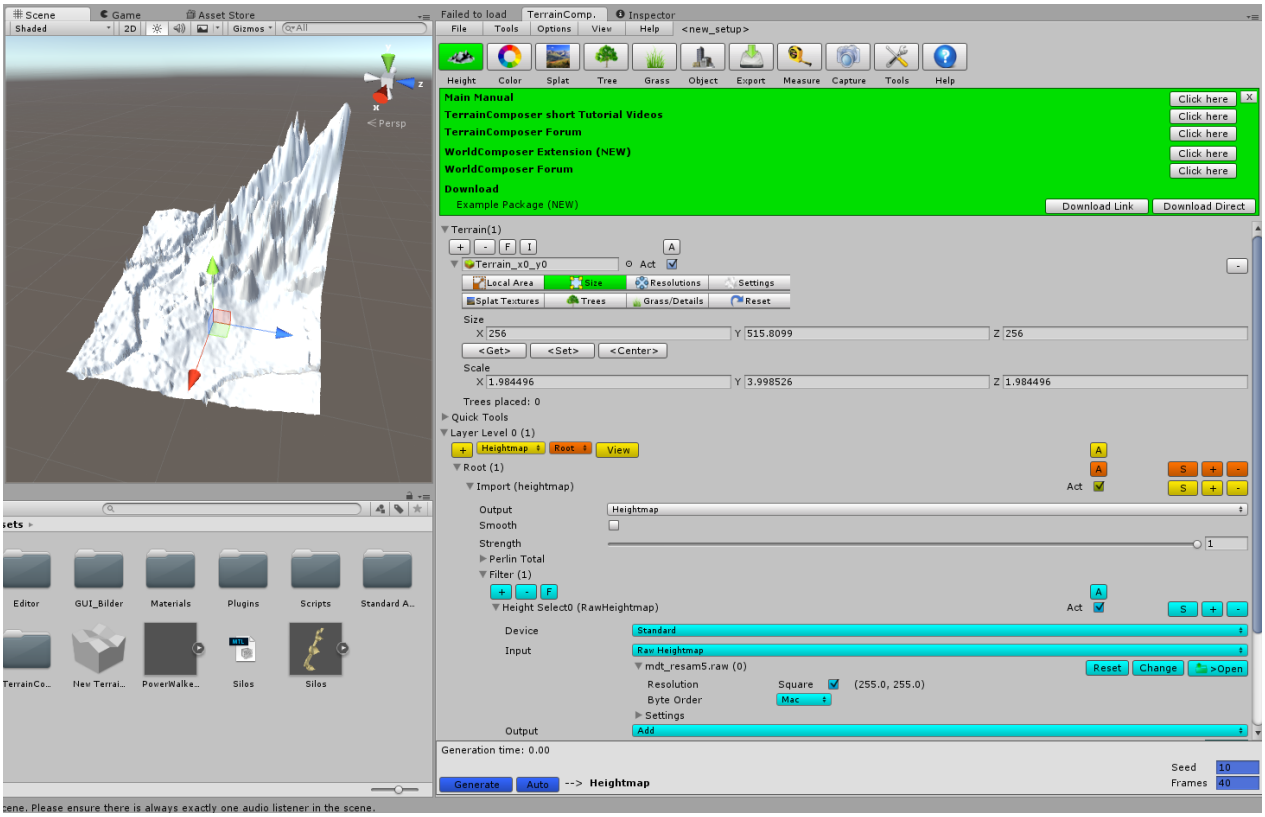

Figure 149. Generating the terrain with the DEM heights.

The final step was to modify the X and Z coordinates of the terrain to the real size, in that case 8824,713m, this distance was the real size of DEM. In figure 149, it could be seen as the heights are so exaggerated. To project the orthophoto on the DEM created it is necessary to add a “Splat Texture” from the Terrain Composer options, choosing the .PNG file of the orthophoto and putting a “Tile Size” of 8824,713m, the distance size of the orthophoto (Figure 150).

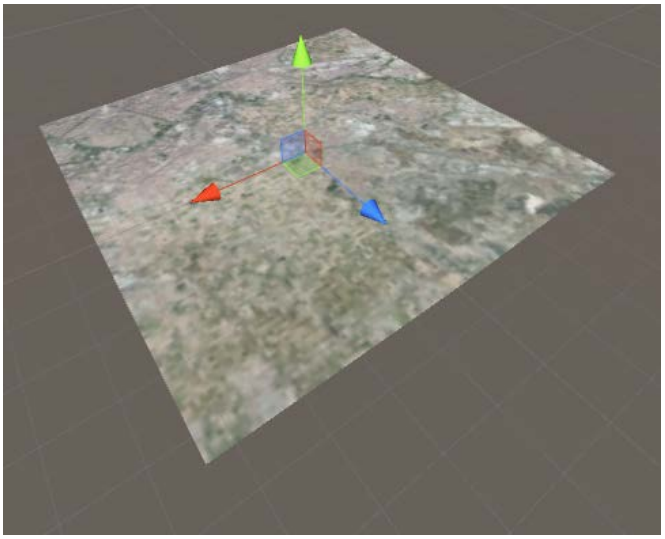

Figure 150. Real landscape height of Burjassot in Unity.

3.9.2 Creation of the town of Burjassot

3.9.2.1 Workflow in ArcScene

To create the representation of the town of Burjassot the first step was to get the urban cadastral map of the town of Burjassot. This information is available in shapefile format from the web of the Spanish Cadastre[36]. The polygon shapefile downloaded of the city of Burjassot contains a polygon per parcel with different fields as cadastral reference, type of construction, number of floors of the construction, or the coordinates of the centroid of the polygon. In this project only the number of floors of the construction was necessary, for this reason the other fields were deleted, keeping only the field called "CONSTRU" (Figure 151).

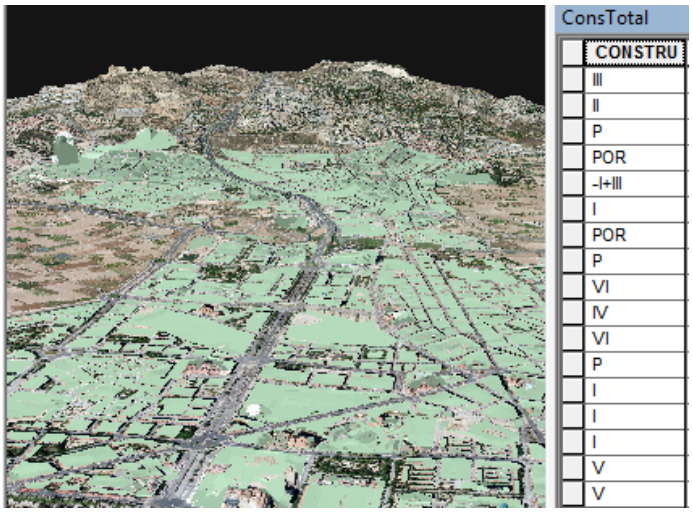

Figure 151. The town of Burjassot in ArcScene, with the cadastral shapefile table.

Seeing field "CONSTRU" (Figure 151) the user could visualize the main problem to create a 3D representation of the buildings, the floors of the buildings are introduced in Roman numerals, indicating with a negative Roman numeral the existence of underground floors. Furthermore more nomenclature exist, such as "P" that means *patio* (yard in Spanish) or "POR" that means *porche* (porch in Spanish) not used in this project (Catastro, 2011). To convert this string field to a float field, it was necessary to create a Pre-Logic Script Code in the Field Calculator of ArcScene (Annex IV).

After this process, an "Elevation from surfaces" was performed using the DEM of the area of Burjassot to the buildings shapefile, in order to put the real height of the buildings on the terrain, because in Unity the terrain was elevated using the same DEM. This process was done from the "Layer Properties" of the shapefile in ArcScene, then click on the tab "Base Heights" and select the option "Floating on a custom surface", selecting the DEM created before. Finally an extrusion of the different buildings were done from the tab "Extrusion", activating the option "Extrude features in layer" and introducing the extrusion expression "Height * 2.5". This number, 2.5 meters, is a mean number of the height floors.

ConsTotal

CONSTRU	Height
III	3
II	2
P	0
POR	0
-I+III	3
I	1
POR	0
P	0
VI	6

Figure 152. Creation of the field "Height" with the number of floors.

[36] The Spanish Cadastre is principally a fiscal cadastre, whose databases of cadastral values of rural and urban real estate are the basis for the calculation of real estate tax and other local, regional and national taxes.

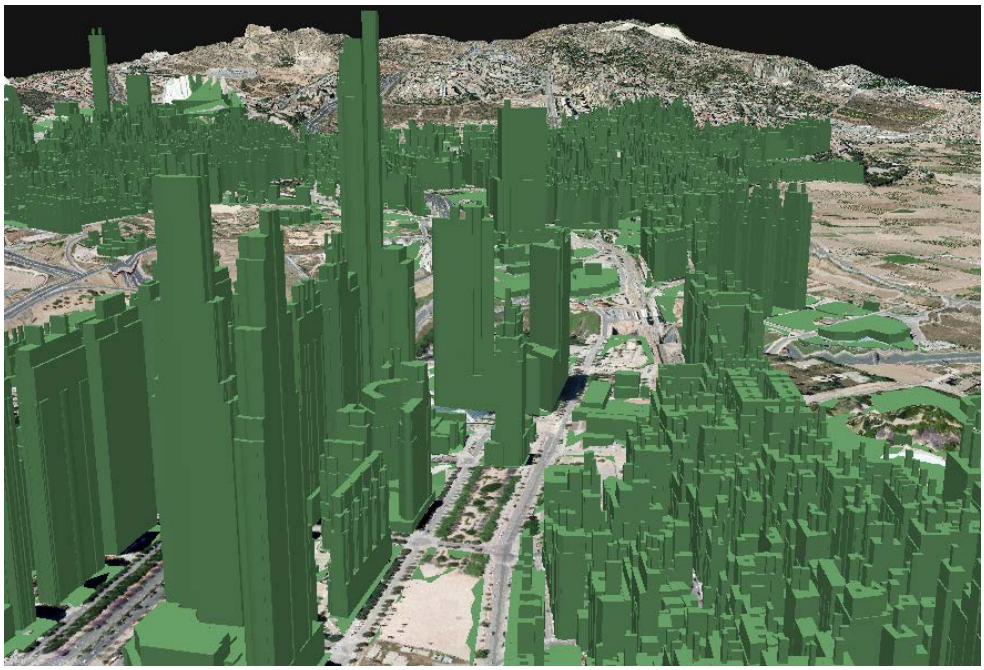

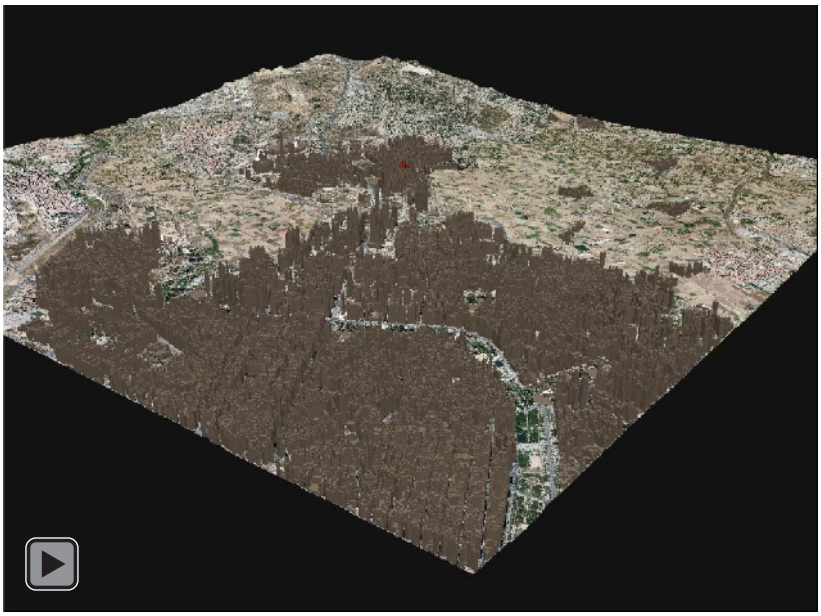

Figure 153. 3D visualization of the Burjassot area in ArcScene.

Finally this shapefile was exported to VRML (.wrl) this is the only format to export 3D objects in ArcScene. But this format is not supported by Unity, so a conversion of this format is required.

3.9.2.2 Workflow in Blender

The job done in Blender was to import the VRML file from ArcScene and export it to an .OBJ file, but once the file was imported into Unity a visualization problem showed up. This problem was the orientation of the normals of each face created in the 3D model. A normal vector is a vector that is perpendicular to its underlying surface. In 3D rendering each vertex can have a surface normal to simulate a different shape than the original geometry has. The normal is used by a shade when it is calculating the

lighting. The figure 154 shows the visualization problems in Unity, collapsing different parts of the buildings.

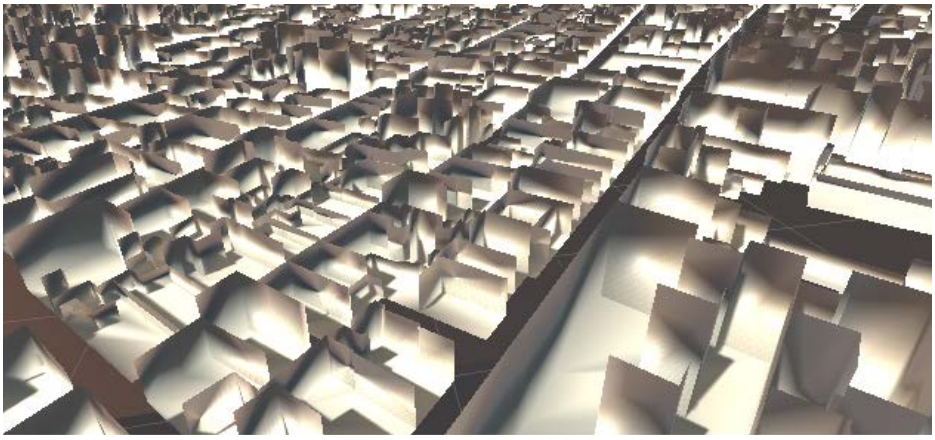

Figure 154. Normals problems in Unity.

To fix this problem the VRML file was imported into Blender again, but in this case the normals were recalculate from the "Shading/UVs" tab of the tool shelf. Once the normals were recalculated, the model was exported as .OBJ file fixing the normals problems and obtaining an optimal model (Figure 155).

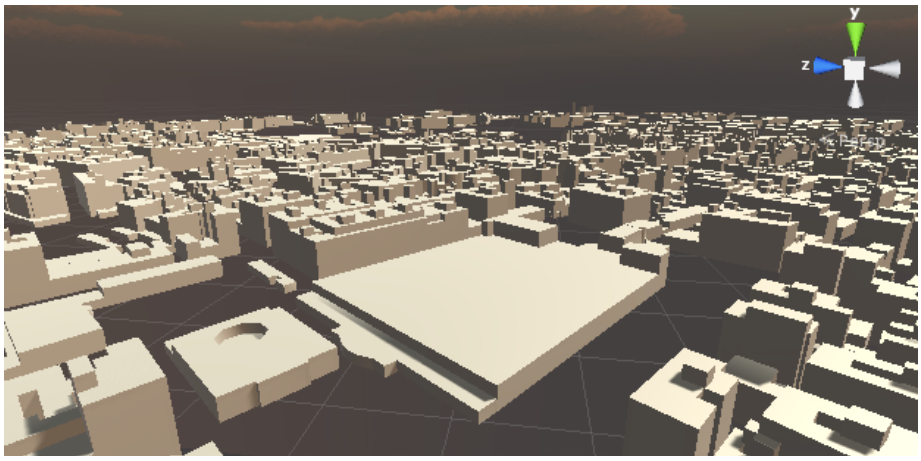

Figure 155. Visualization of Burjassot in Unity.

3.9.2.3 Workflow in 3DReshaper

To finish, a process of texture was performed with 3DReshaper, this software allows one to project different pictures on a 3D Mesh. The tool "Texture Mapping" is found in the tab "Image", in this tool the user can load one or more photos. Defining point couples between the 2D texture and the 3D model the camera position is symbolized and the image appears. 3DReshaper has an option to select the zones to texture, in this project the option selected was "Include invisible parts", and with this option all the triangles in the frame of the camera are textured, giving a blurring effect in the faces which the image is not projected directly.

To create the texture mapping, six point couples were selected between the model and the orthophoto.

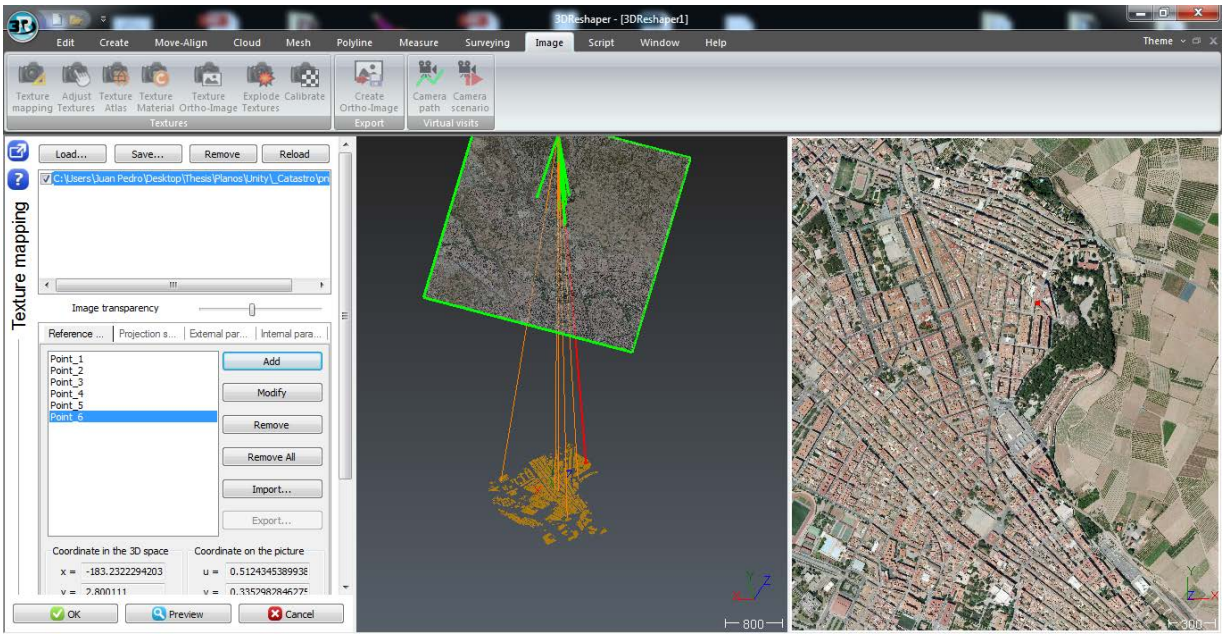

Figure 156. Selecting point couples between the 3D model of Burjassot and the orthophoto.

After this process the .OBJ file of the town of Burjassot was split in two files, one file contains the Valencian Silo-Yard and the other file contains the rest of the buildings. This process was done in order to ease the modelling of the Silo-Yard.

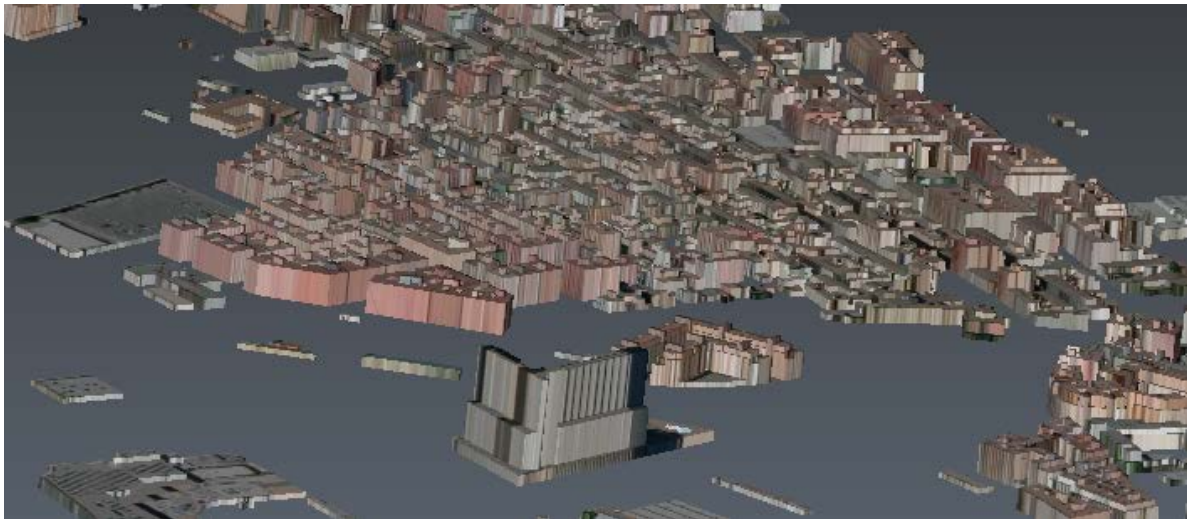

Figure 157. 3D model textured of the town of Burjassot.

3.9.3 Creation of the Valencian Silo-Yard

The 3D model of the Valencian Silo-Yard was extracted from the .OBJ of buildings in the previous step, this model was modified in order to import the 3D model created of the first three connected silos, a visible model of silo 1 and two thermal models from silos 2 and 3. These silos were selected in order to compare a visible silo and a thermal silo with the same characteristics, for this reason the silos selected were the silo 1 for the visible and the silo 3 for the thermal. Lastly, the silo 2 was shown with the thermal 3D model.

All this was performed using Blender, in this workflow the first step was to improve the texture of the side of the Silo-Yard, adding the texture from a photo with the surface of the Silo-Yard (Figure 158). To add a texture of a face into Unity, the different faces to texture must be selected, opening the "UV/Image Editor" the selected faces in the 3D view will appear, and these faces need to be selected again in the "UV/Image Editor" by pressing the button A of the keyboard. Once the faces are selected, pressing the button S of the keyboard the faces could be scaled, adapting them to the size of the texture.

Figure 158. Texture applied on the side of the Silo-Yard.

Once all the sides of the Silo-Yard had the correct texture, the different 3D models of the silos were imported.

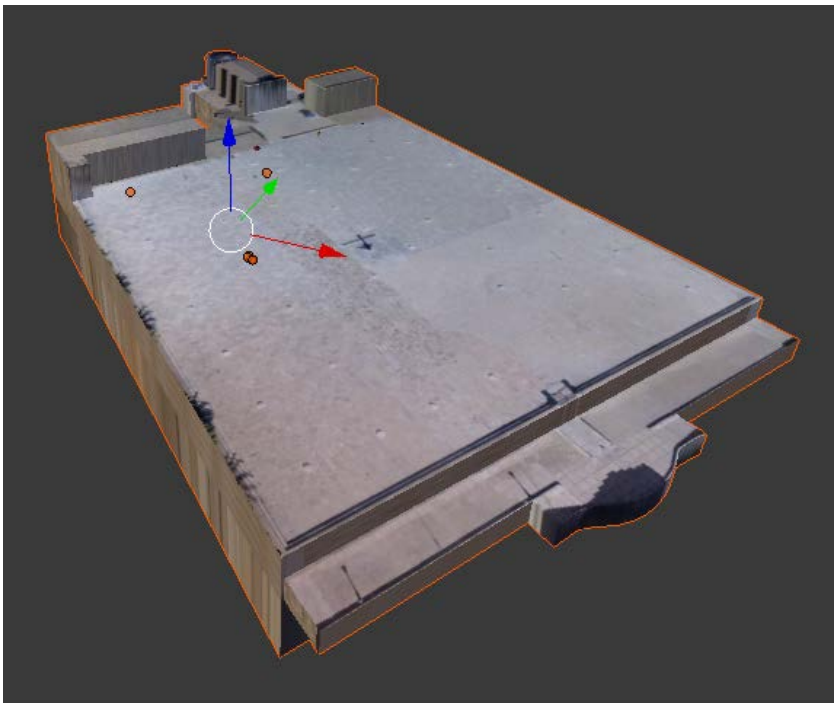

Figure 159. 3D model of the Silo-Yard.

Into this 3D model, the following models created were exported:

- Visible 3D model of the silo 1.
- Thermal 3D model of the silo 2.
- Thermal 3D model of the silo 3.
- 3D model of the silos created from the laser scanner point cloud.

All these models were placed correctly, deleting the areas of overlap between the laser scanner 3D model and the different models of the silos to represent, keeping only the ground and the tunnels of this model. Also, a 3D model of the rest of silos connected by the tunnel was added to the 3D model of the silos created from the laser scanner point cloud. This last 3D model was created by David Montalvá España (Montalvá, 2016). David Montalvá España's model added continuity to the virtual tour, adding the other three silos connected by the Spanish Civil War tunnel, which they were not studied in this project.

In addition, the door of the silos was opened using a Boolean modifier in Blender. The type of operation to be performed from the Boolean operation menu was “Intersect”, using this tool each face of the new object has the material properties of the corresponding surface that contributed to the new volume based on the Intersect operation.

All these models were merged in one object that was exported as an .OBJ file. To represent the different textures it is necessary to save them in different files, for this reason five .PNG files were exported from Blender to apply the textures in Unity.

3.9.4 Creation of a scene in Unity

The scene contained the objects of the virtual tour. It is used to create a main menu, environments, obstacles, and decorations, essentially designing and building the town of Burjassot. In the scene created in the reference 3.9.1.2 it was modified in order to import the buildings of Burjassot and the Silo-Yard, also different lights were introduced to illuminate the silos and the tunnel, ultimately a character was introduced to walk freely around the scene created.

Firstly, the models of the buildings of Burjassot and the Silos were imported to Unity. To import them is necessary import the .OBJ file, the .MTL file and the different textures. Once the objects were imported, they were placed in their real locations over the landscape.

The buildings of Burjassot were created in ArcScene over the base height of the DEM. This DEM was used to create the real landscape in Unity, accordingly the buildings fit perfectly on the ground.

Figure 160. Buildings of Burjassot into the Unity scene.

In order to illuminate the interior scenes different “Light point” were introduced standing in the same place where the lamps of the silos are. In addition the terrain was modified introducing different trees and grass in the parks of Burjassot.

Figure 161. Environment of Burjassot.

Figure 162. Light point into the silo 1.

This project was built to visualize it in a Windows standalone executable in order to show it into the PowerWall of the Fakultät Informationsmanagement und Medien an der Hochschule Karlsruhe. Furthermore, also the scene created in Unity was built to run it in a web player.

3.9.4.1 PowerWall visualization

The PowerWall is a hardware and software combination that allows the user to visualize a Unity scene in 3D thanks to an active shutter 3D system, it is a technique of displaying stereoscopic 3D images. It works by only presenting the image intended for the left eye while blocking the right eye's view, then presenting the right-eye image while blocking the left eye, and repeating this so rapidly that the interruptions do not interfere with the perceived fusion of the two images into a single 3D image.

The character of unity is controlled through different sensors of the system using 3D active glasses with targets and a Wii Remote with other targets. Thanks to these targets a system with two cameras detects the position and orientation of the operator.

To execute a Unity project into the PowerWall only is necessary to modify the character, adding a package called “CustomPlayerV5Final.unitypackage”, this package adds a PowerWalker.prefab into the assets of the project, having the same characteristics than the First Person Character, the default character of Unity.

In this character different settings were modified in order to adapt it into the Valencian Silo-Yard project. The first modification was the position and rotation of the character, locating it in front of the Silo’s door. In addition the options of radius and height of the character was changed to a values of 0.3 meters and 0.8 meters respectively, thus it is not necessary to bend the character to walk through the tunnels of the silos.

Ultimately, different audio sources were added to the character to sound footstep when it is walking and a song to make the walk around the scene more pleasant.

3.9.4.2 Web player visualization

To create the web player visualization was used a different character. In that case the character used was the FirstPersonController, the default character of Unity.

The modifications of the features of this characters were the same previously used in the PowerWall character in order to have the maximum similarity between the two scenes built with different platforms.

The next video shows the web virtual tour created.

Figure 163. Virtual tour of the Valencian Silo-Yard.

4 Conclusion

4.1 Summary of the result

The past is around us. Humanity live around a rich backdrop formed by historic buildings, landscapes and other physical survivals of our past, also all of us create heritage with customs, knowledge and traditions. Heritage may be built, written, recited, remembered, re-enacted, worn, displayed, and taught. Heritage is the only way to connect with our past, to determine right from wrong, beautiful from repulsive, interesting or trivial (Britain, 2001).

The Valencian Silo-Yard, placed in Burjassot is an example of underground heritage. This complex constitutes an example of rural and vernacular architecture. This National Historic-Artistic Monument is in a serious state of disrepair and only the preventive conservation, examination, documentation, research, treatment, and education can return it to its original state, preserving the legacy for the next generations.

Thermal characterization of the Valencian Silo-Yard is a cultural heritage documentation project inside “Responsibility for Cultural Heritage through Geomatics”. This tri-national project provided an opportunity for students to learn different geomatics methods, developing guidelines and acquiring techniques for the documentation of cultural heritage. But it is noteworthy that during the project all students and teachers created an excellent social environment atmosphere that will pay off in the coming campaigns, solving the problems that have occurred during the first campaing in Valencia, improving the job done in the Valencian Silo-Yard. This project not only created a great documentation of the silos, also it created a friendship between all participants.

In this project the first idea of create a thermal 3D model of the Valencian Silo-Yard has came true, starting from the purchase of a thermal camera without which this project would not have been possible. Continuing with the creation and develop of an app to take multispectral photos, using the smartphone camera and the Flir One thermal camera. Creating different 3D models of silos and finally using all the documentation created to detect pathologies and improve the current documentation of the complex.

In addition this project opened a new way to create fast and easy thermal documentation, taking photos with the HSKA Flir One App in order to create a thermal 3D model of an object. Using the visible photographs from the smartphone camera a 3D model is created, and after an automatic processing of the thermal photos, they can be projected on the 3D model. This methodology creates fast thermal 3D models automatically, the main objective of this project.

Finally, all data acquired during the campaign and developed during this master thesis were treated to visualize into a game engine, creating a full scale virtual tour of Burjassot and the Valencian Silo-Yard to visualize it into a Windows standalone application and such as web content.

4.2 Future work

Thermal imaging opens a new way in the preservation of cultural heritage. This project shown as a low-cost project can get great results in order to document a building or any other tangible object to detect facts that are not visible to the human eye.

All work done is just a sample of a new way to document more and better the heritage and the continuous development of new sensors, data capture methodologies and multispectral 3D representations contributes significantly to the digital 3D documentation, mapping, conservation and representation of the heritage. The continued development of smartphones are increasing the possibilities for 3D documentation, and such as the visible sensors of the smartphones, the thermal sensors are increasing the resolution while prices are falling. The CAT S60 from Caterpillar was the first smartphone with a Flir thermal sensor integrated who knows if in the future all smartphones would have thermal sensors that make of this pioneer project something common.

Focusing on the project, one future work will be the finish the orientation of thermal images based on the orientation parameters of the visible images. This point was performed in this thesis manually linking pairs of points between the visible smartphone model and the thermal images from the Flir One. The next step will be transform the coordinates of the cameras from the visible model knowing the offset between the thermal camera and the smartphone camera.

In order to create a realistic visualization, the Silo-Yard would be modeled, including the both *embarronats*, and the Chapel of St. Roque. This project was focused in the visualization of the silos and the tunnel, but to create an optimal visualization these elements should be modeled and textured.

As Max Planck once said,

> *"An experiment is a question which science poses to nature and a measurement is the recording of nature's answer.*

5 Bibliography

Agencia Estatal de Meteorología - AEMET (2016) *Climate data by meteorological stations* Gobierno de España, Available at: https://sede.aemet.gob.es/AEMET/es/GestionPeticiones/consultaEstaciones (Accessed: 15 May 2016).

Aldana Fernández, S. (1988) *La lonja de Valencia* Valencia : Consorci d'Editors Valencians, Biblioteca Valenciana, 1988., Valencia

Arora, C.P. (2004) *Thermodynamics*.Education, M. H. (ed.) New Delhi: McGraw Hill Education.

Balageas, D.L. (2007) 'Termografía Infrarroja : una técnica multifacética para la Evaluación No Destructiva (END)', *IV conferencia Panamericana de END*, p. 14.

Betrán, J.L. (2006) *Historia de las epidemias en España y sus colonias: 1348-1919*. Barcelona: La Esfera de los Libros, Historia divulgativa.

Blanes Andrés, R. (1992) *Los silos de Burjassot : (1573-1600). Un monumento desconocido* Valencia : Consell Valencià de Cultura, 1992., Valencia

Britain, D. for C.M. and S. (2001) *The Historic Environment: A Force for Our Future*. Available at: http://www.tourisminsights.info/ONLINEPUB/DCMS/DCMS PDFS/HISTORIC ENV FORCE - 1.pdf (Accessed: 2 August 2016).

Buxton, D.R. (2003) *Silage science and technology*.American Society of Agronomy, I. (ed.) American Society of Agronomy, Inc.

Catastro, S.E. del (2011) *MODELO DE DATOS DE CARTOGRAFÍA VECTORIAL (FORMATO SHAPEFILE)*. Available at: http://www.catastro.minhap.es/ayuda/manual_descriptivo_shapefile.pdf (Accessed: 8 July 2016).

Climate-Data.org (n.d.) *Climate data of Burjassot* Available at: http://es.climate-data.org/location/56923/ (Accessed: 26 May 2016).

Cruz Zapata, B. (2015) *Android Studio Essentials*. United Kingdom: Packt Publishing.

Cusido, J.A. et al. (1996) 'Aplicaciones de la termografía infrarroja y la espectrorradiometría en el estudio del deterioro del Patrimonio Arquitectónico Nacional', *Informes de la Construcción*, 48(443), pp. 15–26.

Expósito Navarro, L.M. (2005) *Los Silos de Burjassot : el granero de Valencia.* Burjassot : Instituto Municipal de Cultura y Juventud de Burjassot, 2005., Burjassot

Fernández-Posse, M.D. (2011) *Arqueología, sociedad, territorio y paisaje.: Estudios sobre prehistoria reciente, protohistoria y transición al mundo romano.* Consejo Superior de Investigaciones Científicas, Instituto de Historia, Biblioteca prehistórica hispana.

Flir Systems (2011) *Thermal imaging guidebook for industrial applications*. p.48, available at: http://www.flirmedia.com/MMC/THG/Brochures/T820264/T820264_EN.pdf (Accessed: 12 May 2016).

Furió i Diego, A. and València, U. de (eds.) (1999) *Historia de Valencia* Valencia : Prensa Valenciana : Universitat de València, 1999., Valencia

García, E. (2009) *Lonja de la Seda de Valencia*. Available at: https://commons.wikimedia.org/wiki/File:Lonja_de_la_Seda_de_Valencia.jpg (Accessed: 16 June 2016).

Generalitat Valenciana (1983) *Catálogo de Monumentos y Conjuntos de la Comunidad Valenciana*.

Gil, V. (1981) *Cuarenta Años Junto a Franco*. Planeta, Espejo de España.

Gutscher, M.-A. et al. (2006) 'The Gibraltar Arc seismogenic zone (part 2): Constraints on a shallow east dipping fault plane source for the 1755 Lisbon earthquake provided by tsunami modeling and seismic intensity', *Tectonophysics*, 426(1), pp. 153–166.

Heriard Dubreuil, M. (1987) *Valencia y el gótico internacional / Tomo I* Valencia : Institucion Alfonso el Magnanimo, 1987., Valencia

Kagan, R. L. and Wyngaerde, A. van den (eds.) (1986) *Ciudades del Siglo de Oro : Las vistas españolas de Anton van den Wyngaerde* Madrid : El Viso, 1986., Madrid

Kaviany, M. (2014) *Heat transfer physics*. Michigan: Springer.

Lerma, M.J.S. de (2012) 'Introducción Histórica a la Geodesia', *Pensamiento Matemático*, (2), pp. 1–63.

Lillesand, T.M. (2008) *Remote sensing and image interpretation* New York : Wiley, cop. 2008., New York

Lòpez i García, S. (1994) *Arquitectura i ingeneria civil de caràcter rural i agrari en el territori de Burjassot*. Burjassot.

Lòpez i García, S.A. de B. (1989) *Aproximación a la historia de Burjassot y su entorno*. Council of Burjassot.

López Laguarda, J.J. (1946) *Burjasot (Apuntes para su historia)*. Valencia.

Marqués, C. (1979) *Guia urbana de Valencia antigua y moderna. Vol. 2* Valencia : París-Valencia, D.L. 1979., Valencia

Mestre, J.M. (2009) *Sistemes tradicionals de conservació dels aliments en fosses i sitges: un enfocament multidisciplinar*.

Montalvá, D. (2016) *Development of complex geometric surface with Geomatics techniques - Processing of TLS data of the silos of Burjassot*. Hochschule Karlsruhe – Technik und Wirtschaft.

MORTE GARCIA, C. (2006) *La corona de Aragón : el poder y la imagen de la Edad Media a la Edad Moderna (siglos XII-XVIII)* Sociedad Estatal para la Acción Cultural Exterior, Barcelona

Mounce, R. (2013) *Get PDF metadata using exiftool* Figshare,

Payne, S. (2014) *La guerra civil española:* . Ediciones Rialp, S.A., Historia.

Planck, M. 1914. The Theory of Heat Radiation. F. Blakiston Son & Co, available at: https://www.gutenberg.org/files/40030/40030-pdf.pdfRevilla, P.S. (2015) *arteygeografiadelgris*. Available at: http://arteygeografiadelgris.blogspot.de/2015_02_01_archive.html (Accessed: 16 June 2016).

Valls Ayuso A., Ramírez Blanco M. J. & Llinares Millán J. 2014. Silos de Burjassot (S.XVI). Origen y desarrollo constructivo. Evolución de sus estructuras y estado de conservación. PhD thesis at UPV, Valencia.

Valls Ayuso A., García García F., Ramírez Blanco M. J., & Benlloch Marco J. 2015. Understanding subterranean grain storage heritage in the Mediterranean region: The Valencian silos (Spain). Valencia: Elsevier.

Zielinski, S. (2008) *Absolute Zero.*, *SMITHSONIAN.COM* Available at: http://www.smithsonianmag.com/science-nature/absolute-zero-13930448/?no-ist= (Accessed: 25 April 2016).

6 Annex I. Graphic Materials

List of graphics in the Annex 1:

- Location of Burjassot
- Location of the Silos of Burjassot
- Thermal orthophoto of the Silo No. 1
- Thermal orthophoto of the Silo No. 2
- Thermal orthophoto of the Silo No. 3
- Visible orthophoto of the Silo No. 1
- Visible orthophoto of the Silo No. 3

* The top view of the different orthophotos was extracted from "*Silos de Burjassot (S. XVI). Origen y desarrollo constructivo. Evolución de sus estructuras. Estado de conservación."* (Valls Ayuso, 2014)

Spain

Comunidad Valenciana

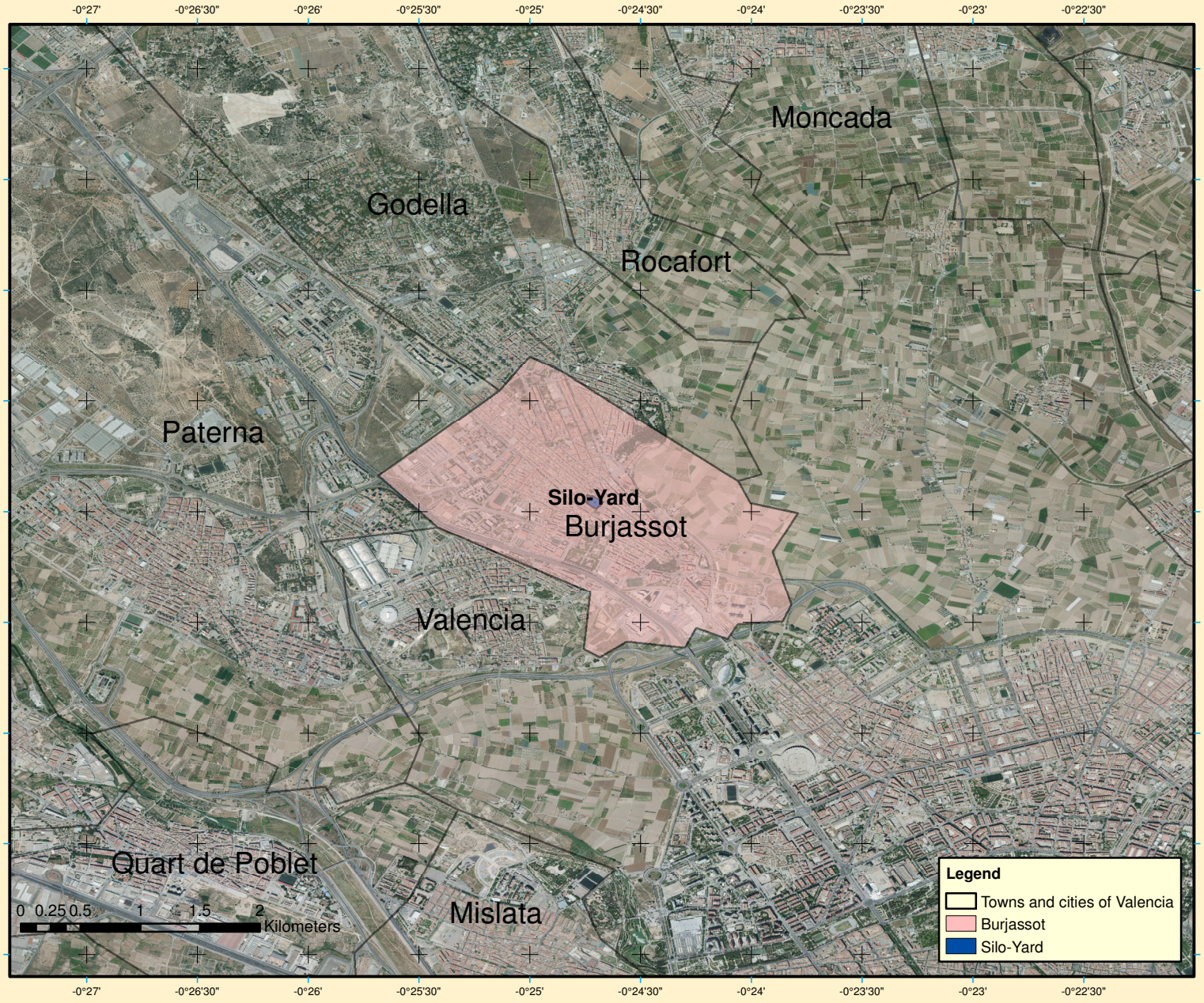

UNIVERSITAT POLITÈCNICA DE VALÈNCIA

Hochschule Karlsruhe Technik und Wirtschaft
UNIVERSITY OF APPLIED SCIENCES

Location of Burjassot

Thermal Characterization of the Valencian Silo-Yard

Juan Pedro Carbonell Rivera

Coordinate System: WGS84
Prime Meridian: Greenwich (0.0)
Semimajor Axis: 6378137.000
Seminor Axis: 6356752.314
Inverse Flattening: 298.257

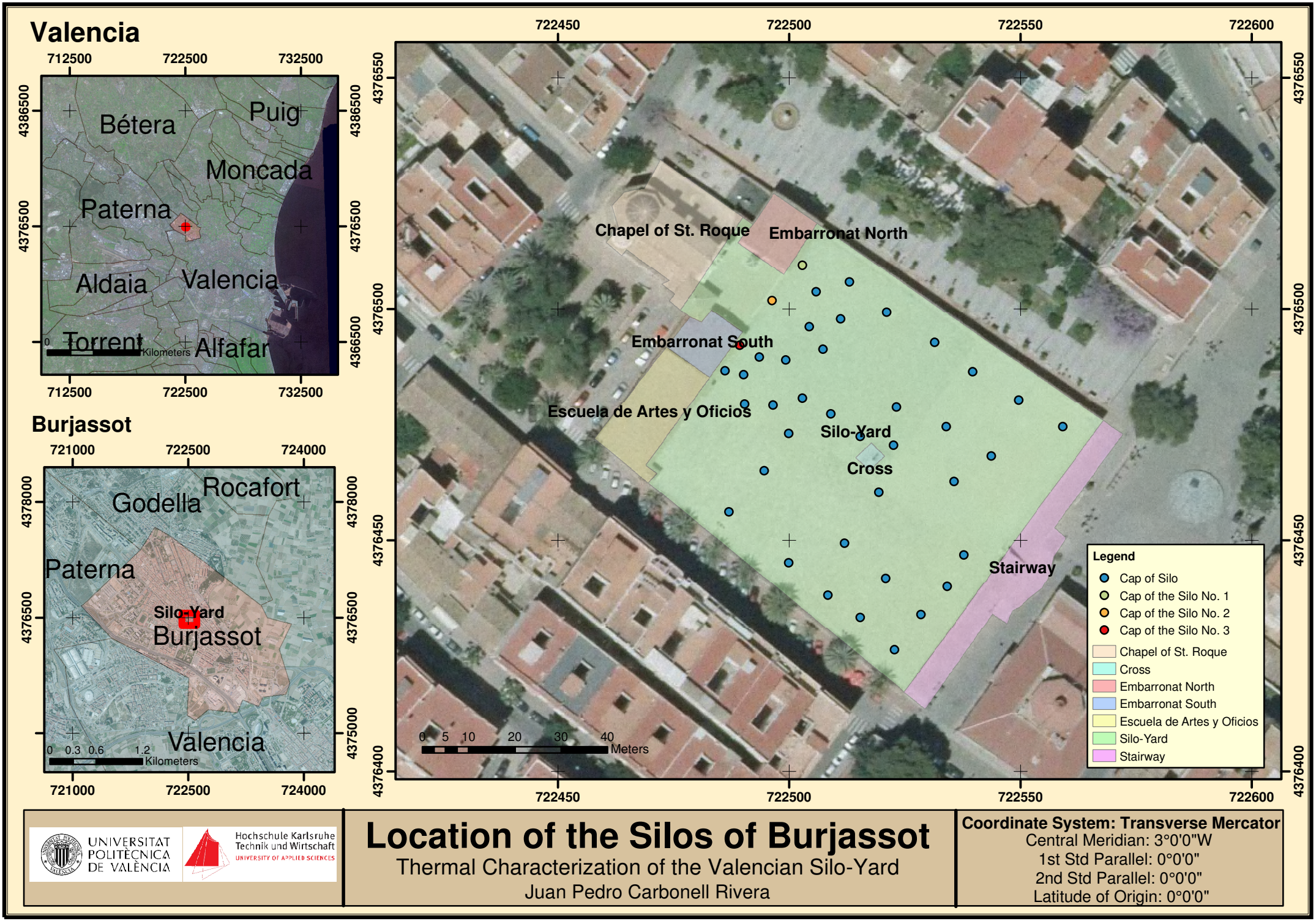

UNIVERSITAT POLITÈCNICA DE VALÈNCIA

Hochschule Karlsruhe Technik und Wirtschaft
UNIVERSITY OF APPLIED SCIENCES

Location of the Silos of Burjassot

Thermal Characterization of the Valencian Silo-Yard

Juan Pedro Carbonell Rivera

Coordinate System: Transverse Mercator
Central Meridian: 3°0'0"W
1st Std Parallel: 0°0'0"
2nd Std Parallel: 0°0'0"
Latitude of Origin: 0°0'0"

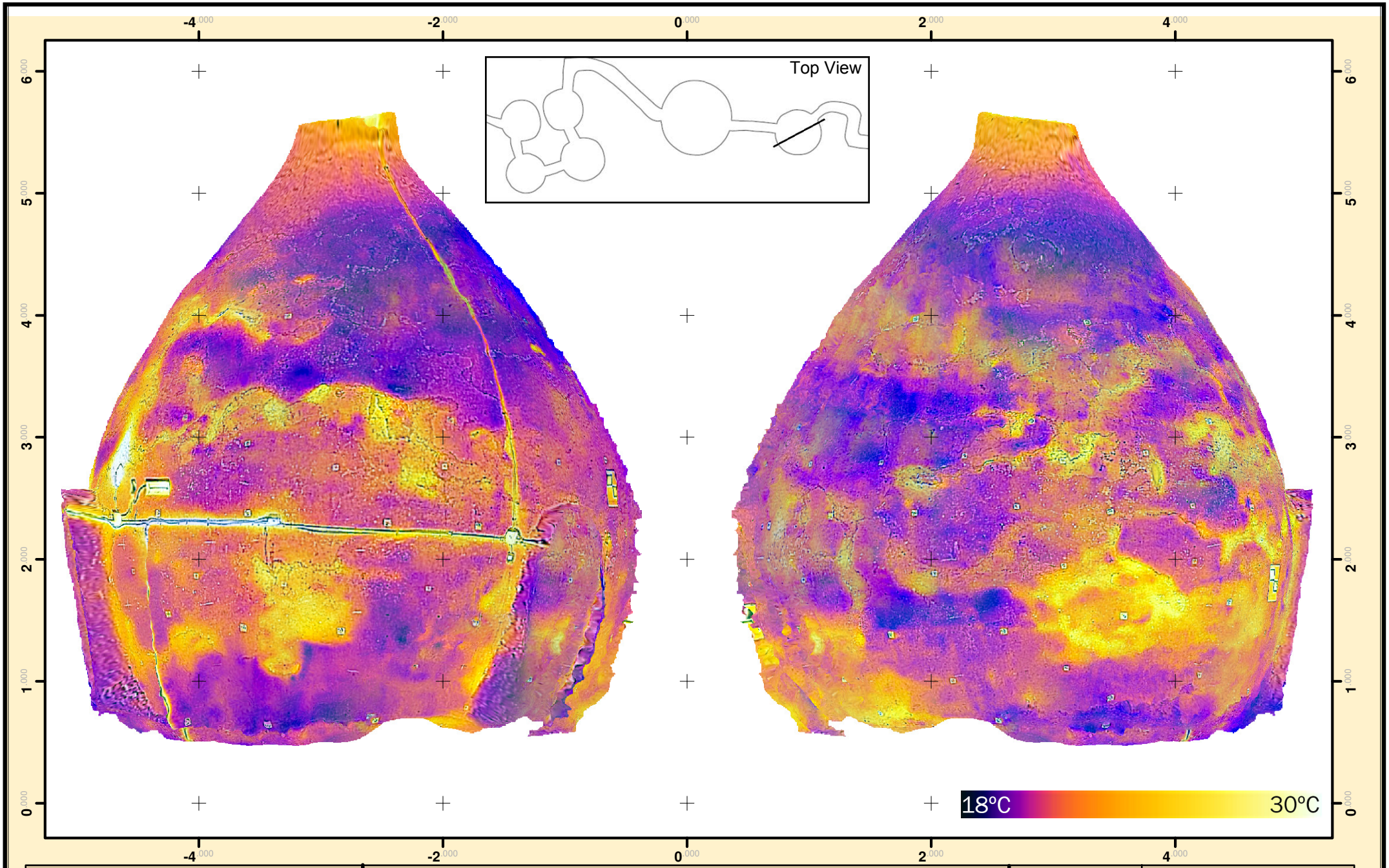

UNIVERSITAT POLITÈCNICA DE VALÈNCIA

Hochschule Karlsruhe Technik und Wirtschaft
UNIVERSITY OF APPLIED SCIENCES

Thermal orthophoto of the Silo No. 1

Thermal Characterization of the Valencian Silo-Yard

Scale: 1:40 | **Date:** August 2016

Author: Juan Pedro Carbonell Rivera

Signature:

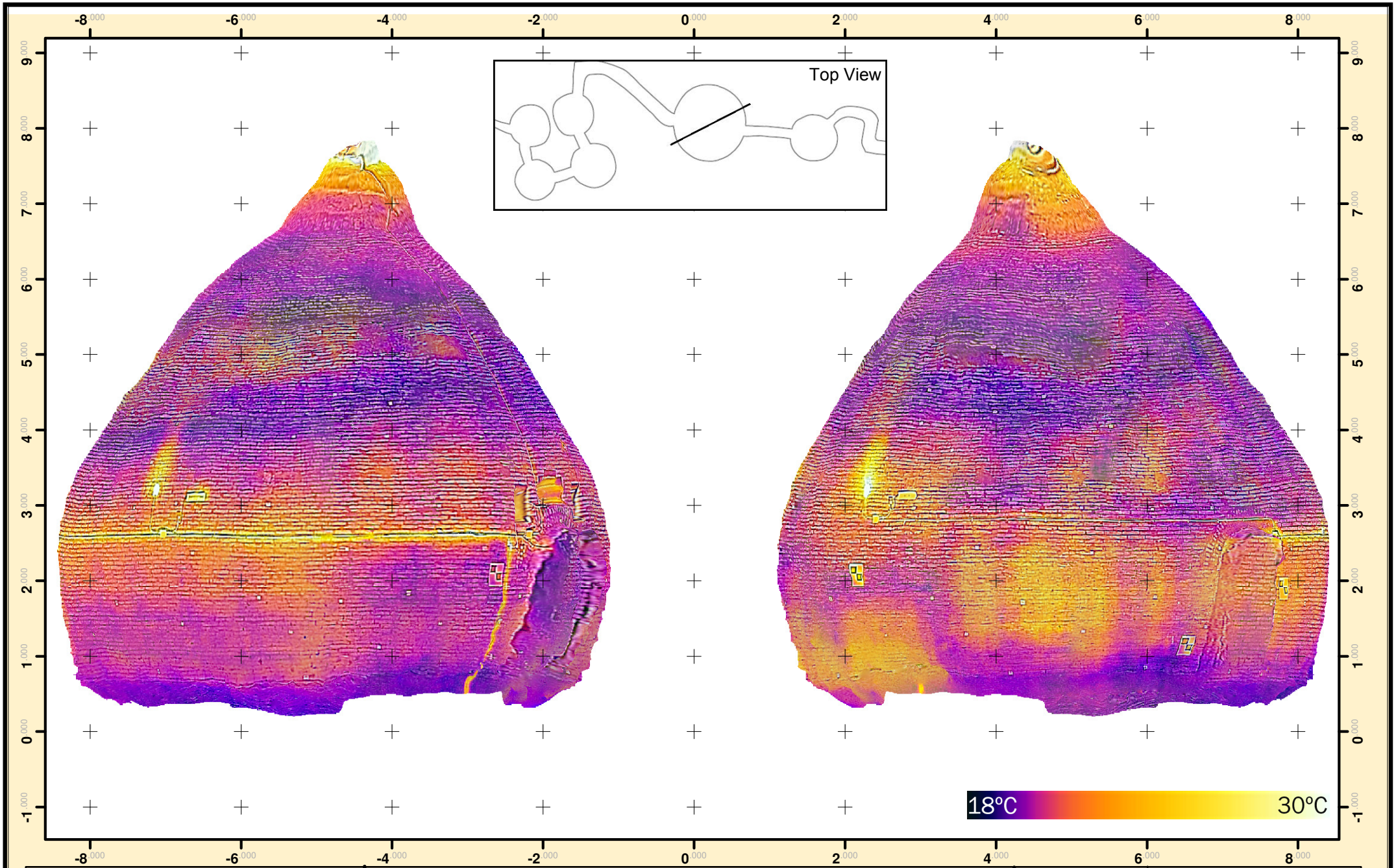

UNIVERSITAT POLITÈCNICA DE VALÈNCIA

Hochschule Karlsruhe Technik und Wirtschaft
UNIVERSITY OF APPLIED SCIENCES

Thermal orthophoto of the Silo No. 2

Thermal Characterization of the Valencian Silo-Yard

Scale: 1:60 | **Date:** August 2016

Author: Juan Pedro Carbonell Rivera

Signature:

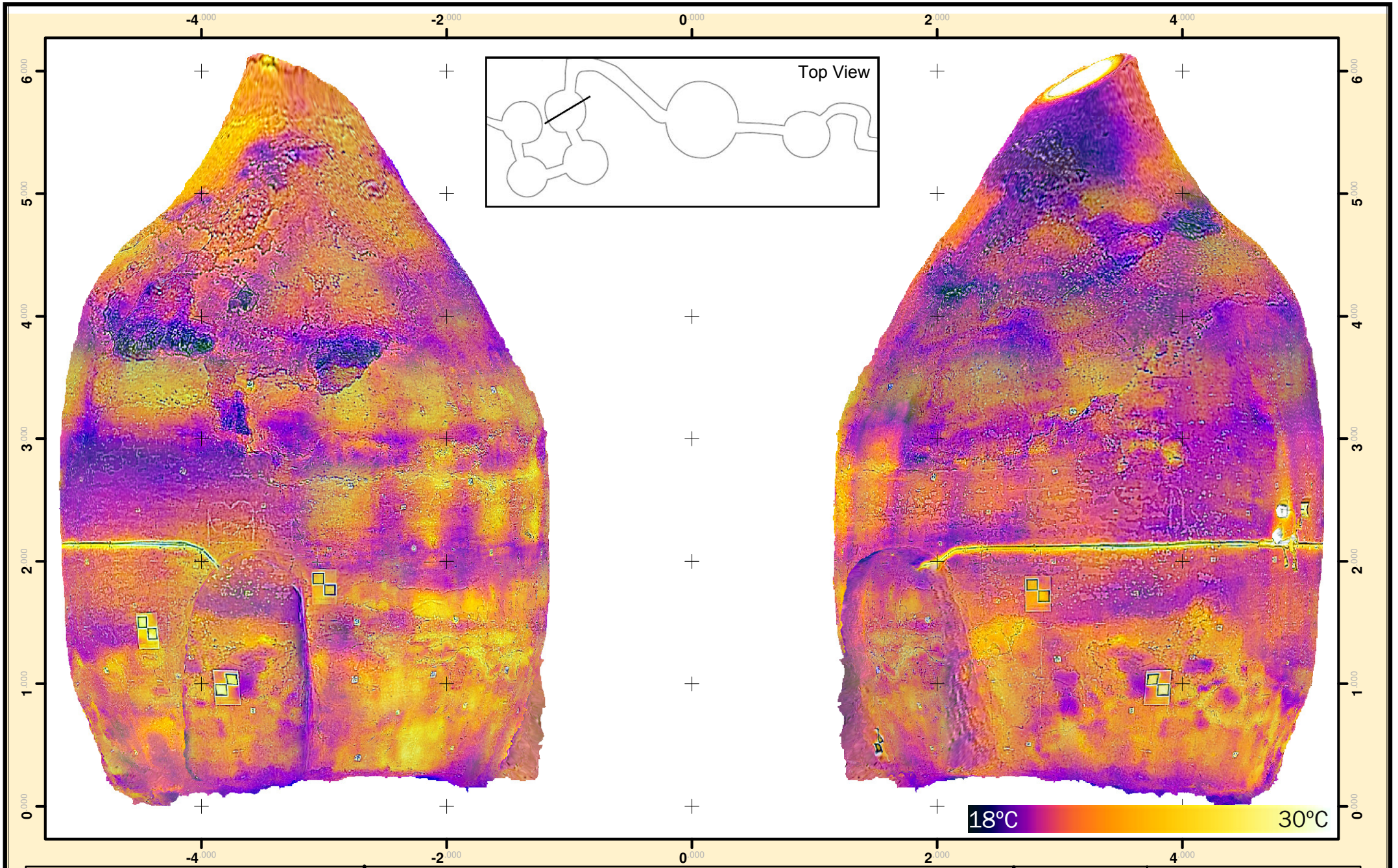

UNIVERSITAT POLITÈCNICA DE VALÈNCIA

Hochschule Karlsruhe Technik und Wirtschaft
UNIVERSITY OF APPLIED SCIENCES

Thermal orthophoto of the Silo No. 3

Thermal Characterization of the Valencian Silo-Yard

Scale: 1:40	**Date:** August 2016
Author: Juan Pedro Carbonell Rivera	
Signature:	

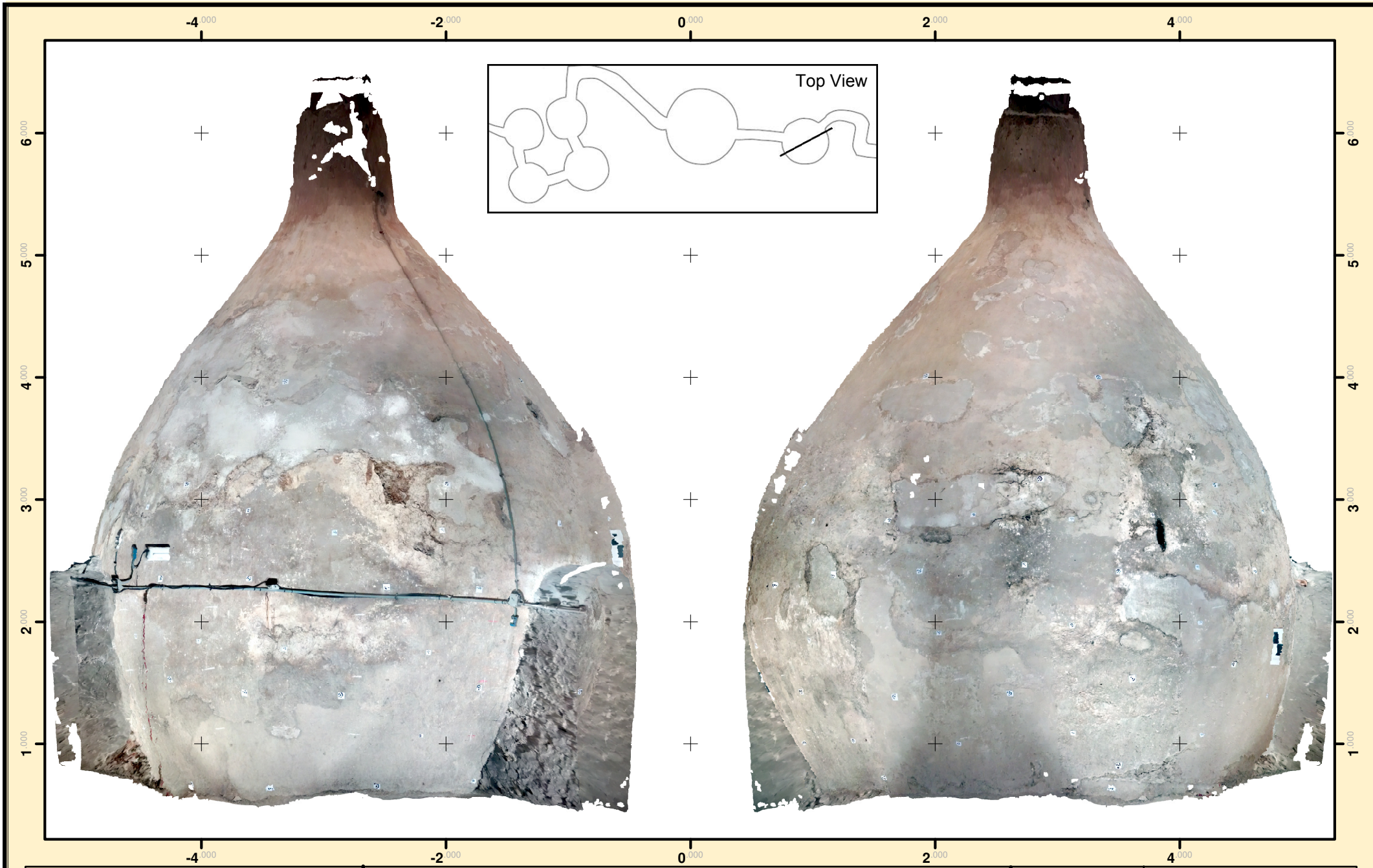

UNIVERSITAT POLITÈCNICA DE VALÈNCIA

Hochschule Karlsruhe Technik und Wirtschaft
UNIVERSITY OF APPLIED SCIENCES

Visible orthophoto of the Silo No. 1

Thermal Characterization of the Valencian Silo-Yard

Scale: 1:40	**Date:** August 2016
Author: Juan Pedro Carbonell Rivera	
Signature:	

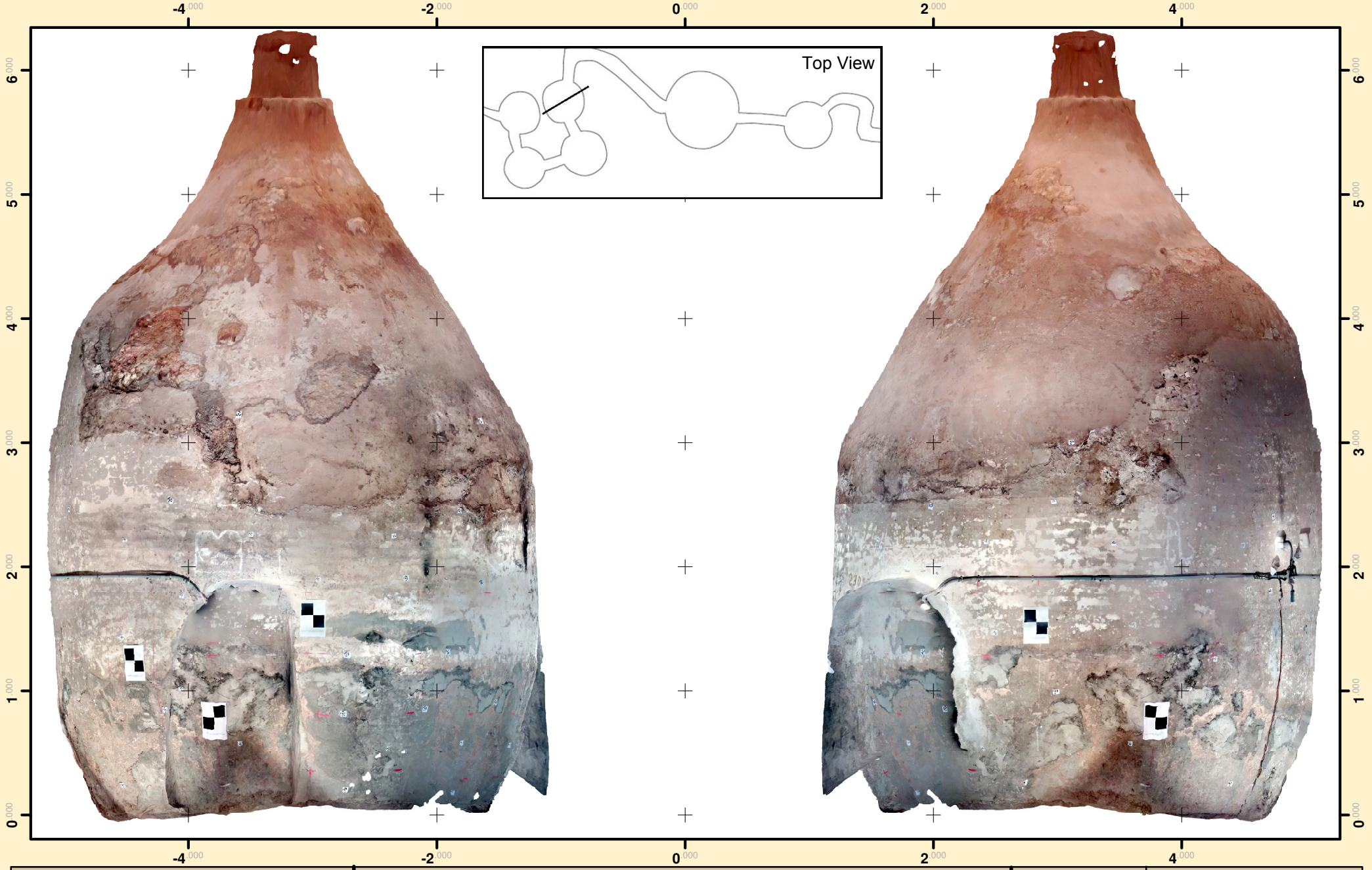

UNIVERSITAT POLITÈCNICA DE VALÈNCIA

Hochschule Karlsruhe Technik und Wirtschaft
UNIVERSITY OF APPLIED SCIENCES

Visible orthophoto of the Silo No. 3

Thermal Characterization of the Valencian Silo-Yard

Scale: 1:40	**Date:** August 2016
Author: Juan Pedro Carbonell Rivera	
Signature:	

7 Annex I. Graphic Materials

7.1 AndroidManifest.xml

7.2 EditorActivity.java

7.3 PreviewActivity.java

7.4 Activity_editor.xml

7.5 Emptytextview.xml

7.6 Activity_preview.xml

8 Annex III. Registration report

9 Annex IV. Script code to transform the Roman numerals floor to float numbers

*These annexes can be found in the compact disc included in this project.